Australian Government
Department of Defence
Defence Science and
Technology Organisation

The Effects of Hole-size and Environment on the Mechanical Behaviour of a Quasi-isotropic AS4/3501-6 Laminate in Tension, Compression and Bending

Paul J. Callus

Air Vehicles Division
Defence Science and Technology Organisation

DSTO-TR-2077

ABSTRACT

This report describes the results of open-hole-tension (OHT), open-hole-compression (OHC) and open-hole-four-point-bend (OHB) tests conducted on AS4/3501-6 quasi-isotropic [45/0/-45/90]$_{2s}$ laminates in the room temperature dry (RTD) and elevated temperature wet (ETW) condition. Specimens were 38.1 mm wide with central through-holes ranging in diameter from 0.00 (unnotched) to 9.55 mm. The strain distribution near the hole in an OHT specimen was measured and found to agree well with that predicted for an infinite orthotropic plate subject to uniform remote stress. A simple modification of this model predicted well the strains near the hole on the tensile face of OHB specimens. OHT and OHC strength fell rapidly as hole size increased for small holes and less so for larger holes. This effect was much less pronounced in OHB specimens. The ETW environment had little effect on OHT properties but produced significant, and similar, reductions in OHC and OHB strength. OHT and OHC strength was predicted very well, and OHB strength moderately well, by the Whitney-Nuismer Average and Point Stress Criteria when using the strain distribution for that specimen type. OHC strength was also predicted very well by the Budiansky-Soutis-Fleck Cohesive Zone Model. However, each of these models requires experimental data in addition to the strength of the unnotched laminate and thus they are limited to applications where this data can be generated.

RELEASE LIMITATION

Approved for public release

APPROVED FOR PUBLIC RELEASE

The Effects of Hole-Size and Environment on the Mechanical Behaviour of a Quasi-isotropic AS4/3501-6 Laminate in Tension, Compression and Bending

Executive Summary

The design and airworthiness certification of composite aircraft structure is generally performed using the building-block approach. This requires substantial testing at the coupon, element, detail, sub-component and component level. This is necessary because the coupon, element and detail tests generally do not accurately represent the loading experienced by components in complex, built-up, aircraft structure.

A more cost-effective approach would be to replace at least some of the element, detail and sub-component tests with a suite of coupons that provide data suitable for the design of the full-scale structure. The Defence Science and Technology Organisation, in collaboration with the Co-operative Research Centre for Advanced Composite Structures, has conducted a program developing one such representative coupon, a laminate with an open hole subjected to combined axial and bend loading.

A series of reports are being prepared that describe the behaviour of composite laminates under both uniaxial and combined loading. This is one of the reports in that series. It provides baseline data regarding the effect of hole size and environment on mechanical properties in tension, compression and bending.

Open hole tension (OHT), compression (OHC) and four-point bend (OHB) tests, in the room temperature dry (RTD) and elevated temperature wet (ETW) condition, were performed on AS4/3501-6 quasi-isotropic $[45/0/-45/90]_{2s}$ laminates. Specimens were 38.1 mm wide and contained central through-holes ranging in diameter from 0.00 (unnotched) to 9.55 mm.

The strain distribution near the hole of an OHT specimen was predicted well by the model for an infinite orthotropic plate containing a circular hole subjected to a uniform, remote, in-plane stress. A simple modification of this model predicted well the strain distribution near the hole on the tensile face of OHB specimens.

OHT and OHC strength and strain-to-failure fell rapidly as hole size increased for small holes and less so for larger holes. This effect was much less pronounced in OHB.

The ETW environment had little effect on OHT properties but produced significant, and similar, reductions in OHC and OHB strength and strain-to-failure.

The deflection OHB specimens with 0.00 and 6.35 mm diameter holes was represented well by assuming no hole and using classical beam deflection theory.

OHT and OHC strength was predicted very well, and OHB strength moderately well, by the Whitney-Nuismer Average Stress Criterion and Point Stress Criterion when using the strain distribution for that specimen type. OHC strength was also predicted very well by the Budiansky-Soutis-Fleck Cohesive Zone Model. The first two of these models are used widely in aircraft design. However, each of these models require experimental data in

addition to the strength of the unnotched laminate and are thus limited to applications where this data can be generated. It is also suspected that they will not predict accurately the strength of laminates subjected to combined axial and bend loading.

Author

Paul J. Callus
Air Vehicles Division

Dr Paul Callus gained his PhD from Monash University in 1993. He worked with CSIRO developing electrode coatings for ceramic fuel cells then at RMIT investigating the mechanical behaviour of textile composites. He joined DSTO in 1997 and is currently a Senior Research Scientist in the Advanced Composite Technologies Work Group. His major work programs have focused on the development of composite replacement panels with an emphasis on airworthiness certification, and more recently to develop multifunctional aircraft structure for the Australian Defence Force. He recently completed an attachment to the Advanced Structural Concepts Branch of the United States Air Force Research Laboratory at Wright Patterson Air Force Base where he worked on Conformal Load-bearing Antenna Structure.

Contents

Nomenclature

a	(support span – loading span) in four-point bending
a_0	Average Stress Criterion characteristic distance
A_{ij}	ij'th element of the stiffness matrix
ASC	Average Stress Criterion
ASTM	American Society for the Testing of Materials
b	Specimen width
CCSM	Composite Compressive Strength Modeller
CRC-ACS	Cooperative Research Centre for Advanced Composite Structures
CZM	Cohesive Zone Model
d	Specimen thickness
D	Maximum deflection of the centre of the specimen
d_0	Point Stress Criterion characteristic length
DSTO	Defence Science and Technology Organisation
E_1	Elastic modulus in longitudinal (0°) direction
E_1^b	Elastic modulus in longitudinal (0°) direction under bending
E_1^c	Elastic modulus in longitudinal (0°) direction under compression
E_1^t	Elastic modulus in longitudinal (0°) direction under tension
E_2	Elastic modulus in transverse (90°) direction
E_2^t	Elastic modulus in transverse (90°) direction under tension
EKDF	Environmental Knock-Down Factor
$EKDF_{ETW}$	Environmental Knock-Down Factor for the Elevated Temperature Wet condition
$EKDF_{ETW}^{Fcu}$	Environmental Knock-Down Factor for Ultimate strength in compression in Elevated Temperature Wet condition
$EKDF_{ETW}^{Ftu}$	Environmental Knock-Down Factor for Ultimate strength in tension in Elevated Temperature Wet condition
$EKDF_{ETW}^{\varepsilon cu}$	Environmental Knock-Down Factor for Strain-To-Failure in Compression in Elevated Temperature Wet condition
$EKDF_{ETW}^{\varepsilon tu}$	Environmental Knock-Down Factor for Strain-To-Failure in Tension in Elevated Temperature Wet condition
ETW	Elevated Temperature Wet
FE	Finite Element
F_1^{bu}	Ultimate strength in longitudinal (0°) direction under bending
F_1^{cu}	Ultimate strength in longitudinal (0°) direction under compression
F_1^{tu}	Ultimate strength in longitudinal (0°) direction under tension
FWCF	Finite Width Correction Factor

G_{12}	In-plane shear modulus
I	Second moment of inertia
K_c	Critical Stress Intensity Factor
K_t	Stress Concentration Factor
K_T^∞	Orthotropic stress concentration factor for a plate of infinite width
l	Distance from left hand loading roller in four-point bend
l_c	Critical microbuckle length
L	Support span in four-point bending
M	Slope of tangent to initial straight-line portion of load-deflection curve in four-point bending
OHB	Open-Hole-Bend
OHC	Open-Hole-Compression
OHT	Open-Hole-Tension
P	(applied load/2) in four-point bend
P_{max}	Maximum load
P-R-S	Potti-Rao-Srivastava
PSC	Point Stress Criterion
r	Hole radius
R^2	Coefficient of determination
RAAF	Royal Australian Air Force
RH	Relative Humidity
RTD	Room Temperature Dry
S	Stress in outer fibres throughout the load span in four-point bending
SACMA	Suppliers of Advanced Composite Materials Association
SRM	SACMA Recommended Method
x	Distance from edge of hole
w	Specimen width
W-N	Whitney-Nuismer
$\delta_{(l)}$	Deflection of bend specimen location l along the specimen
ε_1^{bu}	Strain-to-failure in longitudinal (0°) direction under bending – average magnitude of tension and compression faces
ε_1^{cu}	Strain-to-failure in longitudinal (0°) direction under compression
ε_1^{tu}	Strain-to-failure in longitudinal (0°) direction under tension
ν_{21}	In-plane Poisson ratio
σ_N	Notched strength of a finite width plate
σ_N^∞	Notched strength of an infinite width plate
σ_0	Unotched strength of a finite width plate
σ_N^∞	Unnotched strength of an infinite width plate
$\sigma_y(x,0)$	Normal stress along the line through the centre of the hole and perpendicular to the loading direction

1 Introduction

1.1 Airworthiness certification of composite aircraft structure

The design and airworthiness certification of composite aircraft structure is generally performed using the "building block" approach. This uses large numbers of simple tests and ever reducing numbers of increasingly complex tests. Design data is generated by testing thousands of simple coupon level specimens, hundreds of structural element and design detail level specimens, tens of more complex sub-component level specimens and a few large, component level specimens. Final designs are verified with one or two full-scale tests.

The building block approach requires a full test matrix (testing all specimen levels under all loading directions) despite adding years and millions of dollars to the cost of aircraft development, because the simple and intermediate level tests do not accurately represent the type of loading experienced by full-scale structures. It is currently not possible to predict accurately the mechanical response of, and thus design, complex built-up composite aircraft structures based on the results of coupon tests alone.

It is proposed that many existing intermediate level tests could be replaced by a suite of coupon tests that accurately represent the loading conditions within full-scale structures. Aircraft structures would be designed on the basis of these tests, rather than the current approach of (i) performing simple coupon tests, (ii) designing then testing the next level of specimen, (iii) adjusting the designs on the basis of these test results, (iv) repeating steps (ii) and (iii) until the full-scale structure is designed and tested. Such an approach has the potential to reduce substantially the cost of airworthiness certification.

The Defence Science and Technology Organisation (DSTO), in collaboration with the Co-operative Research Centre for Advanced Composite Structures (CRC-ACS), have completed a program evaluating one such representative test coupon, a laminate with an open hole subjected to combined axial (tension or compression) and bend loading.

This report describes the results of baseline testing for that program. It describes the effect of hole size on the room temperature dry (RTD) and elevated temperature wet (ETW) properties of a quasi-isotropic AS4/3501-6 laminate subjected to open-hole-tension (OHT), open-hole-compression (OHC) and open-hole-four-point-bend (OHB). OHB tests were also conducted on two additional lay-ups. Subsequent reports will describe the response of laminates tested in combined axial and bend loading.

1.2 Holes in composite laminates

Increasing use is being made of advanced composite laminates in aircraft structure. Holes are an essential feature of components such as skins, control surfaces, ribs, spars, stringers, doors and fairings. An important consideration for the designer is the effect of these holes on the strength of the laminate.

It is well known that the tension and compression strength of composite laminates falls disproportionately with hole diameter. As shown in Fig. 1, this fall is larger than that predicted by simple net section stress, but not as large as that predicted by the stress concentration factor (K_t) for brittle failure. For this reason OHT and OHB strengths are usually measured experimentally. These form part of the coupon level of testing in building-block test programs.

1.3 Length Scale Models

A variety of approaches have been developed to predict the effect of holes on strength in an effort to reduce reliance on experimental test data. One class of model incorporates a concept called the length scale. Failure is predicted to occur when the stress, or strain, at some characteristic distance, the so called length scale, ahead of the hole reaches a critical value. These models are used widely by the manufacturers of composite aircraft structure because they are capable of predicting failure in OHT and OHC with an accuracy that is sufficient for aircraft design.

However, such models suffer from two deficiencies. Firstly, some testing in addition to basic material properties such as the unnotched laminate strength is required to calibrate the models. This partially defeats the purpose of using a predictive model, which is to
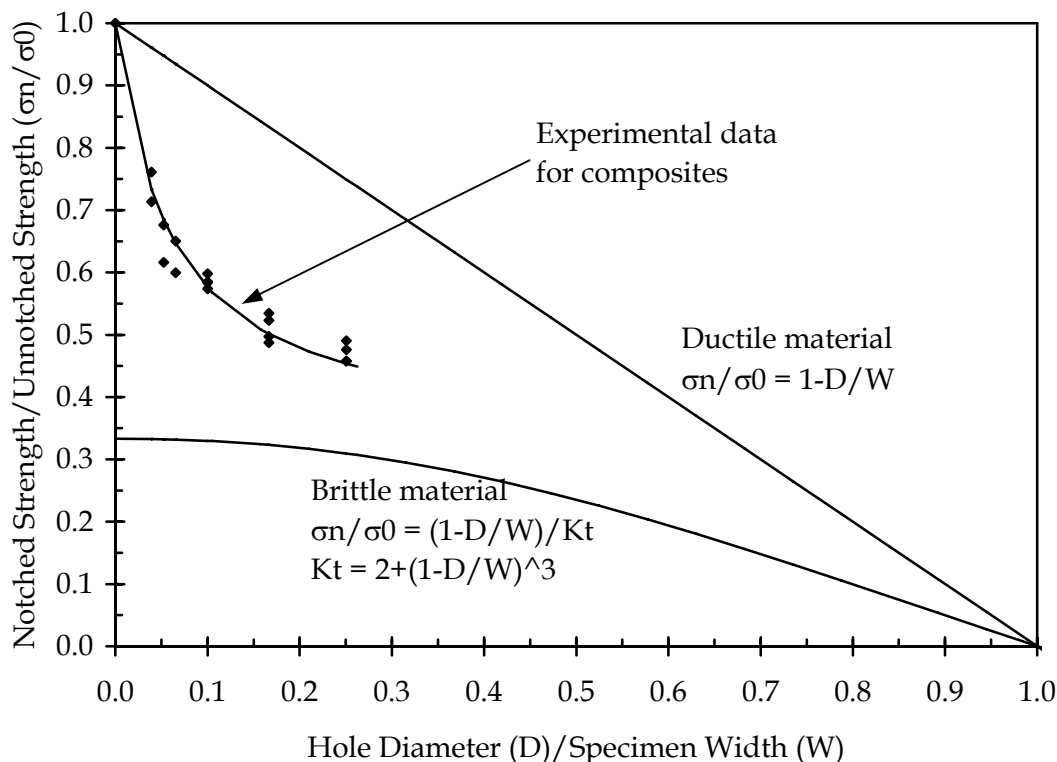

Figure 1: *Plot showing that the tensile strength of a notched composite is less than that predicted for a ductile material but greater than that predicted for a purely brittle material*

reduce the amount of testing. Secondly, these models appear not to be applicable once out-of-plane bending loads become significant.

While the dominant loading in well-designed composite aircraft structure is in-plane so that applied loads may be supported by the strong and stiff fibres, a significant number of laminates are subjected to significant proportions of out-of-plane loading. For example many stiffeners (ribs, hats, stringers, etc.) are flanged and the flange is fastened or bonded to a thin skin. Loads originating in the skin and flowing into the stiffener will create secondary bending in that stiffener because the fastener holes or bonding surface in the attachment flange are offset from the load-bearing body of the stiffener.

In these cases it is presumed that the in-plane length scale models are not sufficiently accurate because manufacturers usually perform additional testing to determine strength in the presence of significant out-of-plane bending, rather than using these models. One of the aims of this report is to quantify the extent of this difference by comparing the predictions from the three commonly used length scale criteria described in Section 2 with experimentally obtained OHT, OHC and OHB strengths.

2 Selected Length Scale Models

2.1 Average and point stress criteria

Whitney and Nuismer (W-N) [1] developed two criteria to account for the effect of holes on the tensile strength of composite laminates. They are commonly referred to as the Average Stress Criterion (ASC) and the Point Stress Criterion (PSC). Both were developed to model the situation shown in Fig. 1, where the loss in tensile strength of notched composites was greater than that due to the reduction in net section but less than that due to a stress concentration factor.

Both of the ASC and PSC require an expression for the stress distribution around the hole. For an infinite orthotropic plate containing a circular hole with a uniform remote stress, σ^{∞}, applied parallel to the y-axis then the normal stress, σ_y, along the x-axis in the remaining ligament can be approximated by Equation 1 [2].

$$\sigma_y(x,0) = \frac{\sigma^{\infty}}{2}\left\{2 + \left(\frac{r}{x}\right)^2 + 3\left(\frac{r}{x}\right)^4 - \left(K_T^{\infty} - 3\right)\left[5\left(\frac{r}{x}\right)^6 - 7\left(\frac{r}{x}\right)^8\right]\right\} \qquad (1)$$

Where:

      r   = radius of hole
      x   = distance from edge of hole
      K_T^{∞} = orthotropic stress concentration factor for a plate of infinite width

The orthotropic stress concentration factor may be expressed as Equation 2 [3] or, in terms of laminate properties, as Equation 3 [4].

$$K_T^\infty = 1 + \sqrt{\frac{2}{A_{11}}\left(\sqrt{A_{11}A_{22}} - A_{12} + \frac{A_{11}A_{22} - A_{12}^2}{2A_{66}}\right)} \qquad (2)$$

$$K_T^\infty = 1 + \sqrt{\left(2\sqrt{\frac{E_2}{E_1}} - \nu_{21}\right) + \frac{E_2}{G_{12}}} \qquad (3)$$

Where:

A_{ij}	=	the ij'th element of the stiffness matrix
E_2	=	transverse elastic modulus
E_1	=	longitudinal elastic modulus
ν_{21}	=	in-plane Poisson ratio
G_{12}	=	in-plane shear modulus

It is noted that the polynomial expression given in Equation 1 is only an approximation to the exact solution for an infinite orthotropic plate containing a circular hole subject to remote uniaxial tension. The exact solution of the in-plane stress distribution has been solved however it is very complicated because it uses a complex variable mapping approach [3]. It was demonstrated [2] that Equation 1 provides a very good approximation to the exact solution for [0], [± 45] and a series of [0/± 45]$_s$ T300/5208 graphite/epoxy laminates. In isotropic plates or laminates with a quasi-isotropic lay-up, $K_T^\infty = 3.00$. In such cases the sixth and eighth order terms may be eliminated, simplifying the relation even further.

2.1.1 Average Stress Criterion (ASC)

The ASC hypothesises that failure in a notched laminate occurs when the average normal stress, at a characteristic distance ahead of the hole, reaches the unnotched strength of the laminate. This criterion can be expressed diagrammatically as in Fig. 2 (a) or mathematically by Equation 4.

$$\sigma_0 = \frac{1}{a_0}\int_{x=r}^{x=r+a_0} \sigma_y(x,0)dx \qquad (4)$$

Where:

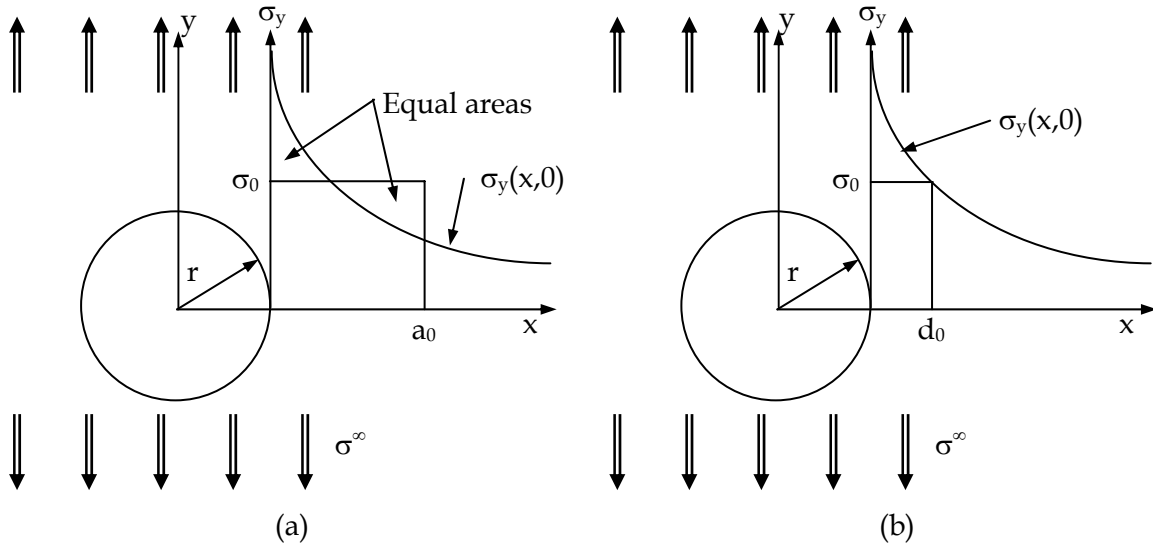|		
a_0	=	ASC characteristic distance
σ_0	=	unnotched strength
$\sigma_y(x,0)$	=	the normal stress along the line through the centre of the hole and perpendicular to the loading direction (x axis as shown in Fig. 2)

Figure 2: *(a) Average and (b) point stress failure criteria for a circular though thickness hole in an infinite plate [1]*

Two material parameters, σ_o and a_o, are required to predict notched strength using this model. The unnotched strength is typically determined from tensile tests on the subject laminate, although it may be determined through laminate plate theory and the application of unidirectional material allowables. The characteristic distance is determined by curve fitting with strength data from tests at two or more hole sizes.

The ratio of notched strength to unnotched strength is a convenient method of representing the effect of hole size on strength. An explicit expression for the notched strength is obtained by substituting Equation 1 into Equation 4 and conducting the integration. The final relation is shown as Equation 5. This equation, solved for a range of r and a_0, is shown in Fig. 3.

$$\frac{\sigma_N}{\sigma_0} = \frac{2(1-\xi_1)}{2-\xi_1{}^2-\xi_1{}^4+(K_T^\infty-3)(\xi_1{}^6-\xi_1{}^8)} \tag{5}$$

Where:

$$\xi_1 = \frac{r}{r+a_0}$$

2.1.2 Point Stress Criterion (PSC)

As implied in Fig. 2 (b), the PSC assumes that failure occurs when the stress at some characteristic distance (d_0) ahead of the hole is equal to the strength of the unnotched material (σ_0). The failure criterion, expressed as the ratio of notched to unnotched strength for an isotropic lay-up, is shown in Equation 6. This relation, solved for a range of r and d_0, is shown in Fig. 4.

Figure 3: *Effect of characteristic dimension a_0 on notched strength of an infinite plate as predicted by the ASC for laminates where $K_T^\infty = 3.00$*

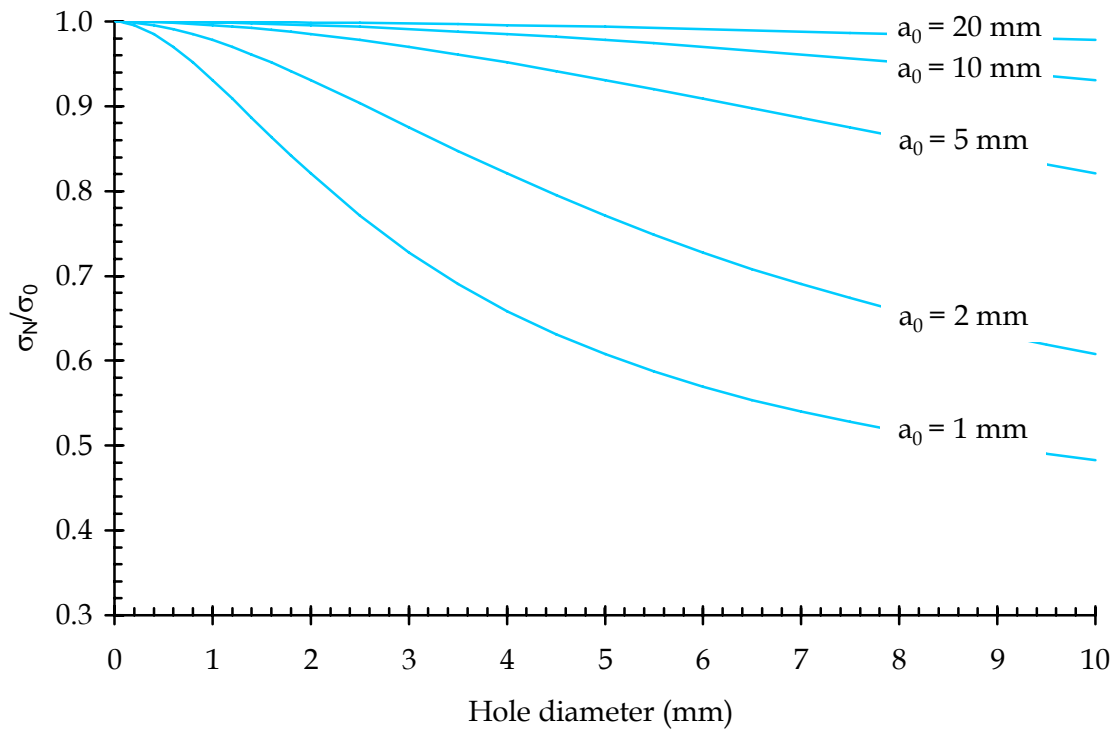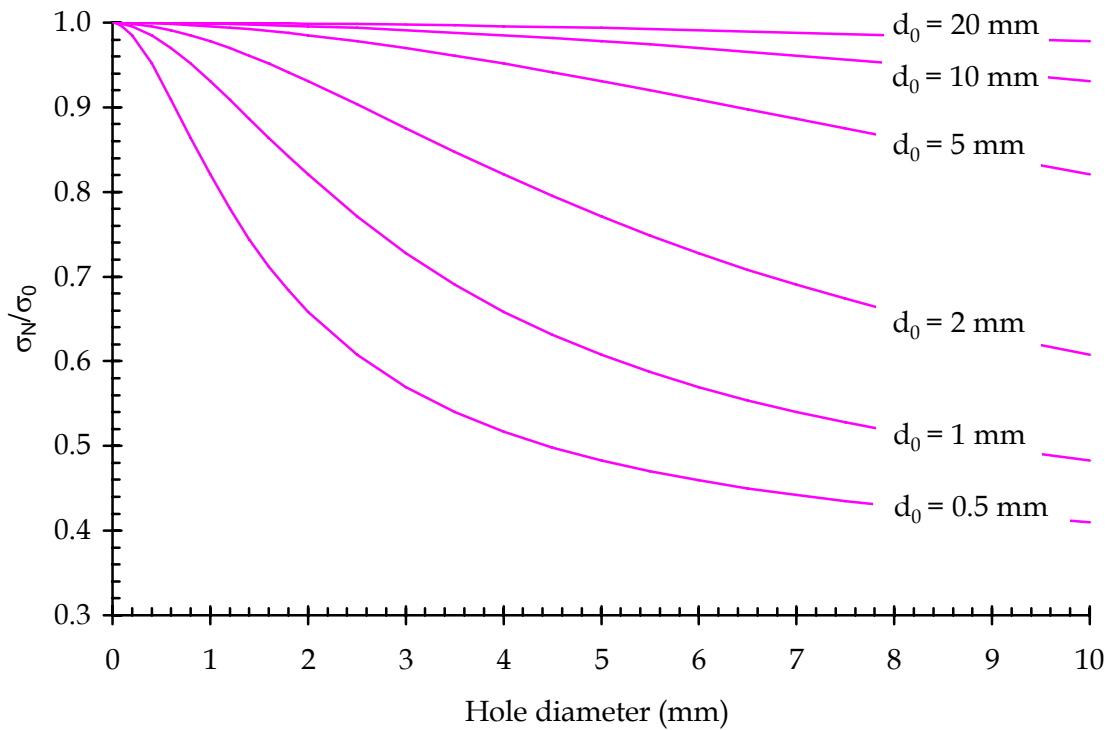*Figure 4:* *Effect of characteristic dimension d_0 on notched strength of an infinite plate as predicted by the PSC for laminates where $K_T^\infty = 3.00$*

$$\frac{\sigma_N}{\sigma_0} = \frac{2}{2 + \xi_2{}^2 + 3\xi_2{}^4}$$ (6)

Where:

$$\xi_2 = \frac{r}{r + d_0}$$

Both Equation 5 and Equation 6 reduce to the stress concentration factor criterion, $\sigma_N/\sigma_0 = 1/3$, for large values of r and to $\sigma_N/\sigma_0 = 1$ for small values of r.

2.2 Cohesive Zone Model (CZM)

The Cohesive Zone Model (CZM) applies to only those specimens loaded in compression. It assumes that compression loads are supported exclusively by the 0° plies (those fibres parallel to the loading axis) and that failure in these plies occurs by microbuckling. The microbuckle initiates at the edge of the hole and, initially, propagates stably. Upon reaching a critical length the microbuckle propagates unstably, thereby producing catastrophic failure of the ply and immediate specimen failure. Experimental evidence supports this model of compression failure in the presence of holes [5].

The following explanation of the model is taken from ref. [5]. Microbuckle initiation is assumed to occur when the stress at the edge of the hole reaches the unnotched strength of the laminate. The damage process zone, including the microbuckle, delamination, matrix cracking, plastic deformation and damage in off-axis plies, is represented by an equivalent line crack. Given that the microbuckle constitutes the majority of the damage then the length of this equivalent crack can be thought of as largely representing the length of the microbuckle. This equivalent crack is loaded on its faces by a normal bridging traction that decreases linearly with the closing displacement of the crack. When the load on the specimen is increased the equivalent crack grows in length, representing microbuckle growth. The length of this equivalent crack is predicted by requiring that the total stress intensity factor, the sum of stress intensity factor due to the remote stress and stress intensity factor due to local bridging traction, equal zero. The equivalent crack length is solved as a function of the remote stress by matching the crack opening profiles from the bridging law with that deduced from the elastic solution for a cracked body. The crack length is plotted as a function of applied stress. There is a maximum that corresponds to the compression strength. The crack length at this stress is the critical length of equivalent crack, l_{cr}. This may be visualised as the length of microbuckle required to initiate catastrophic failure of the laminate.

This model requires two parameters, the unnotched compression strength and the fracture toughness expressed as the critical stress intensity factor (K_c), of the laminate. This fracture toughness is that of the laminate loaded in-plane, with a through-thickness crack propagating perpendicular to the loading direction. It is measured using centre notch coupons loaded in compression. Values of 35-50 MPa $\sqrt{m}$ were measured for a range of T800/924C laminates [5] although these workers have stated that typical values for carbon fibre composites are 40-50 MPa $\sqrt{m}$. The family of curves representing the prediction of the cohesive zone model, for a range of r and K_c, are shown in Fig. 5.
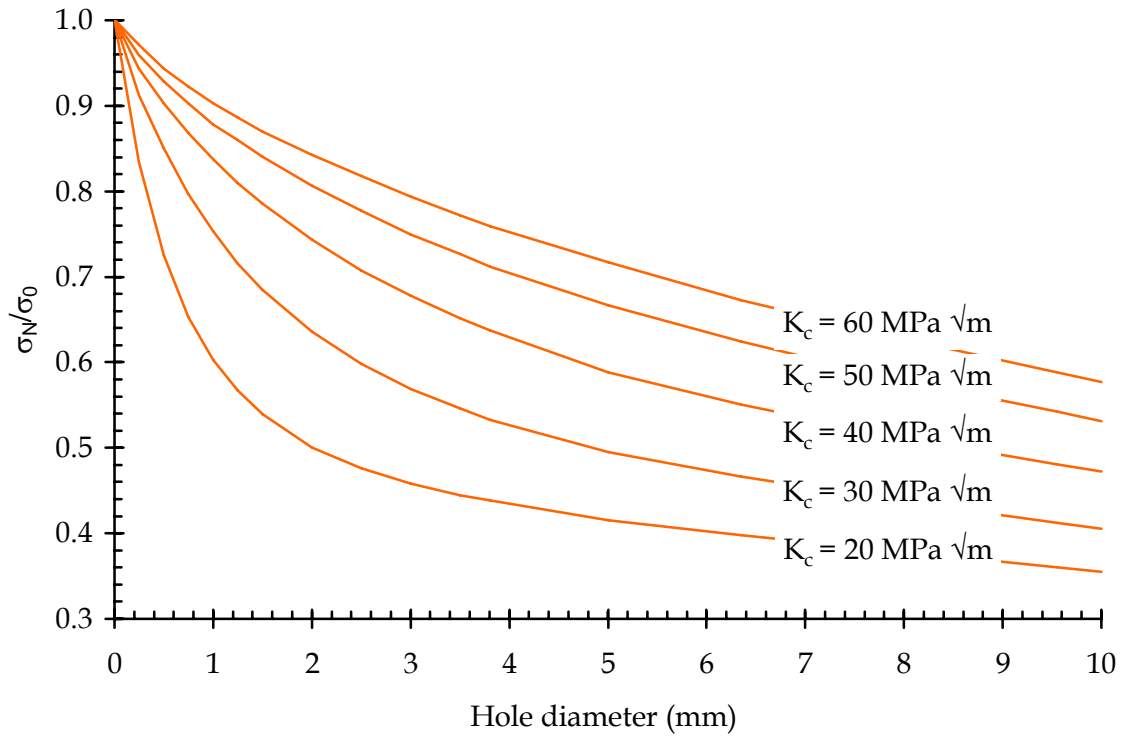
Figure 5:   Effect of composite K_c on notched strength as predicted by the Cohesive Zone Model for OHC

2.3 Finite Width Correction Factor (FWCF)

The models described in Sections 2.1 and 2.2 were formulated on the basis of plates of infinite width. Coupon specimens, such as those tested in this work, are of finite width. For the large holes, the specimen width was only 4 times larger than hole diameter. A Finite Width Correction Factor (FWCF) was therefore used to convert the strengths measured on coupon specimens to strengths that can be used in the models. The FWCF is the ratio of the stress concentration factor at the root of the discontinuity in the finite width specimen compared to the same discontinuity in an infinite plate.

The stress at failure of the notched coupons, σ_N, was calculated by dividing the failure load by the average gross cross-sectional area of the specimen. The hole diameter was not subtracted from the width because the stresses in Equation 5 and Equation 6 are based on the full plate cross-sectional area (far field stress).

A variety of FWCF's are available. Tan [6] presented two derivations, one based on the exact two-dimensional anisotropic normal stress distribution and another by considering an approximate orthotropic stress distribution for an infinite plate. The isotropic finite width correction factor [7] shown in Equation 7 was used in this work. The experimentally determined strengths were multiplied by these factors to produce corresponding σ_N^∞

strength. The values of σ_N, FWCF and σ_N^∞ for each of the test specimens are shown in the tables of results in Sections 4, 5 and 6 of this report.

$$\frac{\sigma_N^\infty}{\sigma_N} = \frac{K_T}{K_T^\infty} = \frac{2 + \left(1 - 2\frac{r}{w}\right)^3}{3\left(1 - 2\frac{r}{w}\right)} \tag{7}$$

Where:

w = specimen width

An alternative FWCF applies when using the net cross-section rather than the gross cross-section. This stress concentration, K_{Tn}, is related to K_T by Equation 8. Obviously, if using this factor, the FWCF must be applied to the net section stress.

$$K_{Tn} = K_T\left(1 - 2\frac{r}{w}\right) \tag{8}$$

3 Experimental Procedure

3.1 Test matrix

OHT, OHC and OHB tests were performed in the RTD and 77°C/85% relative humidity (RH) ETW conditions. The numbers of unnotched (hole size = 0.00 mm) and notched specimens are shown in Table 1.

3.2 Test specimens

All tests were manufactured from AS4/3501-6 prepreg tape, a common first generation aerospace grade composite material and that used on the Royal Australian Air Force (RAAF) F/A-18 aircraft. 320 mm x 800 mm panels of 16 ply, quasi- isotropic [45/0/-45/90]$_{2s}$, lay-up, were prepared. A small number of RTD OHB specimens were prepared with [45/0/0/-45/90/90/0/90/90]$_s$ (High 0°) and [45/-45/0/45/-45/90/45/-45]$_s$ (High 45°) stacking sequence. Curing was performed in accordance with the manufacturer specifications and no manufacturing defects were detected by post-cure ultrasonic C-Scan inspection. A diamond saw with water cooling/lubricant was used to cut 38.1 mm wide straight sided specimen blanks from the panels. The 0° fibre direction was parallel to the long axis of the specimens. OHT and OHC specimens were 305 mm long while the OHB specimens were 102 mm long.

Holes were drilled in the centre of the specimen blanks using "one-shot" drills of the same

Table 1:   Test matrix for OHT, OHC and OHB coupons

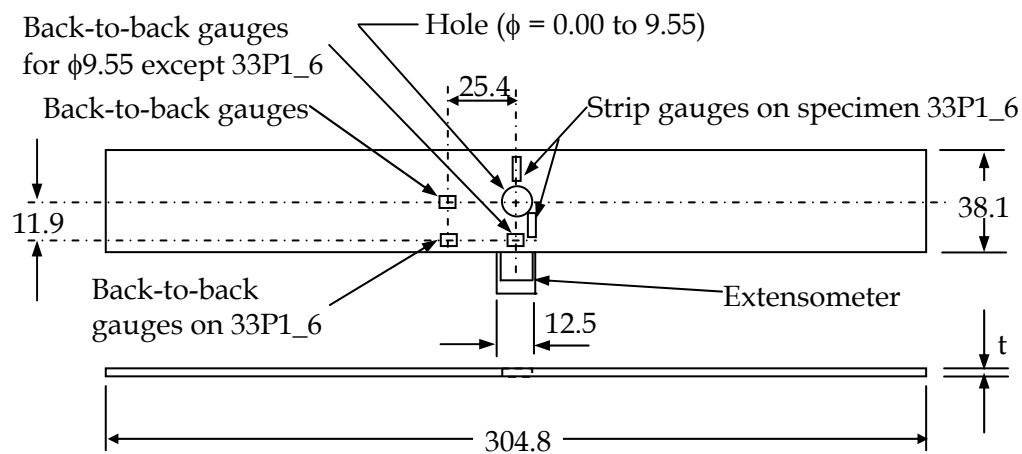| Hole diameter (mm)	Number of tests					
	OHT		OHC		OHB	
	RTD	ETW	RTD	ETW	RTD	ETW
0.00	5	8	4	8	21	2
1.50	2	2	2	2	0	2
2.00	2	2	2	2	0	2
2.50	2	2	2	2	0	2
3.81	7	2	4	2	5	3
6.35	7	2	4	2	14	3
9.55	7	2	4	2	5	3

diameter as the hole diameter indicated in Table 1. It was found that the quality of the hole, in terms of the presence of frayed fibre ends and delamination as observed under a binocular microscope at 20X, varied markedly with drilling technique. The drilling procedure described below was found to minimise the damage and this procedure was followed for all holes. All holes were inspected and only those specimens where no defects were detected visually at 20 X magnification were tested.
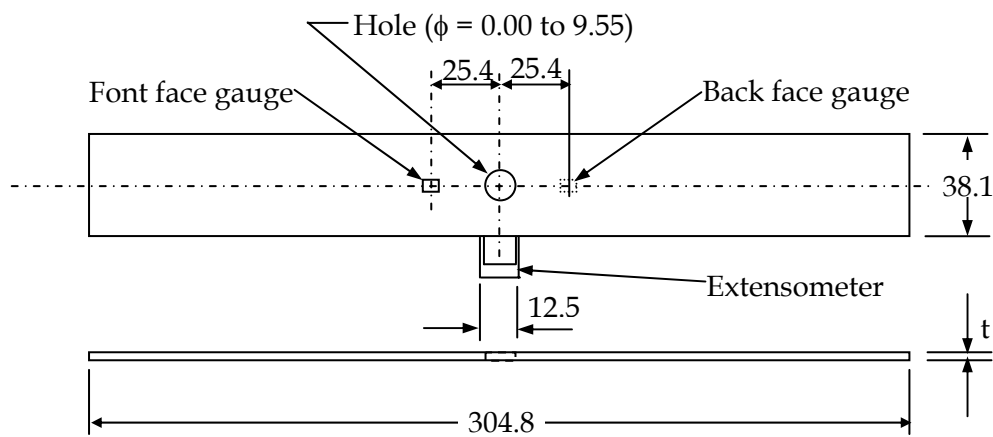
The drilling procedure was to:

(1) sandwich specimen blanks between scrap composite laminates,
(2) firmly clamp the sandwich to the bed of a milling machine,
(3) ensure the drill was sharp. Each drill was discarded after drilling 40 holes,
(4) drill at 1050 rpm (this was the maximum drilling speed permitted by the milling machine on which drilling was conducted. The recommended speeds for the one-shot drills used in this work were 3000 to 5000 rpm) while completely immersing the drilling head and holes with water lubricant, and
(5) stop the drill rotating after the drill had fully penetrated the sandwich but before the drill was withdrawn.

Strain was measured using strain gauges, an extensometer and actuator displacement. Micro-Measurements CEA-06-125UW-120 strain gauges were bonded onto approximately half of the OHT, all of the OHC and almost all of the OHB specimens. The geometry of the specimens and nominal strain gauge locations are depicted in Fig. 6. Typically, strain gauges were mounted on the front and back face of specimens, along the centreline of the specimen at 25.4 mm from the hole. On OHT and OHB specimens, the gauges were located in a true back-to-back arrangement, while on OHC specimens the back face gauge was mounted at the opposite end of the specimen to that of the front face gauge. This was required for the gauges to locate in recesses in the SACMA SRM-3 anti-buckling guides. For the OHT specimens with 9.55 mm holes, the back-to-back gauges were located midway between the centre line and the edge of the specimen.

The RTD specimens were stored in ambient laboratory air of approximately 20°C/50% RH prior to testing. The ETW specimens were conditioned in a Heraeus Vötsch HC 4055

Back-to-back gauges
for φ9.55 except 33P1_6

Hole (φ = 0.00 to 9.55)

Back-to-back gauges

25.4

Strip gauges on specimen 33P1_6

11.9

38.1

Back-to-back
gauges on 33P1_6

Extensometer

12.5

t

304.8

(a)

Hole (φ = 0.00 to 9.55)

Font face gauge

25.4 25.4

Back face gauge

38.1

Extensometer

12.5

t

304.8

(b)

Hole (φ = 0.00 to 9.55)

Strip gauges on convex (tension)
face of specimens XB1, XB3,
TC5, TC6, VC5 and VC6

Back-to-back gauges

38.1

4

t

102

(c)

*Figure 6:   Diagrams of (a) OHT, (b) OHC and (c) OHB specimen showing dimensions in mm,
strain gauge locations and extensometer locations*

11

environmental chamber at 70°C/85% RH. The moisture content of the specimens was monitored by measuring weight gain. Conditioning was considered complete when the weight gain in specimens was less that 0.05% for consecutive readings taken 7 days apart.

Strip gauges were bonded to one of the OHT and six of the OHB specimens in the locations shown in Fig. 6. The strip gauges consisted of five individual gauges, each with a gauge length of 1.5 mm and a pitch (centre-to-centre separation) of 2.0 mm. These were used to measure the strain distribution along the ligament between the edge of the hole and the specimen edge.

A MTS 632 series extensometer with a 12.5 mm gauge length was attached to one RTD OHT and OHC specimen of each hole size at the location shown in Fig. 6.

No end tabs were used on any of the specimens. Prior to testing, the thickness and width of the test section was measured in three locations.

3.3 Test procedure

Except for the variations in hole size and the addition of strain measuring transducers, testing was conducted in accordance with the following standards:

OHT Suppliers of Advanced Composite Materials Association (SACMA) Recommend Test Methods (SRM) SRM 5R-94 [8],

OHC SACMA SRM 3R-94 [9],

OHB American Society for the Testing of Materials (ASTM) D790 [10]. Four-point bend method with 12.7 mm diameter load and support rollers.

RTD tests were conducted in ambient laboratory air. ETW tests were set-up by enclosing the test fixture in an insulated test box. The test box was connected to a Tabai CR-10HL environmental generator via insulated ducts. The box was pre-heated to 77°C with dry air then, immediately prior to testing, the:

(i)   77°C dry air was turned off,
(ii)   door to the test box opened,
(iii)   specimen installed in the grips,
(iv)   door to the test box closed, and
(v)   air from the environmental generator turned on and set to 77°C/85% RH. Testing was commenced between 10 and 20 minutes after the conditions in the test box had equilibrated at 77°C/85% RH.

OHT and OHC tests were conducted at a loading rate of 0.5 mm min^{-1} while the OHB tests were conducted at 5.0 mm min^{-1}. Loading was continued until specimens failed or a major load drop was observed. Selected OHB specimens were photographed as loading proceeded to provide a record of the deformed coupon profile.

The majority of OHT and OHC tests were conducted in a 250 kN Instron Model 1343 servo hydraulic test machine, some in a 100 kN MTS Model 810 test machine and the ETW OHC tests in a 100 kN screw driven 1185 Instron test machine. The OHB tests were conducted in

the 1185 Instron. The MTS machines were fitted with hydraulic grips while the Instron was fitted with flat compression platens for OHC tests and a four point bend fixture for the OHB testing. It was assumed that the change in test machine had no effect on the test results.

Personal computer based data acquisition systems were used. For each test the machine load, actuator displacement and strains from the strain gauges and extensometer were recorded.

4 Results and Discussion - Tension

4.1 Stress-strain behaviour

4.1.1   Strain gauge

The stress-strain response of RTD and ETW specimens was expected, and observed, to be linear to failure. All transducers for the RTD, and the extensometer and actuator displacement for the ETW, specimens were linear as shown in Fig. 7.

The strain gauge response for 12 of the 20 ETW specimens was unexpectedly non-linear, with some apparent stiffening. A typical example is shown in Fig. 7. The likely explanation for this apparent strain stiffening was reorientation of fibres in the surface plies toward the direction of the loading axis. It is hypothesised that the fibres in the outer 45° ply, to which the strain gauges were bonded, rotated sufficiently during testing to cause the apparent stiffening. Supporting this claim are the observations that the plies (i) were only supported on their back face thus less restrained from rotating as the test progressed, (ii) experienced a significant component of load in the direction of the loading axis, and (iii) were supported by a relatively soft matrix in the ETW condition. A similar phenomenon, where the tows in woven composites straightened at high load (termed plastic tow straightening) has been reported elsewhere [11].

Two observations that further support the hypothesis of fibre rotation in the outer ply are that, firstly, the strain gauge measurements initially matched those of the extensometer and only began deviating from linearity after the load had exceeded the yield strength of the matrix (yield strength ≈ 70 MPa, deviation commenced ≈ 120 MPa). Secondly, a very fine feathering was observed on the edges of some of the ETW specimens after testing. This feathering was of the same type as that found on the edges of failed ±45° tension specimens, where plies are known to disbond and move in a "scissor" action during testing. This contrasted with failed RTD specimens where the edges were almost as smooth as prior to the testing.
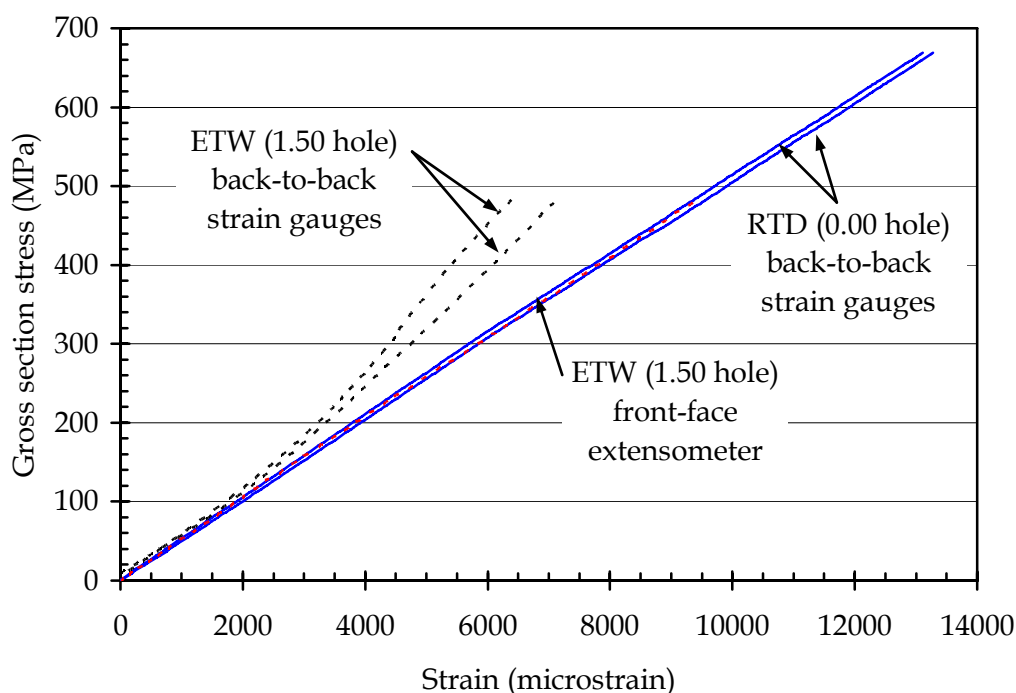
Figure 7: *Typical stress-strain response from a RTD (0.00 mm hole, specimen 33p2_13) and ETW (1.50 mm hole, specimen JC3) specimen. Both the strain gauge and extensometer data are shown for the ETW specimen*

The strain measured by the extensometer, even on the ETW specimens, was not expected to exhibit this apparent stiffening because the extensometer was located on the edge of the specimen and so measured the averaged strain through-the-thickness of the specimen. This averaged strain was dominated by the behaviour of the 0° plies, where any fibre rotation would be very small.

The response of the back-to-back gauges in both the RTD and ETW specimens diverged, indicating bending in these specimens. There was no bending limit prescribed in ASTM D 3039, however it recommended that to be consistent with good testing practice the bending should be limited to 3-5%. The average bending, calculated at the maximum load that the back-to-back gauges functioned reliably, was 1.3% for RTD and 5.0% for ETW, indicating an acceptable level of bending.

4.1.2 Extensometer

An extensometer was used to measure the displacement across the hole on some RTD specimens and on all of the ETW specimens. The results were very similar to those shown in Fig. 7. There was very little difference in the strains measured by the strain gauge and extensometer on RTD specimens. The strains measured by the extensometer were therefore used for further analysis. In contrast, the ETW extensometer response was linear to failure whereas the strain gauges exhibited the apparent stiffening. As indicated in Section 4.1.1, the non-linear response of the strain gauges was judged to not be a true

reflection of material behaviour. Therefore the extensometer data was used for analyses of ETW OHT behaviour.

4.1.3 Actuator

A technique was developed to calibrate the strains calculated from displacement of the test machine actuator with those from the strain gauge. This allowed strains to be estimated in those specimens where no strain gauges were installed or where there were obvious errors in the strain gauge data. The calibration process is described in detail in Appendix A. In summary, the approach was to; calculate a nominal strain from the actuator displacement, factor this strain so that it matched the strain measured by strain gauges, account for the offset at zero load then correct for deformation of the load-train.

The correlations obtained using this approach appeared to be very good. For 22 RTD OHT specimens where reliable data from both strain gauges and the actuator were available, the average difference in failure strain as determined by the strain gauge and corrected actuator displacement was 260 µε. This value was skewed by large errors in two specimens. Ignoring these outliers reduced the typical difference to 170 µε, which was equivalent to less than 2% of the failure strain, well within the experimental scatter of results. Similarly, for the 9 ETW OHT specimens where reliable extensometer and corrected actuator displacement data was available, the average difference in failure strains was 75 µε or less than 1 % of the failure strain. Again, this was an excellent match.

4.1.4 Stress-strain behaviour

In a few cases the response from strain gauge, extensometer and actuator displacements matched. For most specimens there was a gradual deviation of one of the transducers, a typical result being shown in Fig. 8. The hierarchy shown in Table 2 was therefore developed to select which strain transducer would be used for further analysis. Unless stated otherwise the OHT strain data was obtained from the most preferred transducer indicated in Table 2.

Typical stress-strain behaviour for each of the hole sizes are shown in Figs 9 and 10. The elastic modulus from 1000 to 3000 µε, failure strength and strain were determined using the most preferred data source available and the approaches described in Sections 4.3 to 4.5. These data are shown in Tables 3 and 4.

4.2 Strain distribution

A strain survey was conducted on a RTD specimen with a 9.55 mm hole (33P1_6) to

Table 2:   Hierarchy of strain transducers for OHT tests

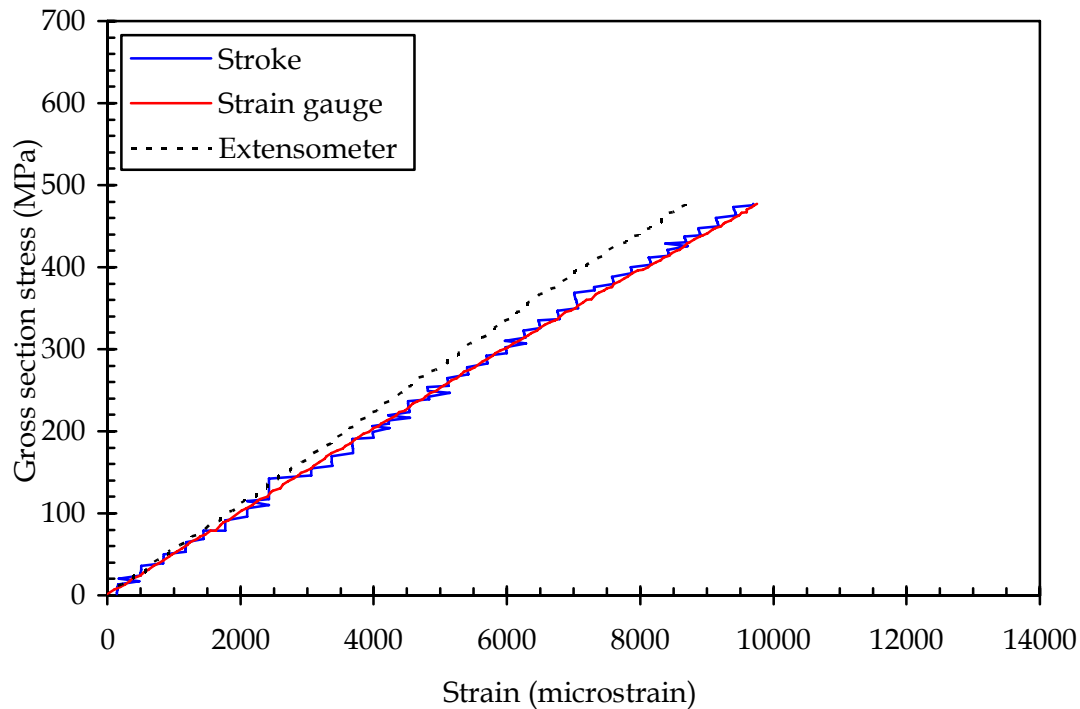| Priority	RTD	ETW
Most preferred	average back-to-back strain gauge	extensometer
Second preferred	extensometer	actuator displacement
Least preferred	actuator displacement	average back-to-back strain gauge

Figure 8:   Typical OHT stress-strain response as determined by strain gauges, extensometer and calibrated actuator displacement (2.50 mm hole, RTD, specimen LA4)

measure the strain distribution near the hole. This specimen was instrumented with two strip gauges as described in Section 3.2. A photograph of the specimen is shown in Fig. 11. The first strip gauge (Gauges 1-5) was located centrally in the ligament between the hole and specimen edges, while the second (Gauges 6-10) was offset from the minimum length ligament by 5.1 mm in the left-right direction and 0.9 mm in the up-down direction. The aim of this overlap was to produce a single strip of strain measurements with an effective spacing equal to half the pitch of the individual strip gauges. The same coupon also contained two far field back-to-back gauges. The gauge locations were imported from the image in Fig. 11 into AutoCAD and scaled in order to determine the precise gauge locations. These are shown in Figure 12. The loading direction was the "y" axis as shown in Fig. 12.

Static strain surveys were conducted at 2.1 and 4.0 kN. For each of the 12 strain gauges shown in Fig. 12 the strains at zero load were subtracted from the strains recorded whilst load was held constant at the strain survey level for 30 seconds. The resultant strains were averaged and are depicted in Fig. 13.

The strain recorded by Gauges 1, 2, 9, 3, 10, 4 and 5 appeared to follow the classical stress concentration profile for a plate with an open hole subject to uniaxial tension. Specifically, the strain was relatively uniform remote from the hole (Gauges 10, 4 and 5) and rose monotonically to reach a peak at the root of the hole (Gauges 1, 2, 9 and 3).
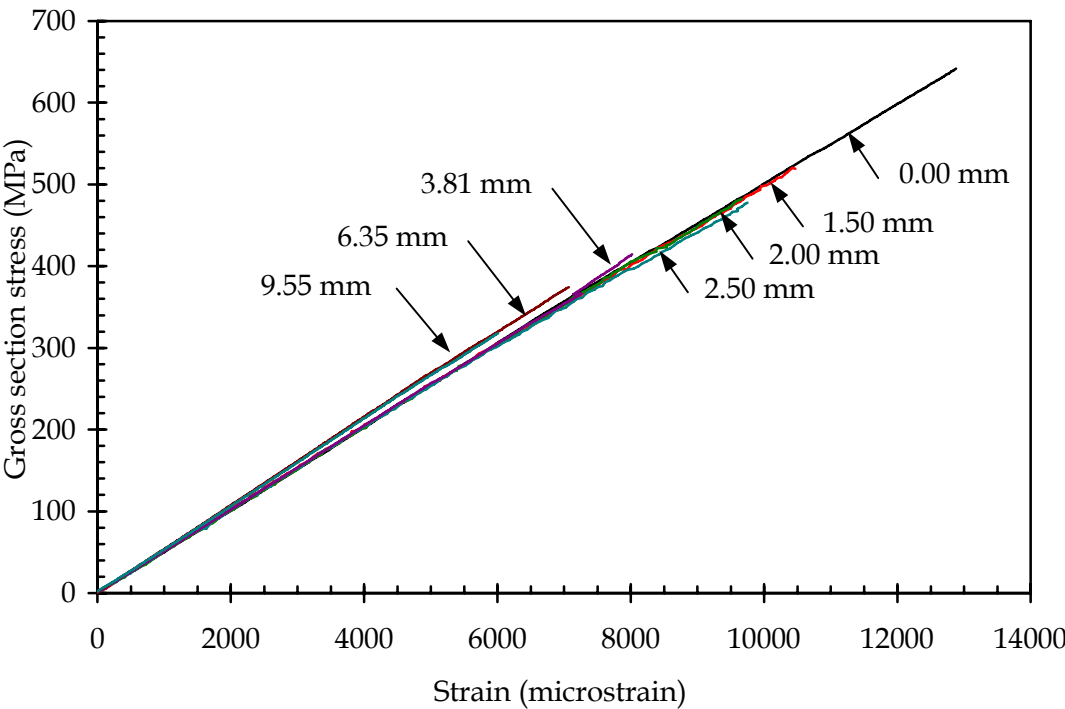
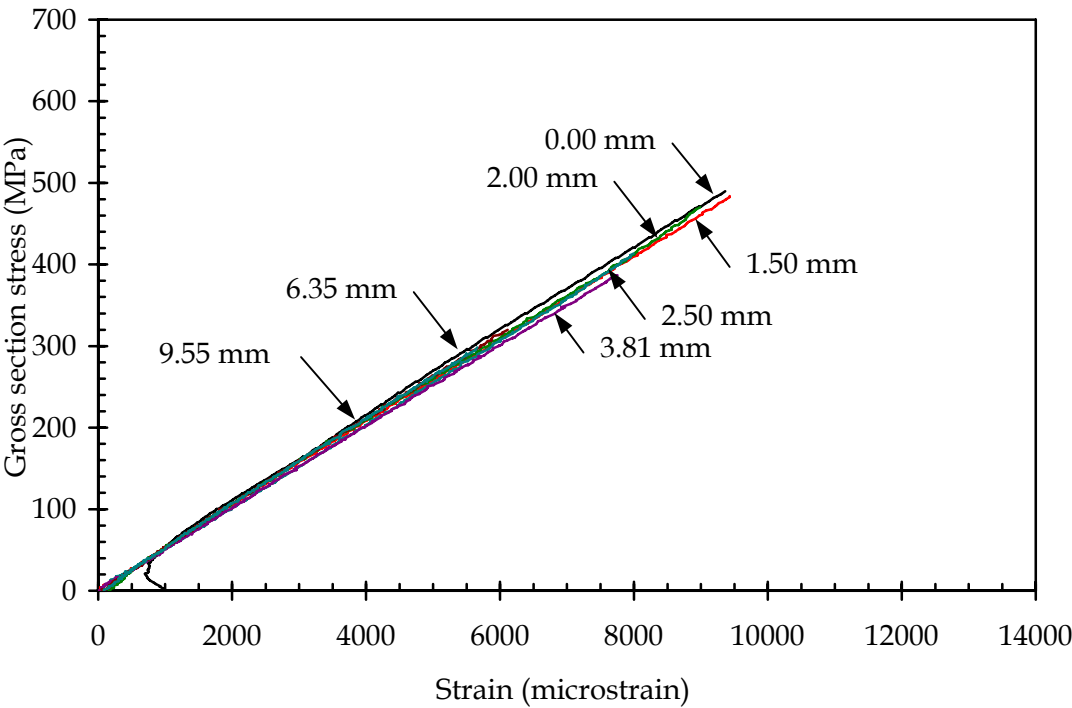*Figure 9:   Typical stress-strain behaviour of RTD OHT specimens at the indicated hole diameter*

Figure 10:   Typical stress-strain behaviour of ETW OHT specimens at the indicated hole diameter

Table 3: RTD OHT results and derived mechanical data

Hole φ (mm)	Specimen number	Thick. (mm)	Width (mm)	P_{max} (kN)	E_1^t (GPa)[1]	ε_1^{tu} (με)[1]	F_1^{tu} (MPa)	FWCF	σ_N^∞ (MPa)
0.00	33P2_13	2.26	38.09	57.7	51.7	13,191	669	1.0000	669
	33P2_14	2.24	38.13	54.7	50.6	12,882	641		641
	33P2_15	2.24	38.21	57.4	51.5	13,220	670		670
	33P2_16	2.28	38.25	53.9	[2]	[2]	[2]		[2]
	33P2_17	2.26	38.02	54.9	49.4	12,836	638		638
	33P2_18	2.28	38.02	55.5	47.1	13,070	640		640
1.50	B4	2.29	38.11	46.3	55.9	8,336	530	1.0016	531
	LA1	2.26	37.98	44.7	51.2	10,468	520	1.0016	521
2.00	LA2	2.29	38.02	42.0	50.4	9,665	482	1.0029	483
	LA3	2.25	38.00	41.5	53.9	9,382	485	1.0029	486
2.50	LA4	2.24	38.00	40.7	51.0	9,753	478	1.0045	480
	LA5	2.26	38.09	40.3	54.9	8,910	468	1.0045	470
3.81	33P1_1	2.29	38.22	35.2	50.4	8,110	402	1.0107	406
	33P1_2	2.29	38.22	36.2	51.1	8,021	415	1.0107	419
	33P1_3	2.26	38.22	33.8	51.5	7,690	391	1.0107	395
	33P2_4	2.29	38.13	33.6	48.6	7,978	385	1.0107	389
	33P2_5	2.26	38.13	35.3	50.9	7,639	410	1.0107	414
	33P2_6	2.26	38.21	35.2	52.5	7,874	407	1.0107	411
	LB1	2.34	38.07	37.5	50.3	8,442	421	1.0108	426
6.35	33P1_7	2.26	38.04	32.2	53.8	7,073	374	1.0316	386
	33P1_8	2.26	38.06	31.2	52.9	6,915	363	1.0316	374
	33P1_9	2.25	38.18	32.0	52.5	7,202	372	1.0313	384
	33P2_7	2.26	38.04	30.5	50.3	7,034	355	1.0316	366
	33P2_8	2.25	38.06	31.6	50.7	7,070	369	1.0316	381
	33P2_9	2.26	38.25	29.9	52.1	6,824	346	1.0312	357
	LA6	2.27	38.08	30.7	52.5	6,885	355	1.0315	366
9.55	33P1_13	2.27	38.10	27.4	53.2	6,010	318	1.0768	342
	33P1_14	2.24	38.14	26.5	53.0	5,890	311	1.0767	335
	33P1_15	2.22	38.17	25.6	53.2	5,706	301	1.0765	324
	33P2_1	2.29	38.24	26.4	50.3	5,864	302	1.0762	325
	33P2_2	2.29	38.15	25.9	48.2	5,809	296	1.0766	319
	33P2_3	2.26	38.09	27.3	51.7	6,042	317	1.0769	342
	LB2	2.28	38.08	26.8	53.7	5,754	308	1.0769	332

[1]   The strain data source for modulus and failure strain is indicated by the colour of the cell, being strain gauge or actuator displacement.

[2]   Maximum load only was recorded. Data not used for further analysis because stress and strain could not be determined.

The stress distribution around the hole on this specimen was calculated using Equation 1 and the strain survey loads. These were converted to strain distributions by assuming linear elastic behaviour and a modulus of 50.0 GPa. These calculated strains are plotted in Fig. 13. The predicted edge and far field strains were 1664 με and 555με at 2.1 kN and

Table 4:   ETW OHT results and derived mechanical data

Hole φ (mm)	Specn no.	Thick. (mm)	Width (mm)	Moisture (%)	P_{max} (kN)	E_1^t (GPa) [1]	ε_1^{tu} (µε) [1]	F_1^{tu} (MPa)	FWCF	σ_N^∞ (MPa)
0.00	JA1	2.56	38.08	1.42	44.09[2]	53.0	10,093[2]	453[2]	1.0000	453[2]
	JA2	2.35	38.16	1.58	43.90[2]	54.9	9,363[2]	490[2]		490[2]
	NB1	2.30	37.96	1.08	55.04	51.0	13,083	631		631
	NB2	2.30	37.99	1.07	53.17	53.8	13,891	610		610
	NB3	2.31	38.02	1.02	46.65[2]	50.7	10,776[2]	531[2]		531[2]
	NB4	2.29	38.05	1.04	56.68	53.3	12,120	649		649
	NB5	2.33	38.01	1.05	55.96	52.2	11,636	632		632
	NB6	2.31	37.98	1.05	55.85	50.6	13,330	636		636
1.50	JC3	2.43	38.21	1.29	44.88	52.7	9,433	484	1.0016	485
	JC4	2.39	38.22	1.33	44.56	54.1	9,332	487	1.0016	488
2.00	JC4C	2.40	38.28	1.35	43.24	53.1	8,989	470	1.0028	471
	JP6	2.44	38.17	1.36	39.36	51.0	8,421	423	1.0028	424
2.50	GC3	2.40	38.19	1.40	39.90	50.9	8,468	435	1.0045	435
	JB4	2.41	38.29	1.36	38.11	50.7	7,997	413	1.0045	415
3.81	GB6	2.44	38.01	1.39	35.38	50.5	7,715	425	1.0108	430
	JB2	2.43	38.19	1.31	35.94	50.8	7,755	387	1.0107	391
6.35	GB5	2.44	38.03	1.39	29.67	53.2	6,116	320	1.0316	330
	JA6	2.39	38.24	1.33	31.28	53.0	6,647	343	1.0312	354
9.55	GA6	2.41	38.03	1.35	27.40	63.9	4,612	299	1.0772	322
	GB3	2.42	38.03	1.34	27.49	53.1	5,659	298	1.0772	321

[1]   The strain data source for modulus and failure strain is indicated by the colour of the cell, being strain gauge, actuator displacement or extensometer.
[2]   Premature specimen failure. This data not used.

3170 µε and 1057 µε at 4.0 kN respectively. The experimental data conformed very closely with the predictions of Equation 1, as indicated by a coefficient of determination $(R^2) = 0.97$. R^2 was calculated using the method shown in Appendix B.

It was noted that the strains from Gauge 11 were 11% lower (498 µε compared to 555 µε at 2.1 kN and 948 µε compared to 1057 µε at 4.0 kN) than the far field strains observed in Gauges 4 and 5 and predicted by Equation 1. As this gauge was located well outside the wake of the hole it is unlikely that this discrepancy was caused by the hole shielding Gauge 11 from the full far-field stresses. Conducting the work to explain this discrepancy was beyond the scope of this report.

The response of Gauges 7 and 8 were much lower than predicted by Equation 1. The 5.1 mm shift along the y axis (Fig. 12) clearly removed these gauges from the peak strain ligament between the hole and the specimen edge. Thus the measurements from these gauges were not considered representative of the strain profile in the ligament (along the x axis in Fig. 12). The strain in Gauge 6 was actually lower than that in the far field. This is consistent with the gauge being in the wake behind the hole where the stress concentration factor $K_t = -1$ at the point x=0, y=r.
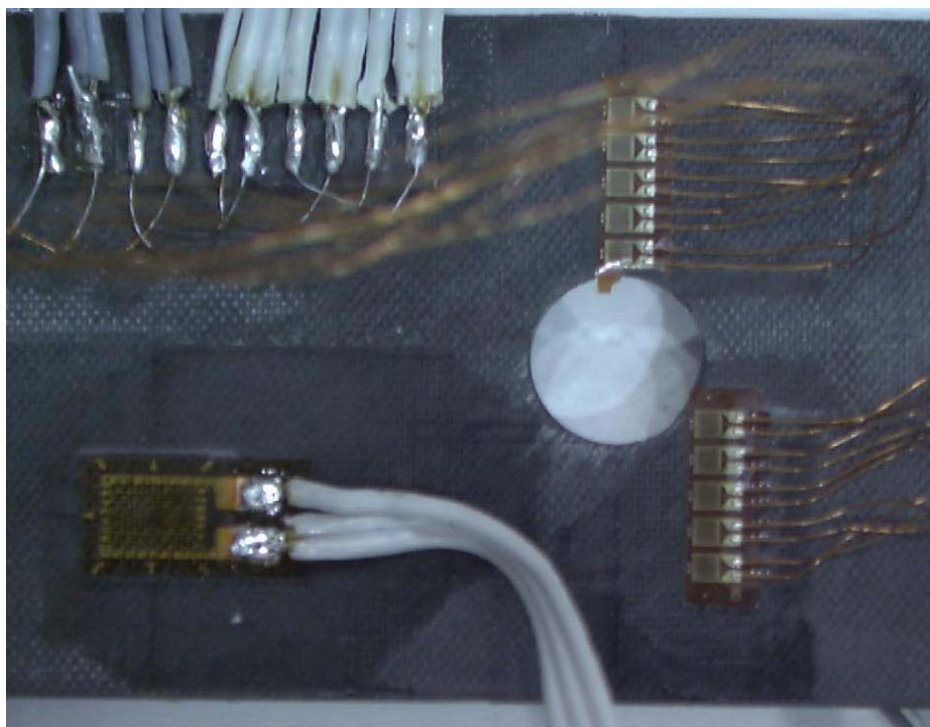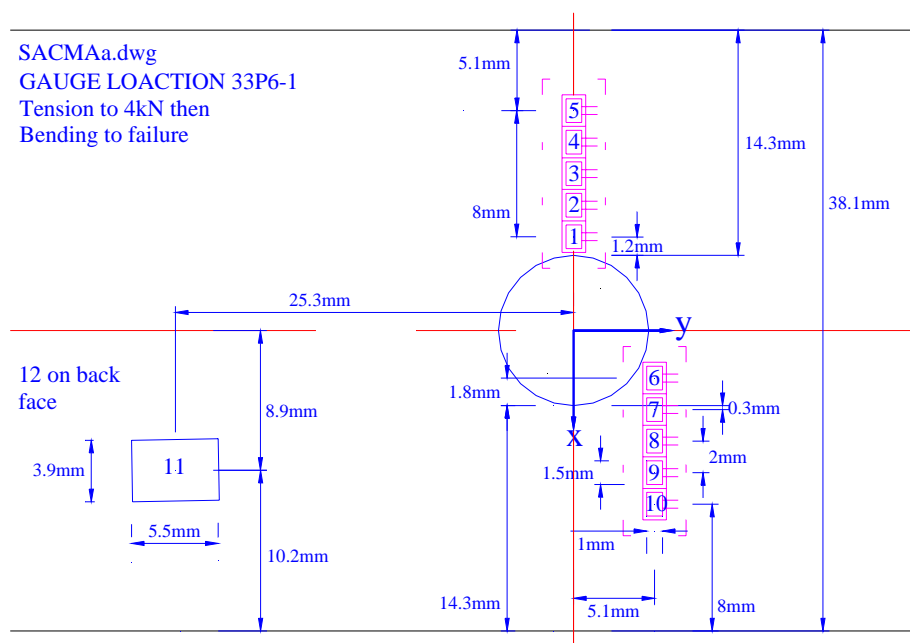
Figure 11: Photograph of strain gauges on specimen 33P1_6

Figure 12: Measured location of strain gauges on 33P1_6 as determined from Figure 11
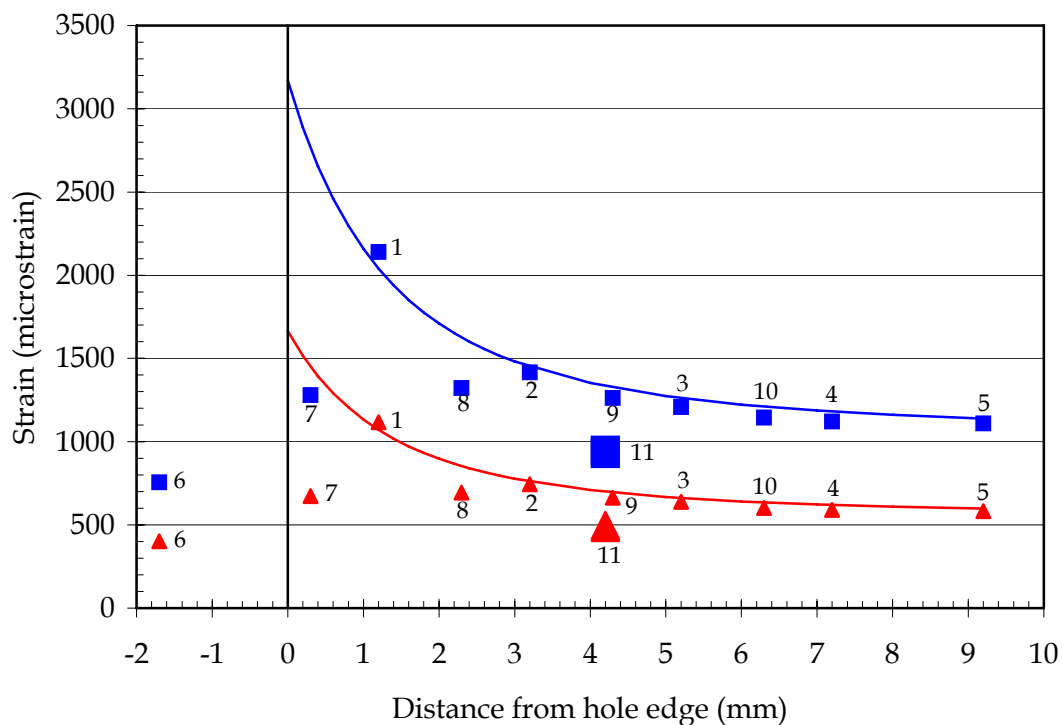
Figure 13:   Strains in the y direction. Data for 2.1 kN is shown as triangles and 4.0 kN as squares. Each data point is labelled with the strain gauge number. The curves are theoretical strains calculated using Equation (1)

4.3 Failure locus

The failed specimens were inspected visually and found to contain significant delamination with very little fibre pullout. There was no apparent difference between the RTD and ETW specimens as shown by the typical failures in Fig. 14.

The notched coupons failed close to the direct line between the edge of the hole and the closest specimen edge. Clearly the stress concentration effects of the hole were sufficient to produce local failure in the load bearing 0° fibres. The delaminations in these specimens were up to approximately 10 mm long and were present between many of the plies on each side of the separated specimen halves. The most obvious delamination was the surface 45° ply. On every specimen this ply separated from the edge of the hole out to the edge of the specimen.

Most of the unnotched coupons failed at or near the grips. This was expected because of the stress concentration created by the hard grips on the relatively soft composite. The unnotched strength data in Tables 3 and 4 must therefore be considered a lower bound.

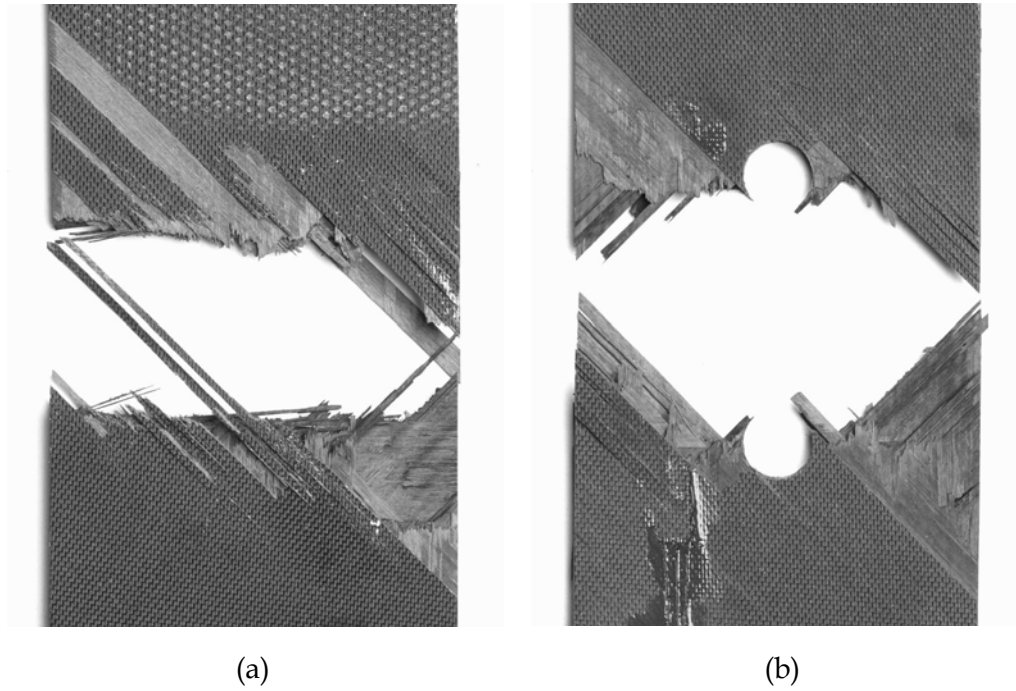<center>(a)   (b)</center>

Figure 14: Photograph of typical failed OHT specimens (a) unnotched ETW (Specimen JA2, 0.00 mm hole) and (b) notched RTD (Specimen LA6, 6.35 mm hole)

4.4 Modulus

The effects of hole size on elastic modulus for the OHT specimens (E_1^t) is shown in Fig. 15.

The modulus was not expected to be strongly affected by hole size because modulus is a measure of the bonding within the material averaged over the volume of the specimen. The holes tested in this work were only a small fraction of the specimen volume. Thus, in terms of volume there was very little difference between the specimens. Fig. 15 shows that indeed there was almost no change in modulus for the RTD case, and a weak increase in ETW modulus caused largely by a single outlier (64 GPa for specimen GA6 with a 9.55 mm diameter hole). It was concluded that, as expected, hole diameter and environment had no effect on elastic modulus for OHT specimens.

4.5 Strength

The effects of hole size on the ultimate tensile strength of OHT specimens (F_1^{tu}) is shown in Fig. 16.

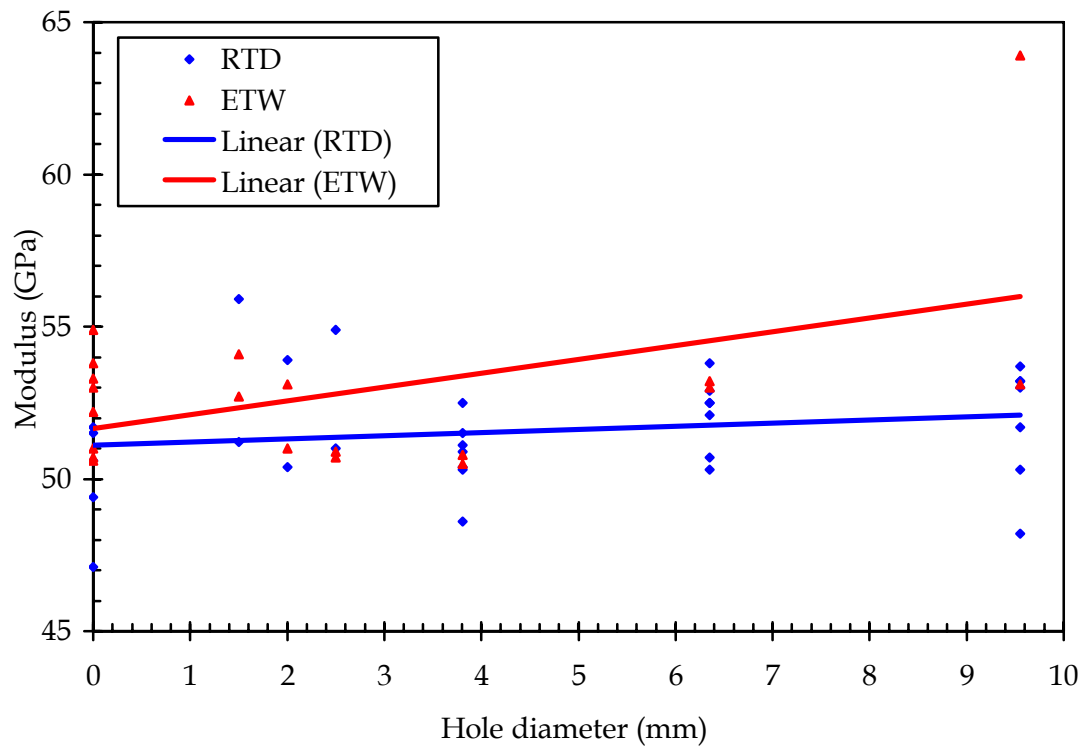Originally, only two unnotched ETW specimens were tested (JA1 and JA2). However

Figure 15: Elastic modulus of RTD and ETW OHT specimens, experimental data and least squares lines of best fit
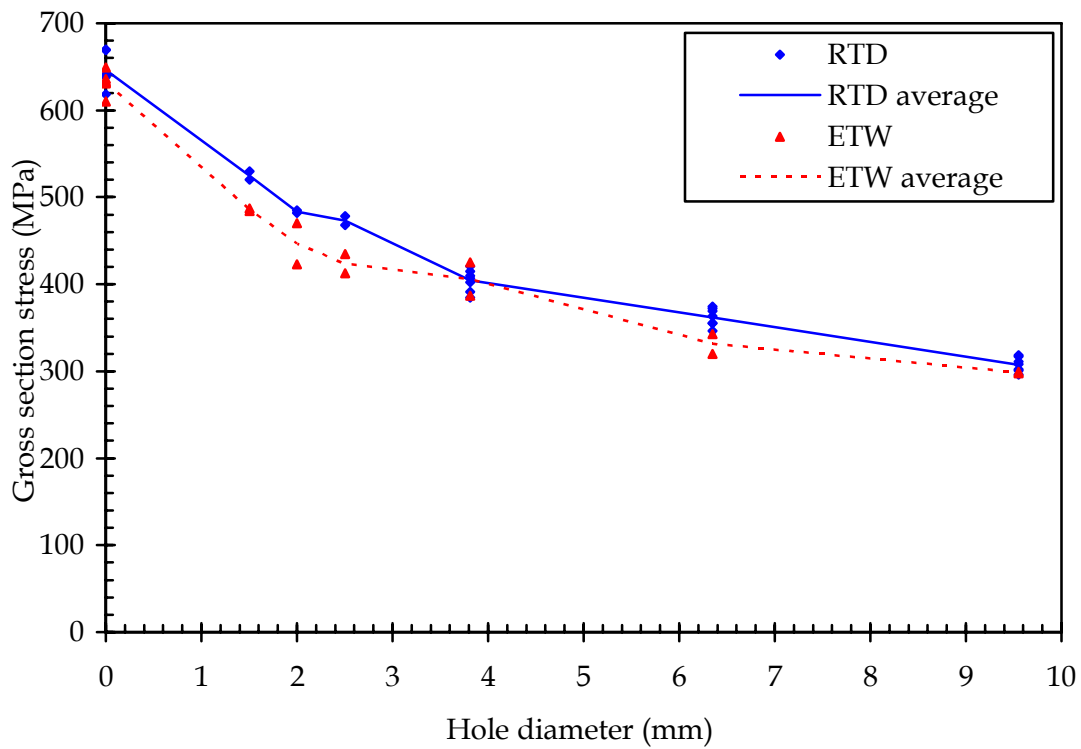

Figure 16: Strength of RTD and ETW OHT specimens

these specimens failed prematurely in the grips at low stress. Therefore an additional six specimens, NB[1-6], were prepared. Care was taken to ensure these specimens were well aligned with the loading axis of the test machine and that a fresh piece of abrasive coated fabric mesh (Norton Metalite Q223) was placed between the specimen and grips immediately prior to testing. The aim of the mesh was to reduce the stress concentration at the end of the grips by softening the grip/specimen interface.

Although these specimens also failed near the grips, except for NB3 that failed within the grips, their failure stress was much higher than for JA1 and JA2, and very similar to that for the RTD specimens. It was concluded that specimens JA1, JA2 and NB3 failed prematurely and so their strength and strain-to-failure data were discarded from the results pool.

The effect of environment on the mechanical properties of composite materials is commonly handled by the use of an environmental knockdown factor (EKDF). As defined in Equation 9 this is the ratio of the property measured in the environment divided by that property measured in the RTD condition. The ETW tests conducted in this work allowed the calculation of the elevated temperature wet environmental knockdown factor (EKDF$_{ETW}$).

$$\text{EKDF}_{ETW} = \frac{\text{property in ETW condition}}{\text{property in RTD condition}} \tag{9}$$

The EKDF$_{ETW}$ was calculated for each hole size specimen by comparing the ETW and RTD strengths for that hole size. These values were averaged to calculate the EKDF$_{ETW}$ for OHT strength (EKDF_{ETW}^{Ftu}) of 0.94. EKDF_{ETW}^{Ftu} was expected to be very close to 1.00 because the tensile strength of fibre composite laminates is controlled by the strength of the fibres, and the AS4 carbon fibres used in these laminates were unaffected by the 77°C/85% RH ETW conditions. The calculated EKDF_{ETW}^{Ftu} = 0.94 was considered to be very close to this expected value.

4.6 Strain-to-failure

The stress-strain curves for RTD specimens with larger holes showed that immediately following maximum load, the strains recorded by the strain gauge and actuator displacement decreased, but strain recorded by the extensometer increased. Fig. 17 illustrates this feature in a specimen with a 6.35 mm diameter hole.

This observation can be explained by considering that, according to the rule-of-mixtures, the four 0° plies support over 85% of the load on these specimens. It is very likely that the stress drop/strain rise was caused by failure of one 0° ply across the ligament between the hole and specimen edge. If this were to occur then the local strain (as recorded by the extensometer) would increase while simultaneously the remainder of the specimen (as recorded by the far field strain gauges) would unload. The failure of one 0° ply in a specimen that contains only four 0° plies would very rapidly lead to specimen failure
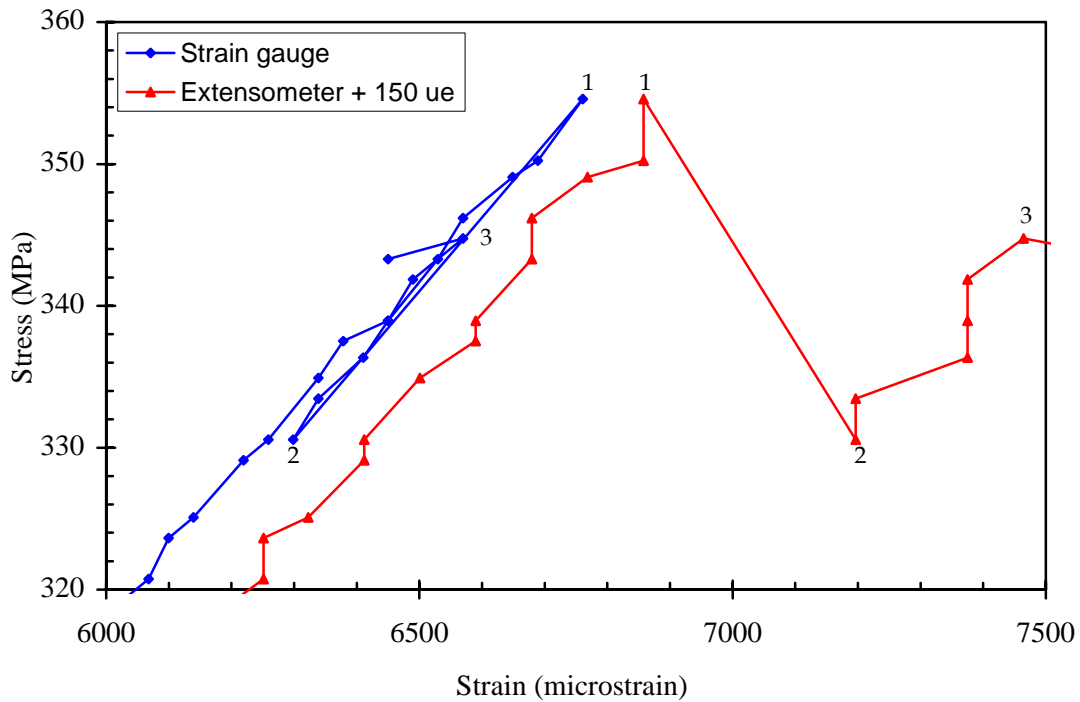
Figure 17: Failure behaviour of a RTD specimen. Points 1 to 4 represent the progression at failure for a strain gauge and extensometer. For display purposes 150 με was added to the extensometer data to separate it from the strain gauge data

because the remaining three plies would be overloaded. All data files were examined closely to ensure that the appropriate data point, equivalent to Point 1 in Fig. 17, was selected as the failure point.

The effects of hole size on the ultimate strain-to-failure in tension (ε_1^{tu}) is shown in Fig. 18. The data used in these plots was obtained from Tables 3 and 4. The strain-to-failure behaviour was very similar to that described for strength and $EKDF_{ETW}^{\varepsilon tu}$ = 0.93.

4.7 Strength prediction

4.7.1 Average Stress Criterion

The ASC requires two parameters, σ_o and a_o. σ_0 was calculated as the average unnotched strength from the data in Tables 3 and 4 (average F_1^{tu} for 0.00 mm holes). a_0 was calculated by fitting the experimental strength data with Equation 5 and assuming K_t =3.00. The least squares values of σ_0 and a_0 and coefficient of determination are shown below. The average stress criterion predictions corresponding to these parameters are compared to the experimental data in Fig. 19.
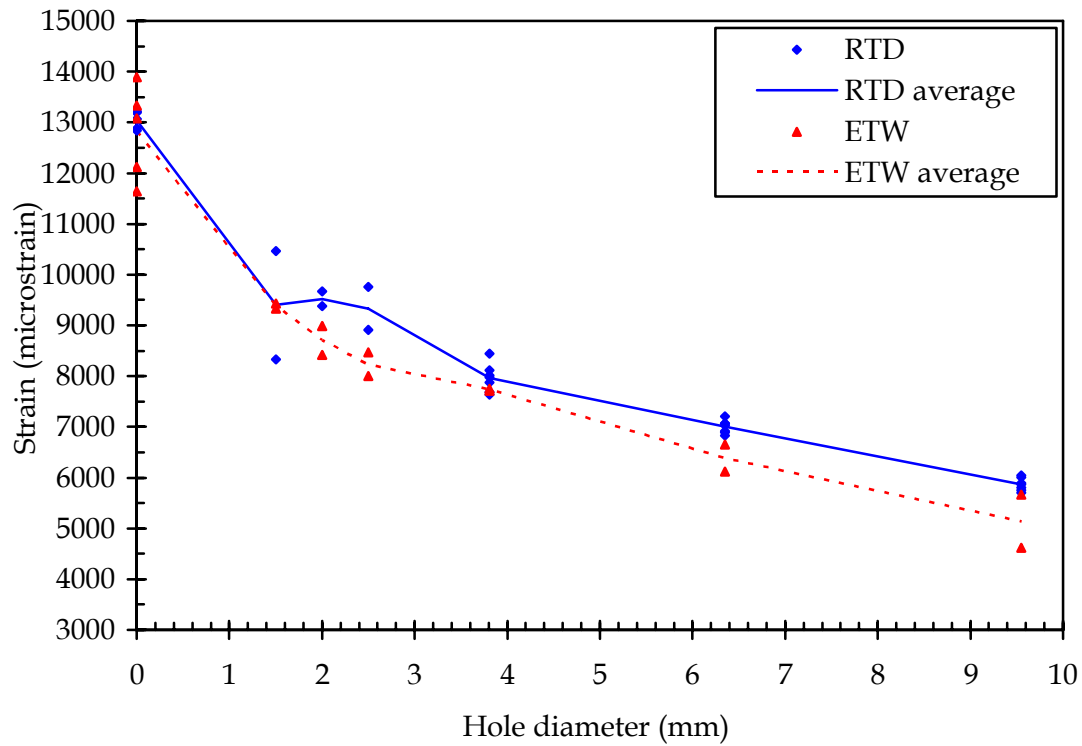
Figure 18: Ultimate strain-to-failure for RTD and ETW OHT specimens

RTD	σ_0 = 646 MPa	a_0 = 2.61 mm	R^2 = 0.986
ETW	σ_0 = 632 MPa	a_0 = 2.26 mm	R^2 = 0.977

4.7.2 Point Stress Criterion

A similar approach was used to determine the PSC characteristic length, except that the experimental strength data was fitted to Equation 6. The best fit curves are shown in Fig. 20 and the calculated parameters are:

RTD	σ_0 = 646 MPa	d_0 = 0.89 mm	R^2 = 0.957
ETW	σ_0 = 632 MPa	d_0 = 0.73 mm	R^2 = 0.943

4.7.3 Compilation

The experimental data and average/point stress criteria predictions are plotted for the RTD specimens in Fig. 21 and the ETW specimens in Fig. 22.

The most appropriate method of comparing the fit of two equations, and thus choosing one model over another, is the F test [12], however performing this test was beyond the scope of this work. Instead it was noted that the coefficient of determination (R^2) for both the ASC and PSC were relatively high. Thus the predictions produced by both criteria

Figure 19: Comparison of notched/unnotched strength for RTD and ETW OHT as determined experimentally and by the ASC
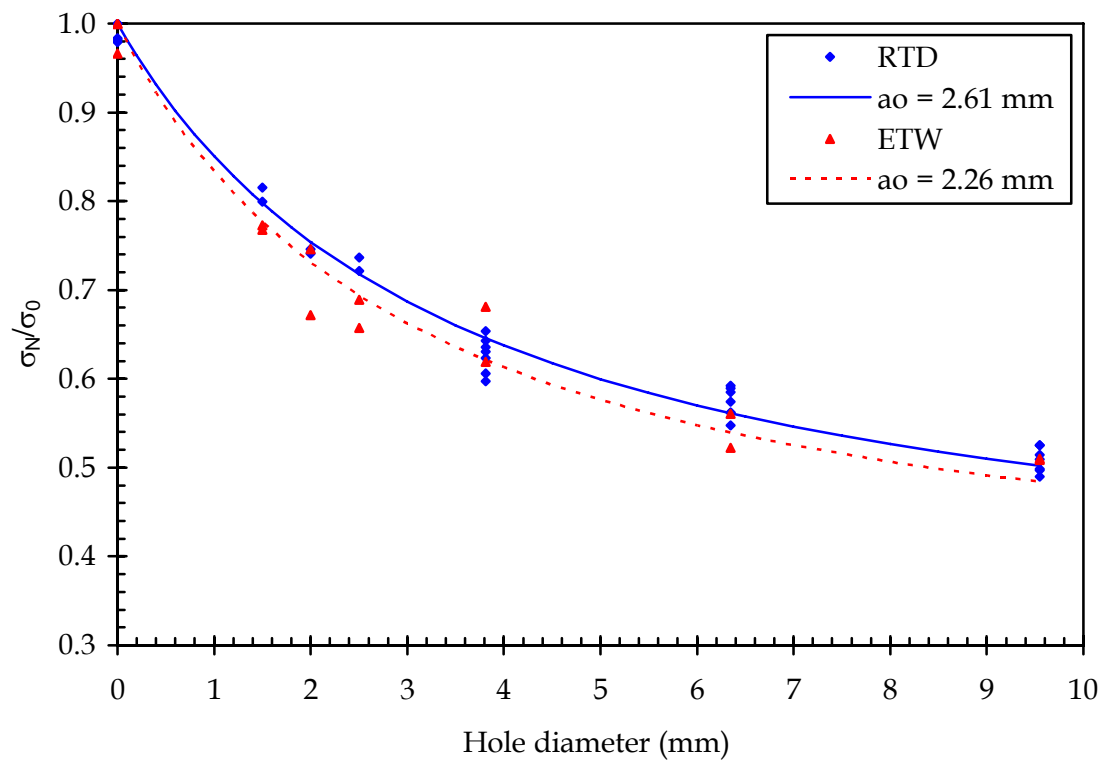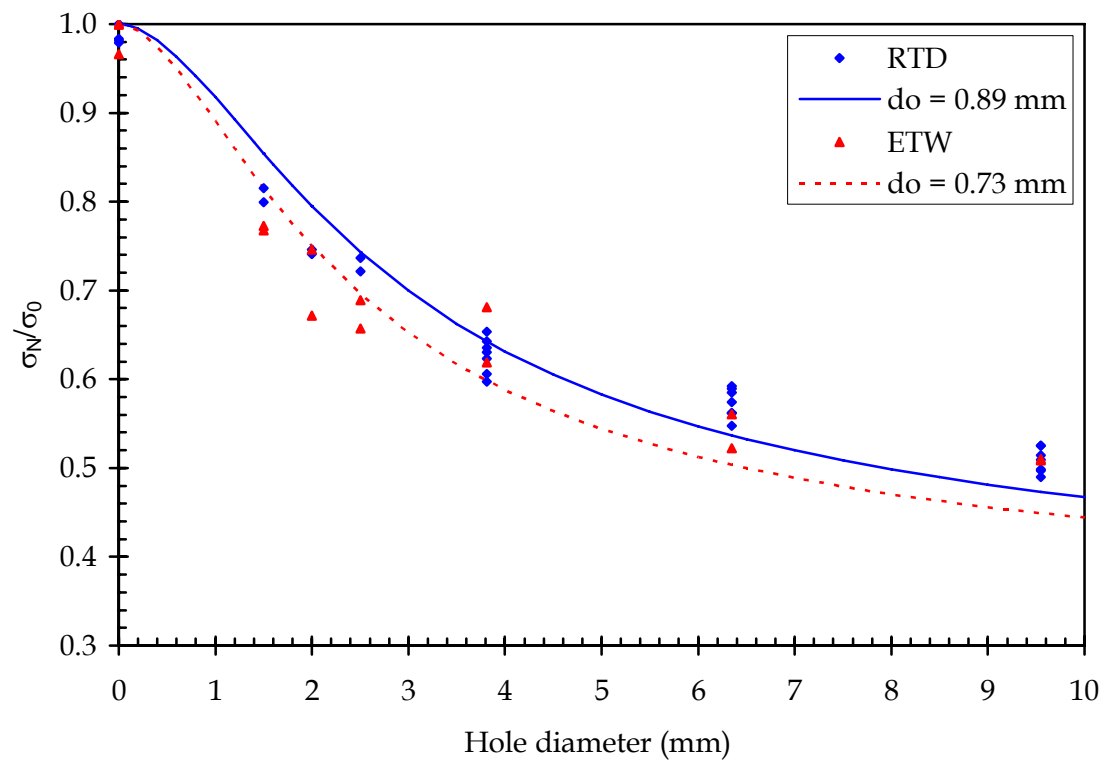

Figure 20: Comparison of notched/unnotched strength for RTD and ETW OHT as determined experimentally and by the PSC
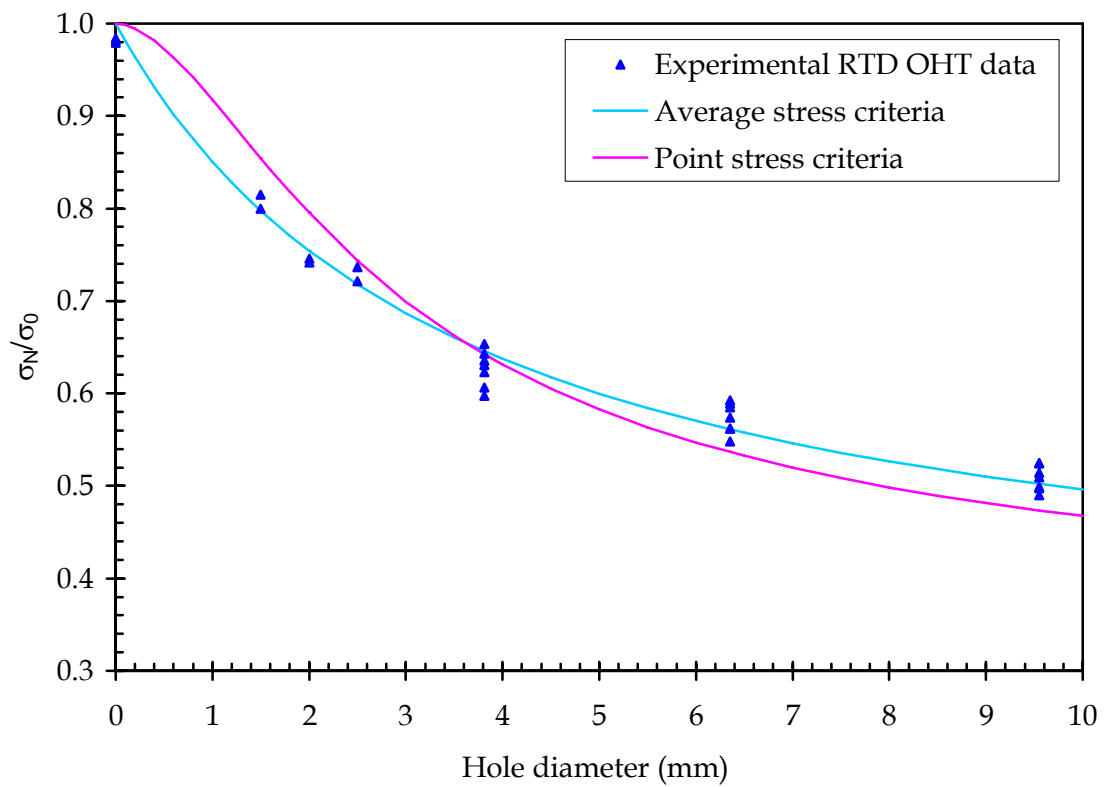
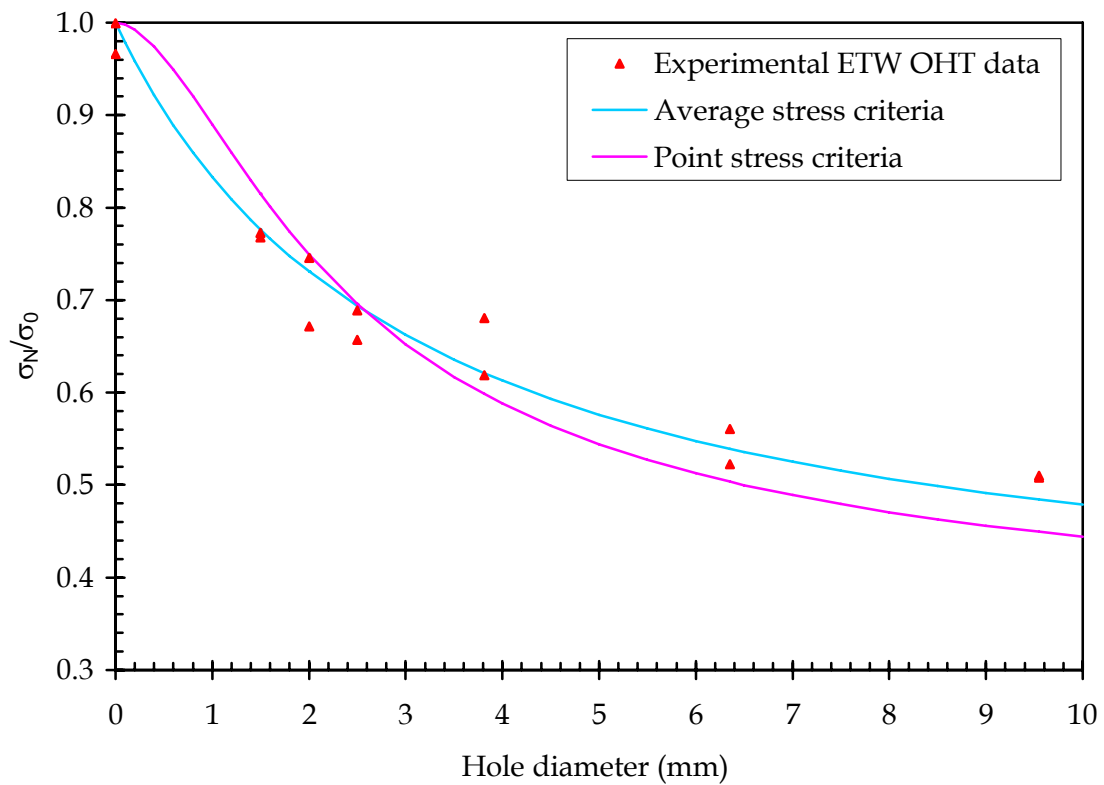*Figure 21: Compilation of the OHT strength predictions for the RTD specimens*

Figure 22: Compilation of the OHT strength predictions for the ETW specimens

were good. Figures 21 and 22 show that, visually, the shape of the ASC curve appeared to match the experimental data more closely than the PSC for both the RTD and ETW conditions.

The improved match of the ASC was also observed in [1] and attributed to the ASC considering a larger volume of material than the PSC ($a_0 \approx 2.8\ d_0$). It was argued that tensile failure in composites is governed by the interaction between flaws (misaligned fibres, disbonded fibres, porosity, matrix yielding) and the local stress field. The distribution of flaws is statistical, therefore those criteria that consider greater volumes of material increase the likelihood of including the critical flaws that precipitate specimen failure. It is possible that the length a_0 is required to fully enclose the flaws that lead to failure within a notched composite while the distance d_0 is insufficient. Detailed microstructural studies would be required to test this hypothesis, however such work was beyond the scope of this program.

4.8 Length scales

The analytical solutions to the ASC and PSC were shown in Section 4.7. The length scales as determined using two other methods were also determined and are shown here for comparison.

Two dimensional finite element (FE) models of specimens at each hole size were created. For each model the stress distribution around the hole was determined at the average RTD failure load for specimens of that hole size. From these distributions, a_0 and d_0 were calculated numerically using the Whitney and Nuismer (W-N) [1] and Potti-Rao-Srivastava (P-R-S) [13] approach. The P-R-S method is a modification of the W-N approach and requires that the length scale be recalculated for each hole size. The detailed results of the FE modelling, including the application of the failure criteria, are reported elsewhere [14].

Some of the experimentally obtained RTD strengths that were shown in Table 3 were not included in the average used for the numerical analysis [14]. Therefore it is not rigorously correct to compare the length scales obtained from the FE modelling with those obtained from the ASC and PSC. However it is unlikely that the inclusion of a small number of additional data points will change the conclusions.

A summary of the results from the experimental and FE studies is shown in Table 5 and data from this table is plotted on Fig. 23. It can be seen that a_0 was substantially longer that d_0, as expected given the method that these parameters are calculated, but the prediction of these lengths by each of the methods were relatively close.

Table 5: *The ASC and PSC characteristic lengths for OHT as calculated using the Whitney-Nuismer (W-N) and Potti-Rao-Srivastava (P-R-S) approaches*

Hole diameter (mm)	ASC length scale a_0 (mm)			PSC length scale d_0 (mm)		
	W-N		P-R-S	W-N		P-R-S
	Analytical	FE		Analytical	FE	
1.50	2.61	2.20	2.49	0.89	1.07	0.66
2.00		2.29	2.53		1.08	0.73
2.50		2.64	2.56		1.16	0.78
3.81		2.17	2.63		1.01	0.89
6.35		2.65	2.71		1.29	1.02
9.55		2.55	2.76		1.14	1.12
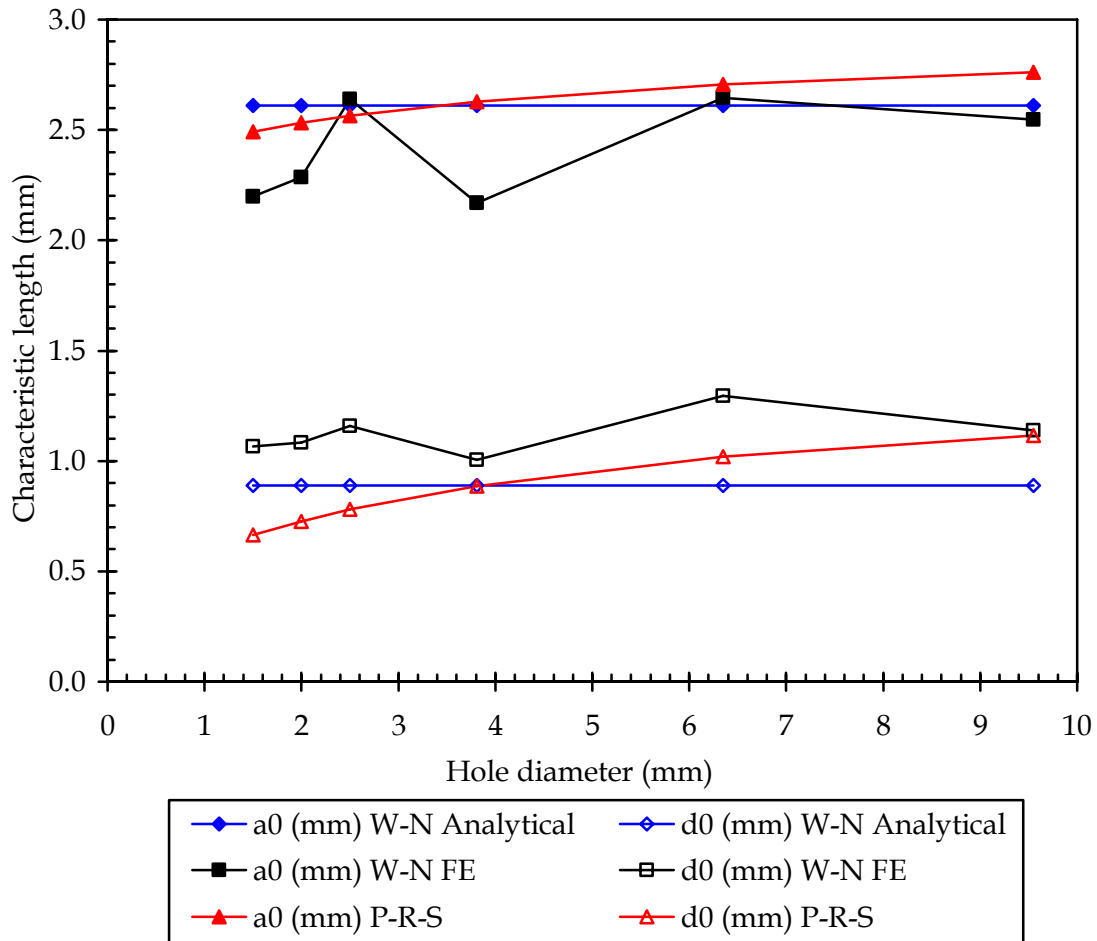
Figure 23: *Effect of hole size on critical length for RTD OHT models*

5 Results and Discussion - Compression

5.1 Stress-strain behaviour

5.1.1 Strain gauge

The stress-strain response of OHC specimens was approximately linear to failure. ASTM D 3410 states that for a compression test to be valid the bending shall be less than 10%. The stress-strain responses measured on the back-to-back strain gauges for both the RTD and ETW specimens diverged, indicating bending. A typical result is shown in Fig. 24. The range of this difference, and the corresponding amount of bending, was 217-3800 με and 4-63% for RTD and 182-911 με and 1-17% for ETW. Typically the amount of bending was less than 8% for RTD and less than 7% for ETW. Although the difference in back-to-back strain gauge readings in some specimens was higher than recommended, the data was not rejected.

The most likely source of the difference in back-to-back strains in the OHC specimens were; (1) gross bending or buckling in the specimen, (2) misalignment of the strain gauges, and (3) interference between the strain gauge and the test fixture as the test proceeded. It is suspected that much of the back-to-back strains difference in RTD specimens was due to actual bending of the specimen, caused by slight misalignment of specimens in the test machine. Specimens were aligned and held in position manually while hydraulic wedge grips were tightened against the anti- buckling guides. The guides often moved slightly as
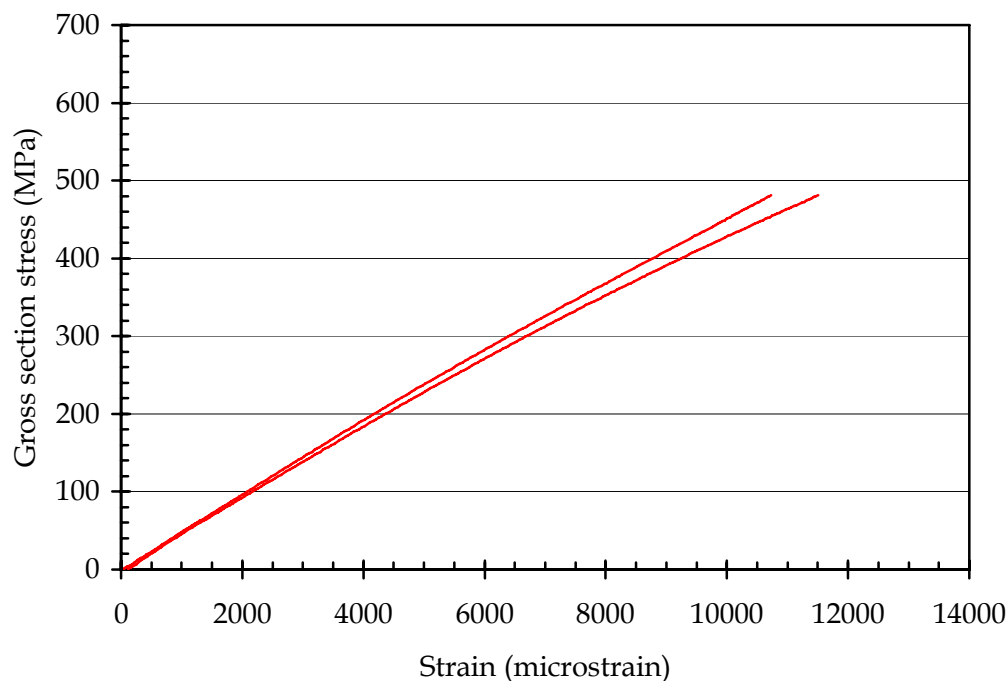
Figure 24: Typical OHC test result (ETW, Specimen NC5, 0.00 mm hole). The divergence between back-to-back strain gauge measurements indicated specimen bending

the grips tightened. Although the gripping process was repeated if movement was observed it was not always possible to eliminate all movement. In future work physical limits will be installed in test machines to prevent specimens from moving during the gripping process.

In support of this conclusion was the observation that the ETW specimens were loaded by clamping the anti-buckling guides to compression platens using rigid, well aligned, mounts. The resultant differences in back-to-back strain readings were much lower than for the RTD specimens.

It is unlikely that the divergence in measured strains was due to gauge misalignment. Post-test examination of nineteen gauges on the RTD specimens showed that the gauge location varied from the nominal location by 1 to 2 mm and the misalignment angle between the gauge and the specimen varied from 0.1 to 0.7°. Such small angles would have very little effect on the measured strains.

5.1.2   Extensometer

An extensometer was installed on the edge of some OHC specimens (see Fig. 6). Figure 25 shows typical stress-strain responses for the extensometer and strain gauge for RTD and ETW specimens. Severe slippage of the extensometer was noted on seven out of eight RTD specimens, as indicated by the horizontal steps in the curve. Prior to slippage the strains
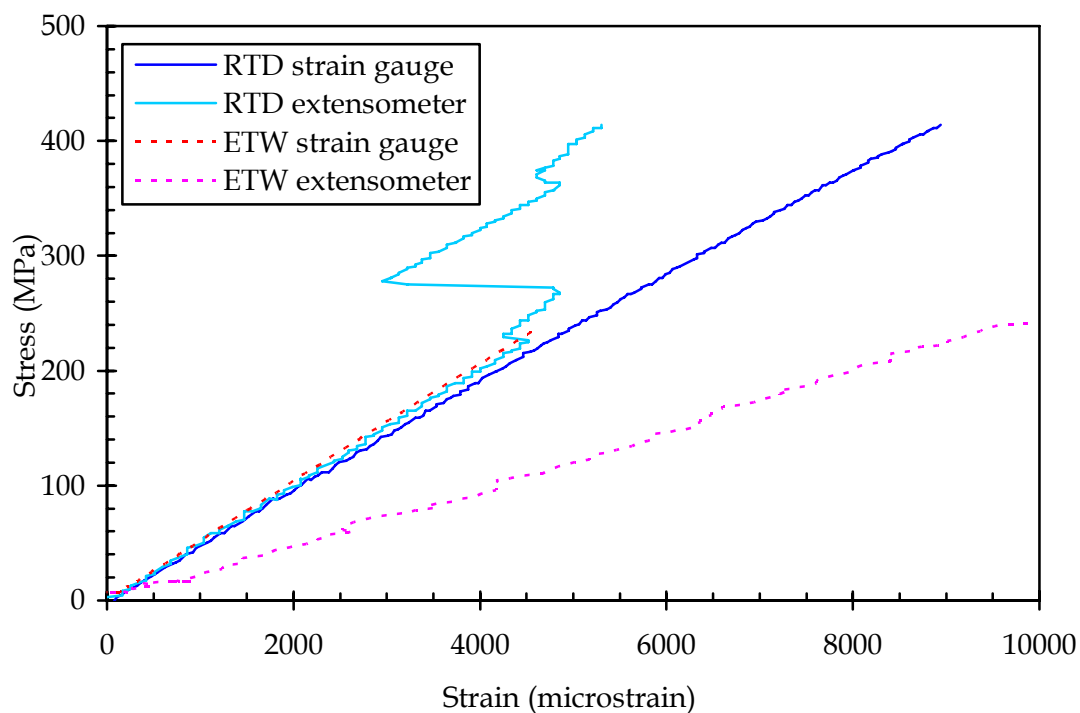
Figure 25:   Comparison between and extensometer and strain gauge showing extensometer slippage for RTD (2.00 mm hole, specimen KB2) and excessive extensometer strain for ETW (6.35 mm hole, specimen JA5)

measured by the extensometer matched well that recorded by the strain gauges. This indicated that the concept of measuring strain using the extensometer was reasonable, however the experimental technique needed to be improved. The most obvious improvement was to increase the force holding the extensometer knife edges against the specimen edge. This will be done in any future tests.

The match between strain gauge and extensometer data was poor for ETW tests, with significantly greater strain being recorded by the extensometer. Although no conclusive reason for this error has been determined, it is possible that it was caused by the non-ambient environment changed the calibration of the extensometer.

It was hypothesised that deformation in OHC specimens would be concentrated in the ligament between the hole and specimen edge because the cross-sectional area of the specimen was minimum in this region. If this were the case then, as hole size increased the strain recorded by the extensometer should have increased greater than that measured by the far-field strain gauges. As indicated in Fig. 26, any tendency for this to occur was masked by a large variability in the test data. Thus no conclusion could be made regarding the validity of this hypothesis.

5.1.3 Actuator displacement

The calibration technique described in Appendix A was used to correlate the strains

Figure 26: Effect of hole size on the difference between failure strains as measured by an extensometer across the hole and a far field strain gauge. Extensometer data has been corrected to account for slippage

calculated from actuator displacement with those from the strain gauge. The correlations obtained using this approach produced a reasonable match for the RTD data. For the 16 specimens with valid strain gauge and corrected ac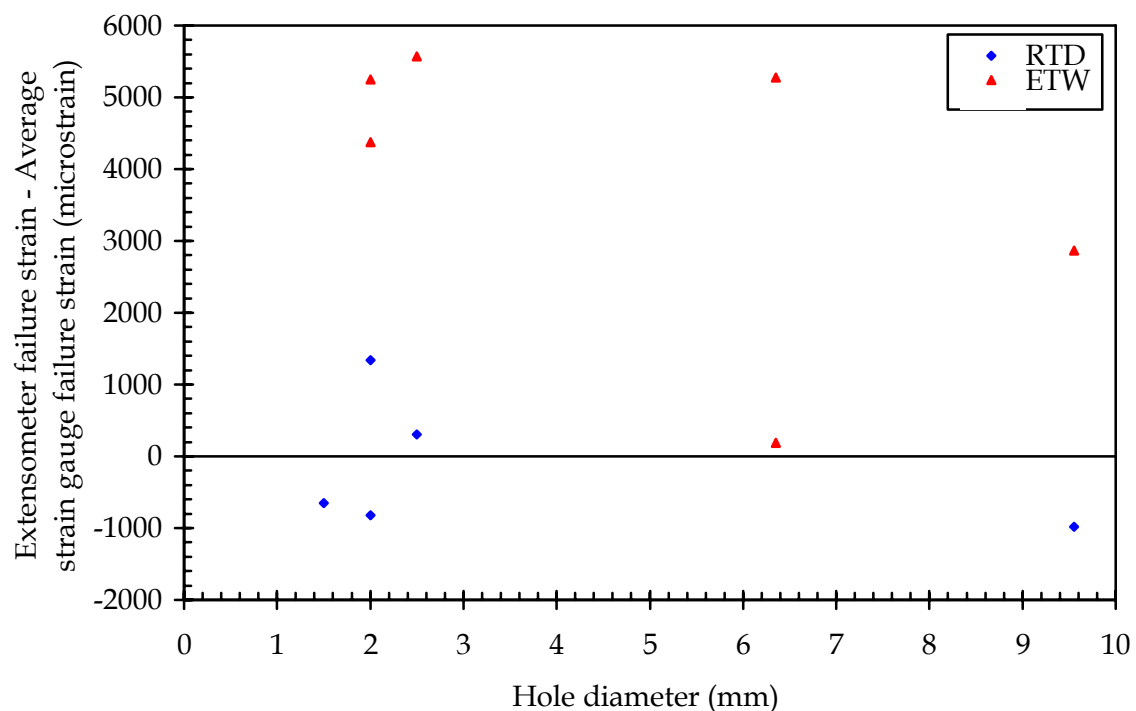tuator displacement data, the average difference in failure strain was 320 $\mu\varepsilon$ or 4% of the failure strain. The fit was not as good for the ETW tests. Data from six specimens was ignored because of gross deviations from the linear stress-strain response. The average difference for the remaining nine specimens was 473 $\mu\varepsilon$, or 7.2% of failure strain. Ignoring data from three outliers in this group reduced differences to 300 $\mu\varepsilon$ or 4%, very close to the RTD values.

5.1.4 Final

As with the OHT data, there were differences between the strains measured by the strain gauges, extensometer and actuator displacements. Differences included step changes in the strain gauge or extensometer response, or a gradual deviation of the measurement from one transducer relative to the other two. The following hierarchy was therefore used to select which strain transducer would be used for further analysis. In order of most preferred to least preferred, the strain transducers were:

(i) averaged back-to-back strain gauge,
(ii) actuator displacement (corrected as per Section 5.1.3), then
(iii) extensometer.

Thus, in this report the average back-to-back strain gauge data is reported for RTD and ETW OHC test results unless stated otherwise.

Typical stress-strain behaviour for each of the hole sizes are shown in Figs 27 and 28. The elastic modulus from 1000 to 3000 $\mu\varepsilon$, failure strength and failure strain were determined using the most preferred data source available and the approaches described in Sections 5.2 and 5.3 respectively. These properties are shown in Tables 6 and 7.

5.2 Failure locus

All failed specimens were inspected visually and typical examples are shown in Fig. 29. All the notched coupons failed across the thin ligament between the hole and specimen edge. Damage was restricted to a narrow band around the relatively flat line of failure with fibre brooming on both failure faces. This failure morphology is typical of that for laminates subject to axial compression.

All but one of the unnotched specimens failed by fibre brooming at one end. Thus the strength and strain-to-failure data for unnotched specimens quoted in Tables 6 and 7 must be considered lower bounds. Although great care was taken to ensure the fixtures were well aligned and additional clamping placed over the anti-buckling guides, it was very difficult to prevent fibre brooming failures when specimens were end-loaded between compression platens.
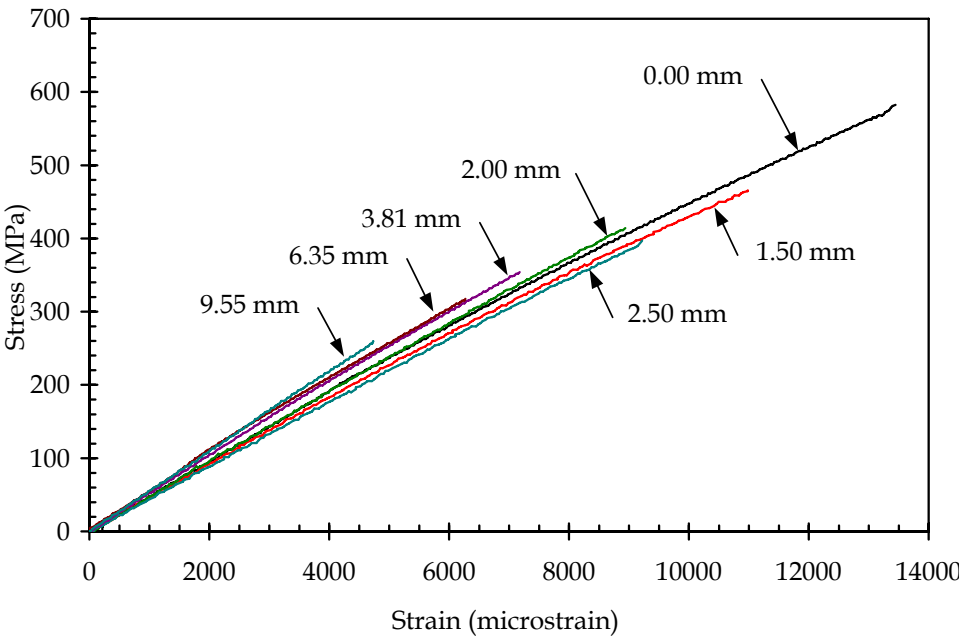
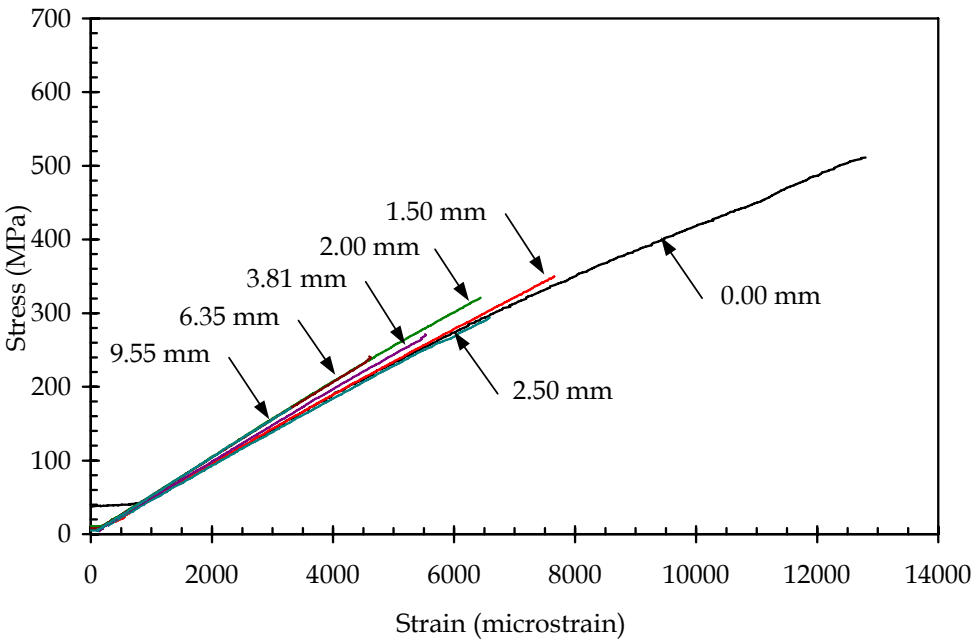*Figure 27: Typical stress-strain response of RTD OHC specimens with the indicated hole size*

Figure 28: Typical stress-strain response of ETW OHC specimens with the indicated hole size

Table 6:   RTD OHC results and derived mechanical data

Hole φ (mm)	Specimen number	Thick. (mm)	Width (mm)	P_{max} (kN)	E_1^c (GPa) [1]	ε_1^{cu} (µε)[1]	F_1^{cu} (MPa)	FWCF	σ_N^∞ (MPa)
0.00	33P3_1A	2.25	38.02	53.8	48.3	14,598	629	1.0000	629
	33P3_12	2.34	38.09	51.8	47.5	13,443	583		583
	33P3_18	2.24	37.94	52.5	56.5	11,681	618		618
	33P3_19	2.22	37.96	52.7	50.2	14,009	625		625
1.50	KB5	2.24	38.14	39.8	46.6	10,981	466	1.0016	467
	KC3	2.31	38.17	38.5	47.8	9,785	437	1.0016	438
2.00	KA6	2.32	38.14	33.3	45.8	8,950	377	1.0029	378
	KB2	2.24	38.02	35.3	49.5	8,940	414	1.0029	415
2.50	KB3	2.31	38.11	34.9	45.0	9,222	397	1.0045	399
	KB4	2.25	38.14	31.4	49.0	7,554	366	1.0045	368
3.81	33P3_4	2.27	37.09	30.4	52.1	7,175	354	1.0114	358
	33P3_5	2.27	37.93	30.5	57.9	6,324	355	1.0108	359
	33P3_6	2.28	37.92	31.4	59.8	6,143	363	1.0108	367
	KA3	2.25	38.02	29.8	53.1	6,602	348	1.0108	352
6.35	33P3_1	2.29	37.95	26.9	48.0	5,284	311	1.0317	321
	33P3_9	2.28	37.99	25.6	49.6	6,260	296	1.0317	305
	33P3_10	2.29	37.95	27.5	54.3	6,272	318	1.0317	328
	KA4	2.27	38.12	25.1	53.2	-	290	1.0314	299
9.55	33P3_15	2.29	38.02	23.6	52.1	5,142	271	1.0772	292
	33P3_16	2.27	37.95	22.3	55.3	4,737	260	1.0775	280
	33P3_17	2.26	37.86	22.3	59.9	4,511	261	1.0779	281
	KA5	2.29	38.05	24.3	50.8	5,850	279	1.0771	301

[1]   The strain data source for modulus and failure strain is indicated by the colour of the cell, being strain gauge or actuator displacement.

5.3 Modulus

The effects of hole size on OHC elastic modulus (E_1^c) are shown in Fig. 30. As with the OHT specimens, the applied compression load was supported primarily by the 0° fibres and total volume of these fibres was not affected significantly by the relatively small holes. Thus E_1^c was expected to be unaffected by hole size. This was observed for the ETW case but it appeared that the average E_1^c rose as hole size increased. This trend was probably an artefact of the broad scatter of results and was not considered a real effect.

5.4 Strength

The effects of hole size on ultimate OHC strength (F_1^{cu}) is shown in Fig. 31.

Using the approach described in Section 4.5, it was calculated that $EKDF_{ETW}^{Fcu}$ = 0.81. This was consistent for all hole sizes is similar to that reported in the literature. The

Table 7: ETW OHC results and derived mechanical data

Hole ϕ (mm)	Specimen number	Thick. (mm)	Width (mm)	Moist. Cont. (wt%)	P_{max} (kN)	E_1^c (GPa)[1]	ε_1^{cu} ($\mu\varepsilon$)[1]	F_1^{cu} (MPa)	FWCF	σ_N^∞ (MPa)
0.00	GB1	2.42	38.02	1.32	47.1	47.4	12,800	511		511
	GB2	2.38	38.12	1.42	33.8[2]	52.2	7,733[2]	373[2]		373[2]
	NC1	2.29	38.05	1.09	37.9[2]	64.8	7,510[2]	434[2]		434[2]
	NC2	2.31	38.09	1.08	42.9	48.8	11,190	488	1.0000	488
	NC3	2.29	38.05	1.03	46.5	48.2	12,695	534		534
	NC4	2.31	37.98	1.06	45.8	51.6	11,268	522		522
	NC5	2.31	38.04	1.00	42.2	47.2	11,116	481		481
	NC6	2.30	38.04	1.03	43.5	53.7	11,024	498		498
1.50	JC1	2.39	38.18	1.34	32.16	47.4	8,247	352	1.0016	353
	JC2	2.39	38.05	1.32	31.81	47.9	7,653	350	1.0016	351
2.00	GC5	2.37	38.02	1.42	29.03	52.3	6,471	322	1.0029	323
	JB5	2.43	38.11	1.41	30.01	45.7	7,383	325	1.0029	326
2.50	GC2	2.40	38.00	0.91	30.20	41.6	8,129	332	1.0045	333
	JB3	2.45	38.07	1.42	27.37	46.5	6,588	294	1.0045	295
3.81	GC1	2.42	38.03	1.56	26.59	46.5	6,476	289	1.0108	292
	JB1	2.39	38.13	1.30	24.73	49.2	5,523	271	1.0107	274
6.35	GB4	2.40	38.11	1.44	24.25	45.5	6,027	265	1.0315	273
	JA5	2.38	38.18	1.29	21.85	51.9	4,600	241	1.0313	249
9.55	JA3	2.38	38.15	1.27	19.61	52.0	4,221	216	1.0766	233
	JA4	2.36	38.17	1.31	18.39	57.4	3,650	204	1.0765	220

[1] The strain data source for modulus and failure strain is indicated by the colour of the cell, being strain gauge or actuator displacement.

[2] Premature specimen failure. This data not used.

compression strength of fibre composite laminates is a "resin dominated" property. Although the applied loads are supported by the fibres oriented parallel to the loading direction, these fibres are supported by the resin matrix. When the resin yields or allows the fibres to rotate sufficiently, then these fibres can no longer support the applied loads. Failure in compression occurs by localized buckling, called microbuckling, of these load-bearing fibres. The strength and stiffness of epoxy resin matrices are degraded significantly by elevated temperature and absorbed moisture. This has a significant effect on OHC strength.

5.5 Strain-to-failure

Figure 32 shows data from a strain gauge on a RTD OHC specimen near failure. It shows three peaks, at data points 17, 19 and 25, immediately prior to catastrophic failure. The real failure strain at point 17 (4626 $\mu\varepsilon$) is lower than the normally recorded value of strain at point 19 (4705 $\mu\varepsilon$). The latter point would normally be chosen simply because it is the final data point prior to the large drop in load. Each data file and stress-strain plot was examined carefully to ensure that the first load drop was used as the failure point.
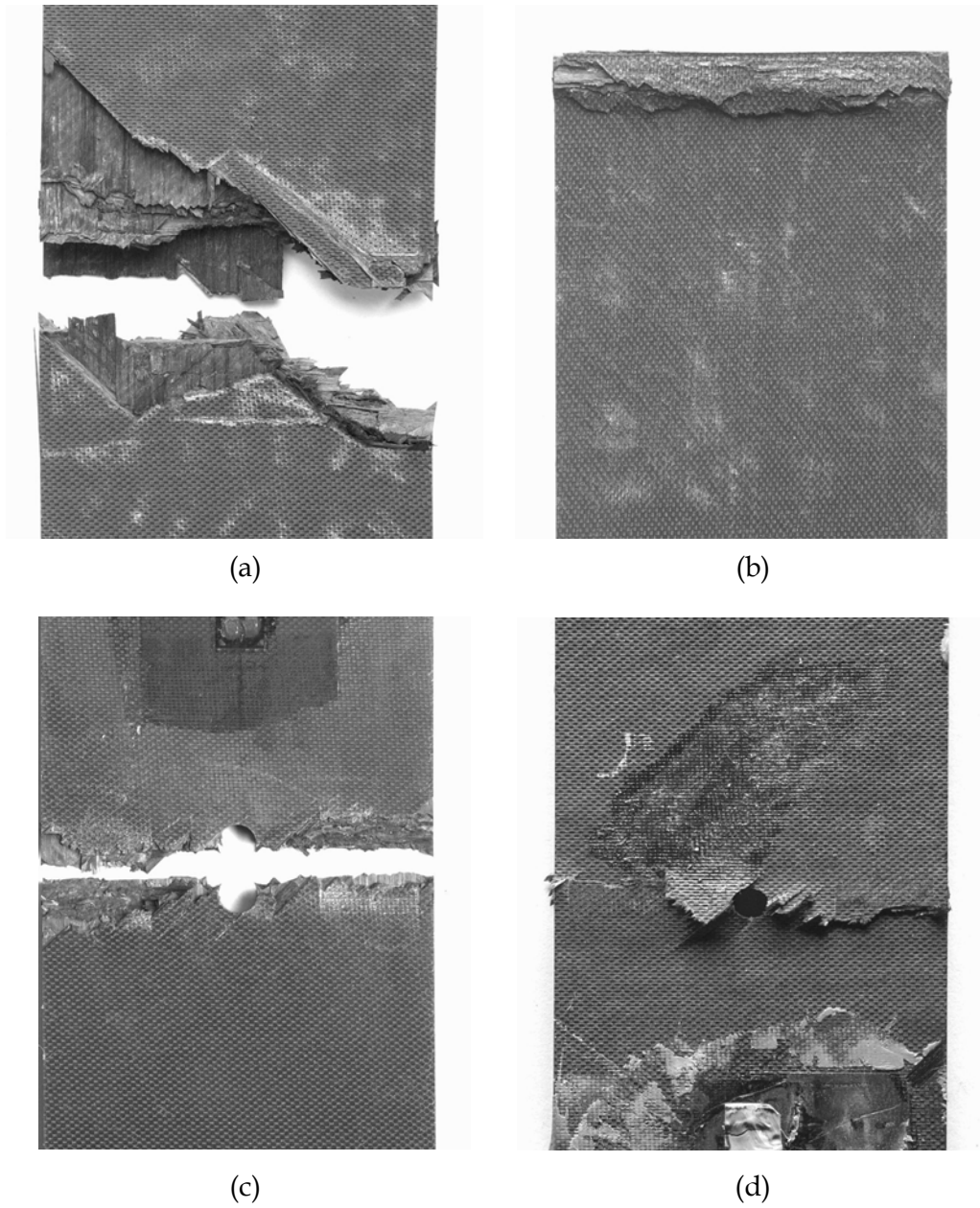
Figure 29: *Photograph of typical failed compression specimens (a) unnotched RTD (P3_19), (b) unnotched ETW (NC5), (c) notched RTD (P3_6, ϕ 3.81 mm hole), and (d) notched ETW (JB1, ϕ 3.81 mm hole)*

The effects of hole size on the OHC strain-to-failure (ε_1^{cu}) are shown in Fig. 33. This behaviour was similar to that for strength shown in Fig. 31. It was calculated that $\text{EKDF}_{\text{ETW}}^{\varepsilon cu}$ = 0.84. The slight difference between this and $\text{EKDF}_{\text{ETW}}^{Fcu}$ was caused by the non-linearity shown in Fig. 28.
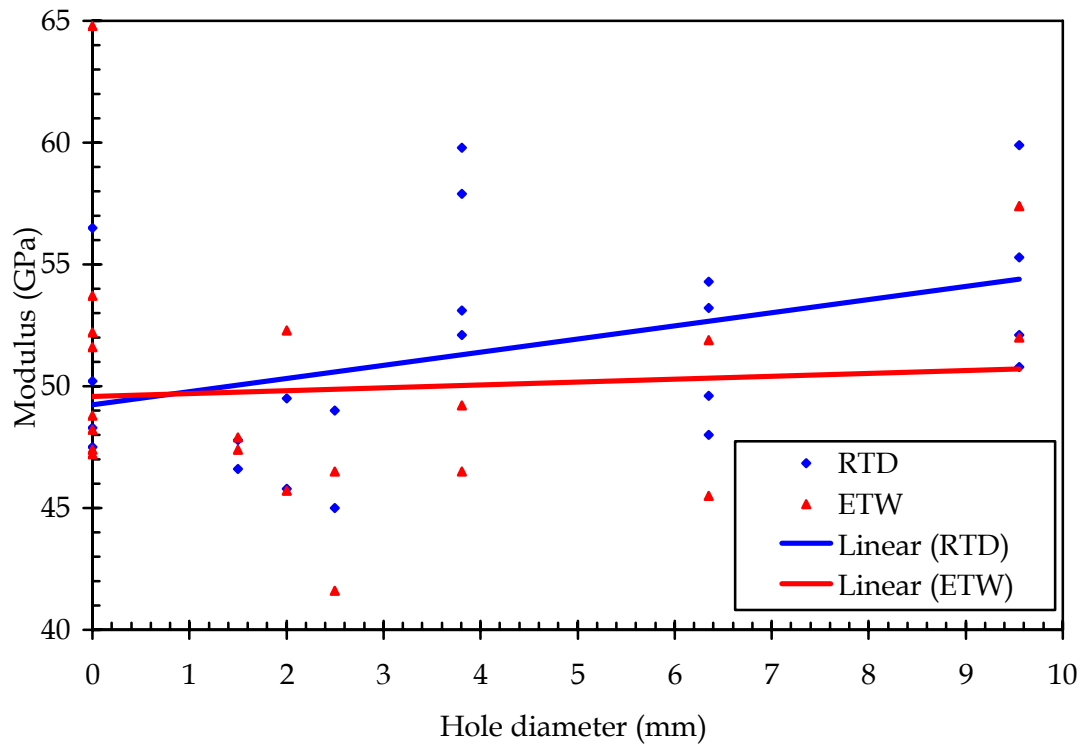
Figure 30: Elastic modulus of RTD and ETW OHC specimens, experimental data and least squares lines of best fit
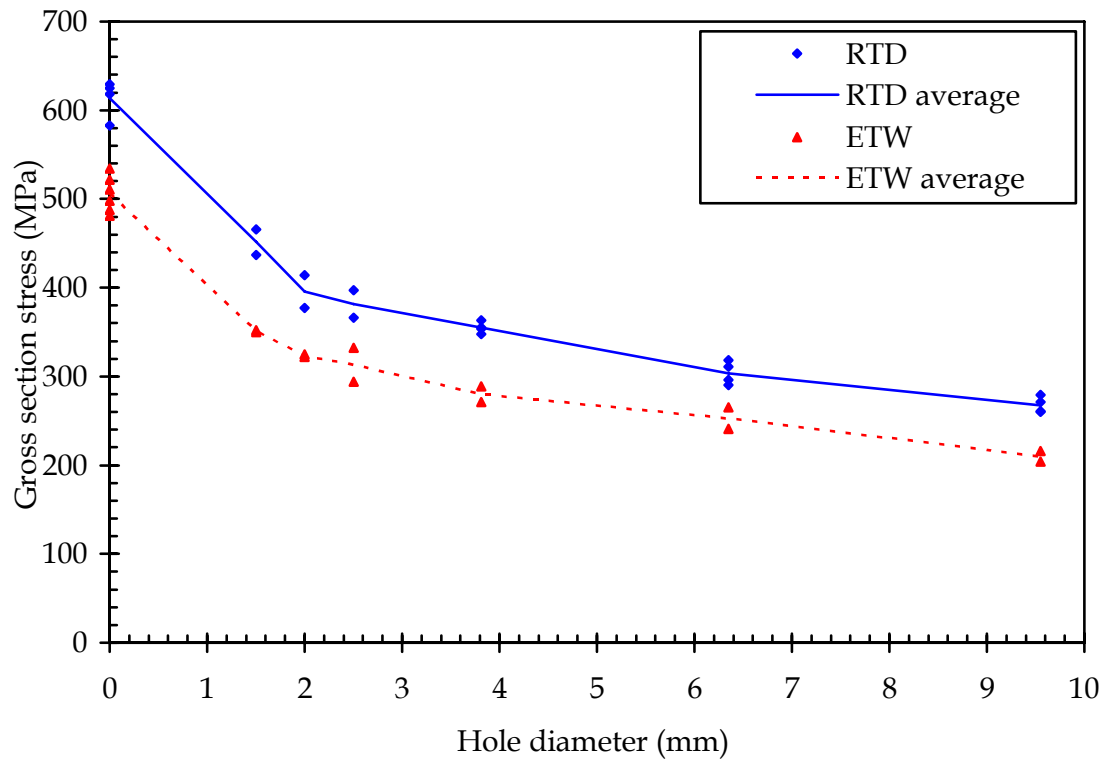
Figure 31: Strength of RTD and ETW OHC specimens
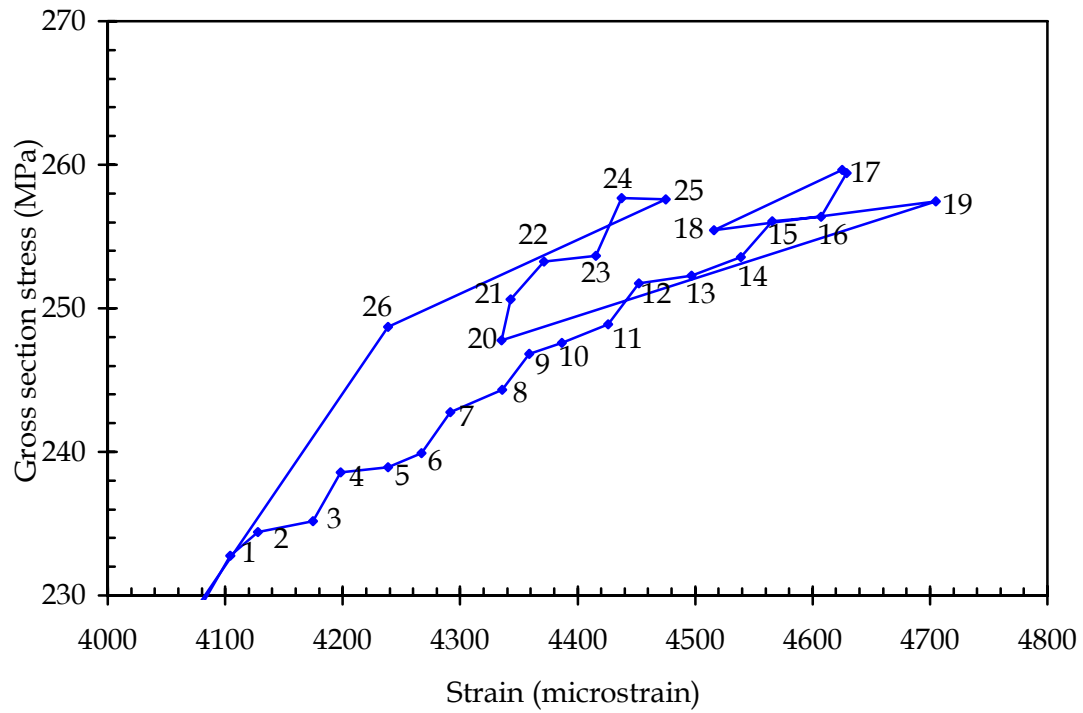
Figure 32: Example of an RTD OHC coupon with a multi-step failure. The data point numbers are indicated (9.55 mm hole, specimen 33P3_16)
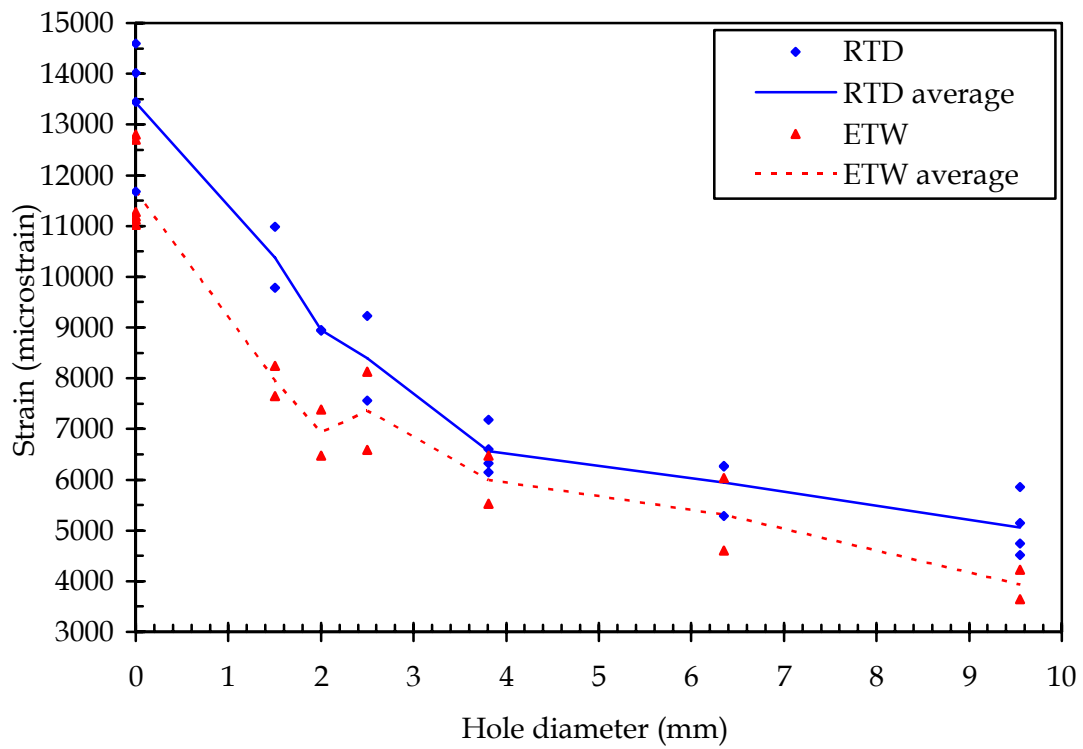
Figure 33: Failure strain for RTD and ETW OHC specimens

5.6 Strength prediction

5.6.1 Average Stress Criterion

The average unnotched compression strength was calculated from the data in Table 3 and 7 and the ASC characteristic length (a_0) from a least squares fit of the experimental data into Equation 5. The resultant parameters are shown below while the experimental data and curves of best fit are shown in Fig. 34:

RTD $\sigma_0 = 614$ MPa $a_0 = 1.71$ mm $R^2 = 0.978$
ETW $\sigma_0 = 506$ MPa $a_0 = 1.49$ mm $R^2 = 0.977$

5.6.2 Point Stress Criterion

The PSC characteristic length (d_0) was calculated by matching the experimental strength data with Equation 6. The calculated parameters are shown below while the experimental data and curves of best fit are shown in Fig. 35:

RTD $\sigma_0 = 614$ MPa $d_0 = 0.60$ mm $R^2 = 0.954$
ETW $\sigma_0 = 506$ MPa $d_0 = 0.52$ mm $R^2 = 0.965$

5.6.3 Cohesive Zone Model

The CZM has been implemented in the Composite Compressive Strength Modeller (CCSM) software package distributed by Cambridge University [15]. This package was acquired and used to predict the OHC strength of the notched laminates tested in this work.

The first input required by the CCSM is the elastic properties of the unidirectional lamina. The program uses laminate theory to calculate the elastic properties of the laminate. Lamina properties are either user defined or selected from a database. In the absence of experimental data, the values for AS/3501 from the CCSM database were selected for this calculation. The inputs required by CCSM and the outputs from this section of the program are shown in Table 8. The predicted failure stress and critical microbuckle length (l_c) are shown in the CCSM "Failure Analysis" page. The data used for these calculations are shown in Table 9.

The K_c was varied until the least squares best fit was found with the experimental data. This was obtained for RTD at $K_c = 34$ MPa $\sqrt{m}$ ($R^2 = 0.975$) and ETW at $K_c = 26$ MPa $\sqrt{m}$ ($R^2 = 0.978$). The experimental data and curves of best fit are shown in Fig. 36. Although K_c for the AS4/3501-6 laminate under test was not evaluated experimentally, the best fit values certainly appear reasonable, being well within the range quoted in the CCSM software.

The CCSM software stated that the predictions for the 9.55 mm diameter hole size must be treated with caution. Reliable bridging data for the laminate may only be obtained for $R/w < 0.25$ while the 9.55 mm hole represents $R/w = 4.775/19.05 = 0.251$. Figure 36 shows
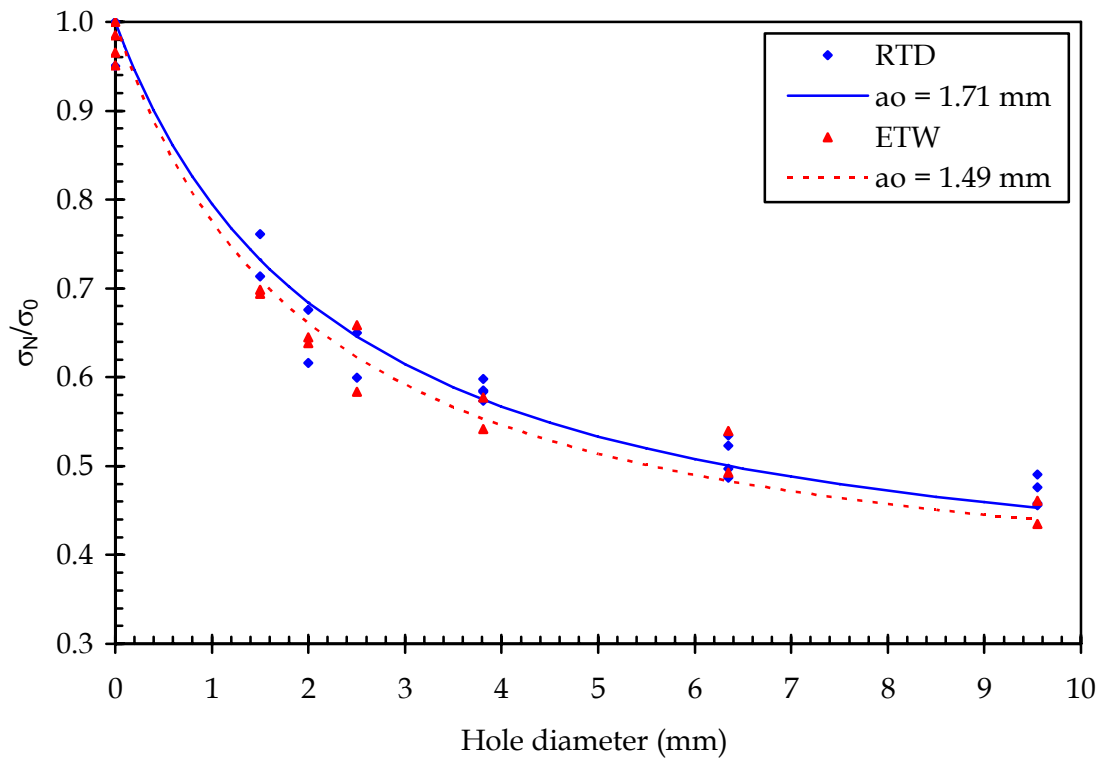
Figure 34: Comparison of notched/unnotched strength for RTD and ETW OHC as determined experimentally and by the ASC
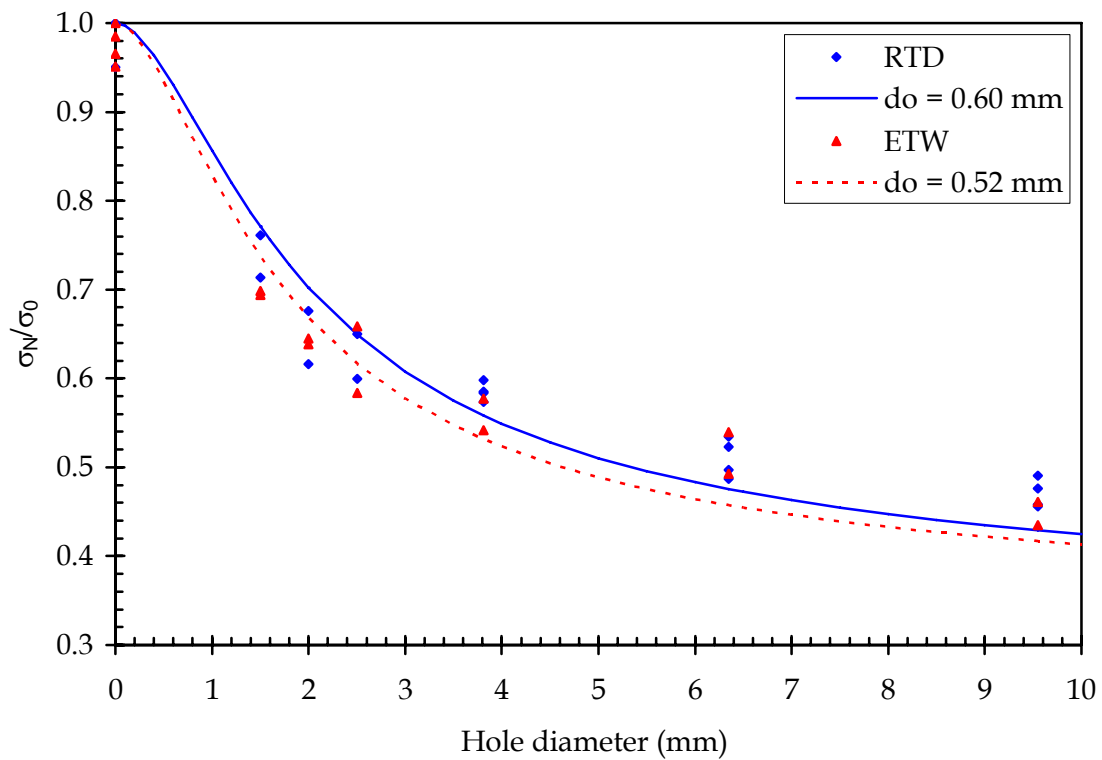
Figure 35: Comparison of notched/unnotched strength for RTD and ETW OHC as determined experimentally and by the PSC

Table 8:   Input data for CCSM and calculated laminate elastic properties

Property	Value
Lamina (default for AS4/3501)	
E_{11} (GPa)	138
E_{22} (GPa)	9
ν_{12}	0.3
G_{12} (GPa)	6.9
Laminate (input)	
Ply thickness (mm)	0.142
Lay-up	$[45\ 0\ {-}45\ 90]_{2s}$
Laminate (calculated)	
$E_{xx} = E_{yy}$ (GPa)	54.7
$\nu_{xy} = \nu_{yx}$	0.29
G_{xy} (GPa)	21.3

Table 9:   Data used in CCSM failure analysis page

Property	RTD	ETW
Relative axial load	-1	-1
Relative transverse load	0	0
Relative shear load	0	0
Laminate unnotched compression strength (MPa)	613.8	442.0
Specimen half width (mm)	19.05	19.05
Hole radius (mm)	0.05 to 5.0	0.05 to 5.0
K_c (MPa $\sqrt{m}$)	20-60	20-60

that this warning appears justified. The strength predicted by the cohesive zone model fell below the experimental data at this large hole diameter.

5.6.4   Compilation

The experimental data and predictions of all models are plotted for the RTD case in Fig. 37 and the ETW case in Fig. 38. The ASC appeared to match the experimental data more closely than the PSC for both load cases.

The predictions of the CZM were almost identical to those of the ASC for 0.00 to 6.35 mm holes, but poor for the 9.55 mm hole. The CCSM acknowledged that bridging data was not available for r/w ≥ 0.25 and so the strength for this hole size (r/w = 0.251) was predicted on the basis of asymptotic values. It appears that the CZM could not be used for situations where the r/w limit was exceeded.

The curve-of-best-fit for the ASC appeared superior to that for the PSC (see Figs 37 and 38). The hypothesis that this improved fit may be caused by the larger volume of material interrogated by the ASC was discussed in Section 4.7.3.
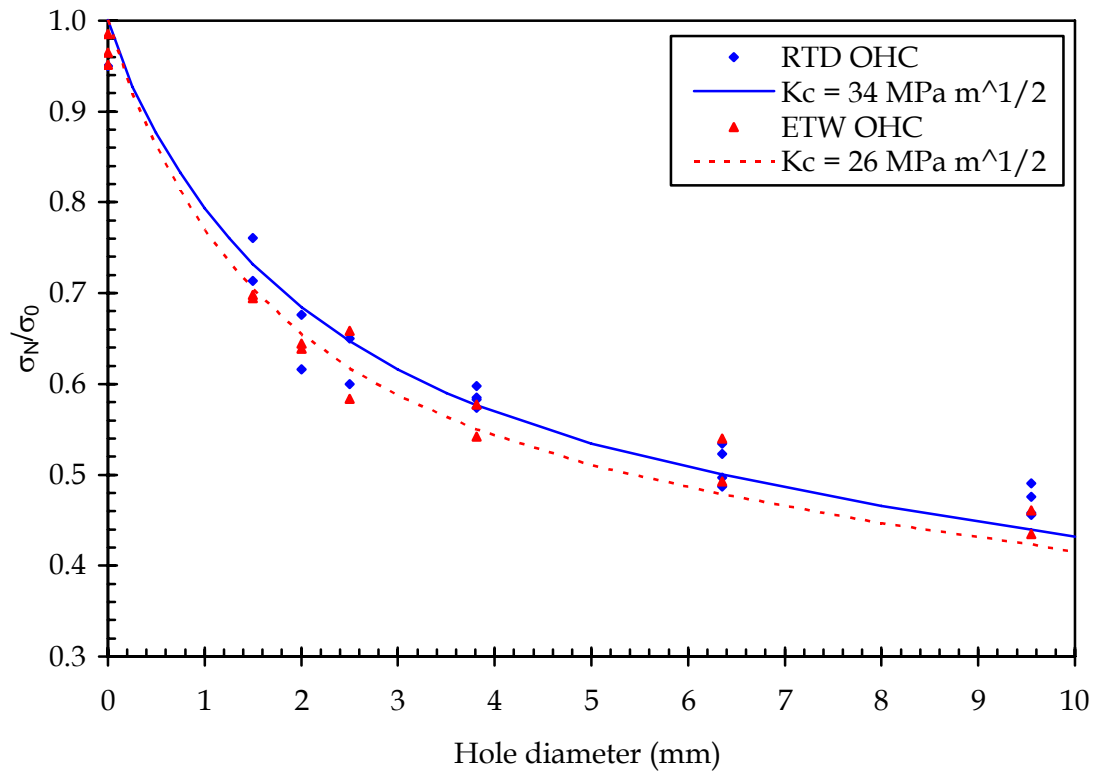
Figure 36: Comparison of notched/unnotched RTD and ETW OHC strength as determined experimentally and by the CZM

5.7 Length scales

The length scales determined from each of the models for OHC are shown in Table 10. There were significant differences in the characteristic lengths predicted by each of the methods, however the predictions from each of the models was excellent, with the ASC and CZM appearing slightly better than the PSC. The creators of these models claimed that each of the respective length scale had some physical significance related to the failure process. This would suggest that the length scale which most accurately captures the effect of the real failure mechanism would produce the best prediction. Clearly this was not observed in this work. It appeared that the different length scales were merely the artefact of using different mathematical equations to model the data.
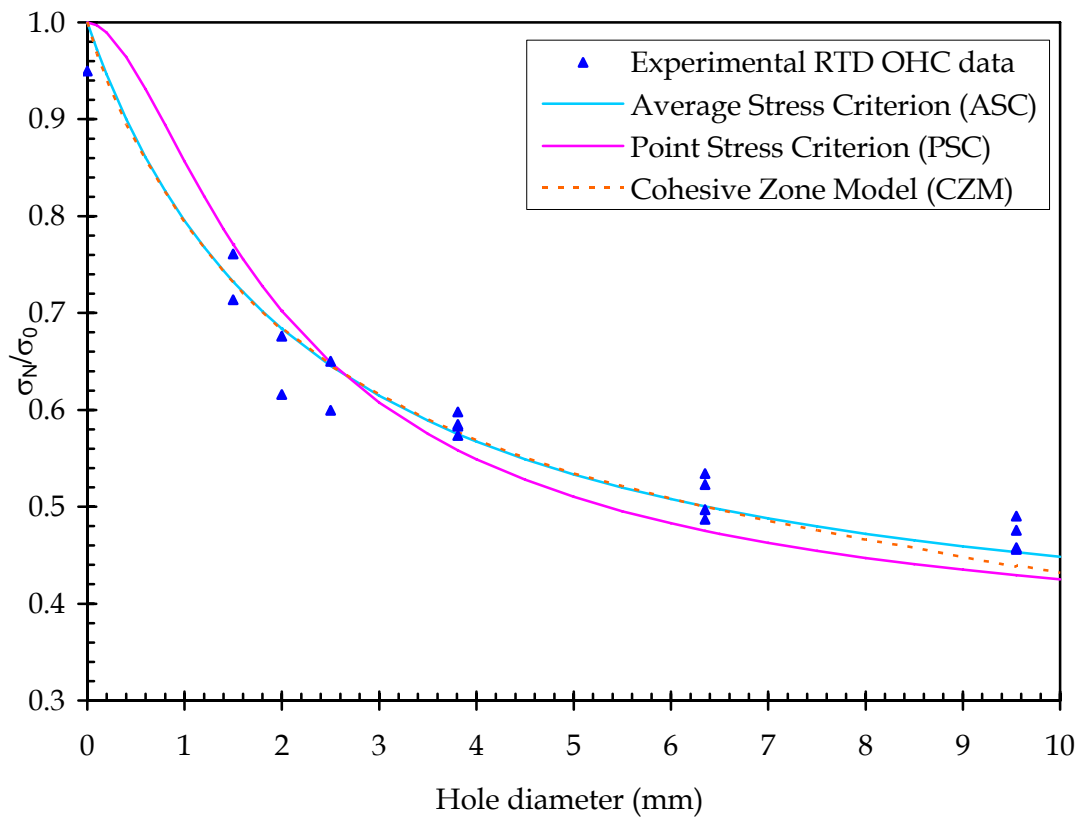
Figure 37:   Compilation of the RTD OHC strength predictions
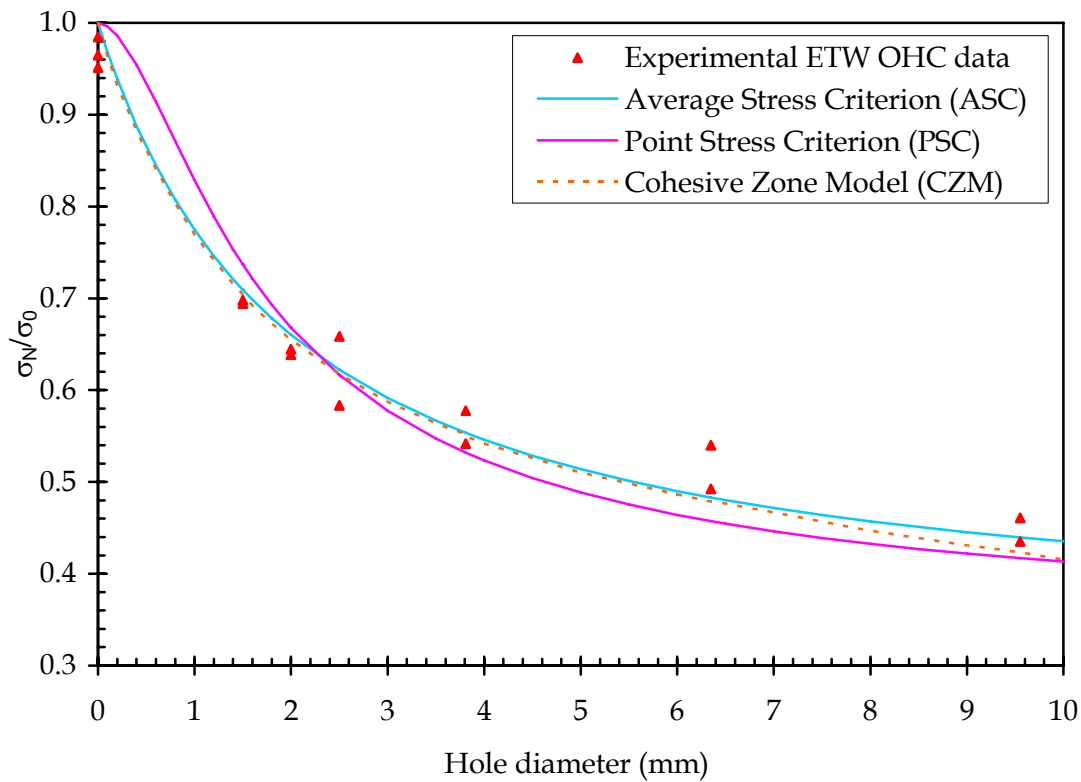
Figure 38:   Compilation of the ETW OHC strength predictions

Table 10:   The OHC characteristic lengths as calculated using the ASC, PSZ and CZM

Hole diameter (mm)	Length scale (mm)					
	a_o		d_0		l_c	
	RTD	ETW	RTD	ETW	RTD	ETW
1.50					2.05	1.80
2.00					2.09	1.83
2.50	1.71	1.49	0.60	0.52	2.11	1.84
3.81					2.10	1.81
6.35					1.97	1.67
9.55					1.75	1.44

6 Results and Discussion - Bending

6.1 Test setup

6.1.1   Bending configuration

The recommended support span/specimen thickness (L/d) ratio for four-point bend specimens will vary according to the properties being evaluated. For the measurement of bending elastic modulus a large L/d (say 64:1) is recommended because this maximises the ratio of bending moment/shear stress and is thus closer to the case of "pure" flexure (i.e. maximum bending moment and minimum shear stress). For the measurement of bending strength the recommended ratio is 16:1 [10] although this may be raised to 32:1. The latter is being considered as the recommended ratio in future editions of the standard [16]. These lower L/d ratios must be used in order to obtain failure without displacements that are so large that the assumptions used to derive the bending equations are violated.

The specimens tested in this work were approximately 2.4 mm thick and holes ranged up to 9.55 mm diameter. Ideally the L/d would have been maximised. Not only would this have produced the most "pure" bending but it would also give the greatest separation between the hole and loading rollers and thus minimised the interference of the rollers on the stress distribution near the holes. Initial tests were conducted with specimens of L/d = 64:1 (support span = 154 mm, loading span = 51 mm), however the centre-span displacement at failure were very large. In some cases the loading rollers pushed the specimen completely through the support rollers without specimen failure.

The recommended L/d = 16:1 would have produced a support span of 38.4 mm and a loading span of 12.8 mm. However this loading span was only marginally larger than the large, 9.55 mm diameter, holes. If this ratio were selected it was expected that the stress distribution close around the hole would have been distorted excessively. As a result of these arguments a ratio of L/d = 32:1 was selected.

The remaining ratio critical to the design of the bend test was that between the loading span and the support span (L). Two standard ratios are specified in ASTM D790, quarter-point loading where load span = L/2 and third-point loading where load span = L/3. Although the former would have given a larger distance between the loading rollers and thus a larger separation from the hole, third-point loading was selected because it produced a more uniform stress distribution in the specimen.

The recommended and actual four-point bend test dimensions are shown in Table 11.

Table 11: Specifications of four-point bend tests

Parameter	Specified in ASTM D790	Actual
L/d	32:1	
Specimen thickness (mm)	2.4	2.0-2.4
Specimen width (mm)	25	38.1
Support span (mm)	76.0	76.0 or 95.0
Loading span (mm)	25.4	25.4 or 31.8
Crosshead speed (mm min^{-1})	4.5	5.0
Specimen length (mm)	102	102

6.1.2   Data reduction

Modulus of elasticity in bending (E^b) was calculated using Equation 10.

$$E^b = 0.21 \frac{L^3 m}{b d^3} \tag{10}$$

Where:

    L   =   support span
    m   =   slope of tangent to initial straight-line portion of load-deflection curve
    b   =   specimen width
    d   =   specimen thickness

The peak strains measured by the strain gauges on both the tension (Tens) and compression (Comp) faces were recorded. The strain gradient was the difference between tension and compression strains divided by specimen thickness.

In most specimens the mid-span deflection at failure exceeded 10% of the loading span. The failure strength was therefore calculated using Equation 11, the large-deflection relation from ASTM D790. To maintain consistency, his approach was used to calculate the strength of, and stress for stress-strain plots in, all specimens. It did not lead to any significant errors because the difference between Equation 11 and the more traditional $S = PL/bd^2$, was a few percent at a deflection of 10% of the loading span and less as deflection reduced.

$$S = \left(\frac{PL}{bd^2}\right)\left[1 + \left(\frac{4.70D^2}{L^2}\right) - \left(\frac{7.04Dd}{L^2}\right)\right] \tag{11}$$

Where:

S	=	stress in outer fibres throughout the load span
P	=	load at a given point on the load-deflection curve
D	=	maximum deflection of the centre of the specimen

6.2 Stress-strain behaviour

Representative bending stress-bending strain curves for RTD OHB specimens are shown in Fig. 39. Specimen dimensions, failure loads and deflections, and derived flexural properties for all RTD specimens are shown in Table 12. The equivalent data for ETW specimens are shown in Fig. 40 and Table 13 respectively.

Figures 39 and 40 show that the responses of RTD and ETW specimens in bending were approximately linear to failure. In addition the magnitude of compression strains on the concave side of the specimens were approximately equal to the magnitude of the tension strains on the convex side of the specimen. The failure stress, and thus failure strain, decreased as hole size increased.

As expected, the bending modulus of the laminates containing a larger fraction of 0° plies was greater and that of laminates containing a larger fraction of 45° plies was lower, than the bending modulus of quasi-isotropic laminates. There was a consistent reduction in bending modulus as hole size increased, particularly for hole sizes of 6.35 and greater.

6.3 Deformation shape

The shape of selected RTD, quasi-isotropic, OHB specimens was recorded during loading and compared to that predicted by classical bending theory. Figure 41 shows one such specimen (0.00 mm hole, MC6) loaded in the four-point bend fixture prior to loading. Figure 42 shows, at higher magnification, MC6 plus a specimen with a 6.35 mm diameter hole (MC10) as loading progressed.

Superimposed over the photographs in Fig. 42 are the predicted deflected shapes. These shapes were created using Equation 12, the parameters of which are defined in Fig. 43. It was necessary to calibrate the predicted deflection shapes with the photographs because the loads at which the photographs were taken were not recorded with sufficient accuracy. Calibration was performed by matching the displacements at the support and load rollers. Thus, for each photograph the predicted curve shape was expanded or contracted until its location at the support and load rollers was as close to the specimen centre-plane as possible given the resolution of the photographs.

$$\delta_{(l)} = \frac{P(L-a)}{6LE_1^b I}\left[\frac{L}{L-a}\langle l-a\rangle^3 - l^3 + \left(L^2 - (L-a)^2\right)l\right] + \frac{Pa}{6LE_1^b I}\left[\frac{L}{a}\langle l-(L-a)\rangle^3 - l^3 + \left(L^2 - a^2\right)l\right]$$
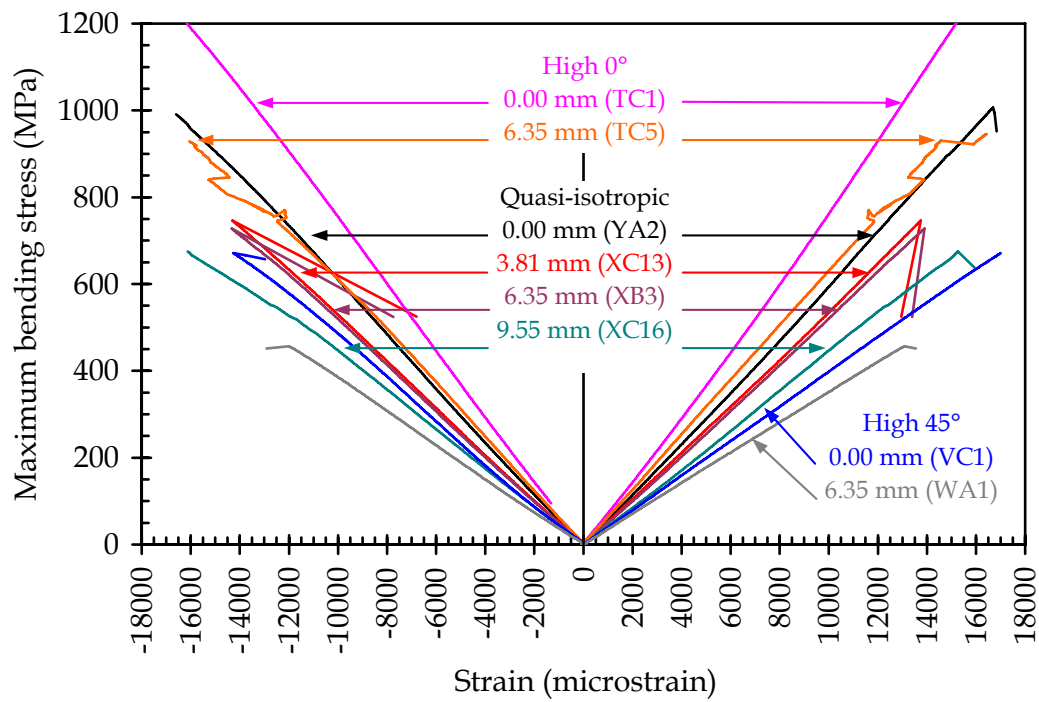
$$\tag{12}$$

Figure 39:   Typical stress-strain responses of RTD OHB specimens with the indicated hole size
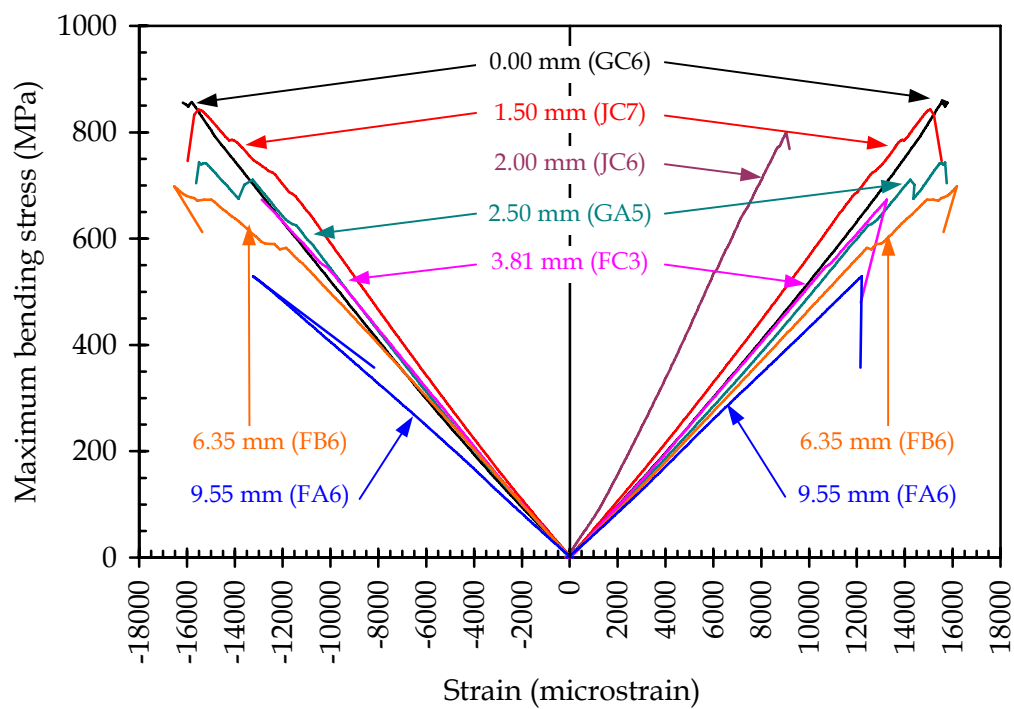

Figure 40:   Typical stress-strain responses of ETW OHB specimens with the indicated hole size

Table 12: RTD OHB results and derived mechanical data

Hole φ (mm)	Specimen ID	Thick. (mm)	Width (mm)	Span (mm) Load	Span (mm) Supp.	P_{max} (kN)	E_1^b (GPa)	Midpt defl. (mm)	ε_1^{bu} (με) Tens. face	ε_1^{bu} (με) Comp. face	Strain grad. (με mm^{-1})	F_1^{bu} (MPa)	FWCF	σ_N^∞ (MPa)
Quasi-isotropic lay-up - [45 0 –45 90]$_{2s}$														
0.00	LC2	2.24	37.94			2.463	56.8	9.68	17111	-16127	14855	1035	1.0000	1035
	YA1	2.06	38.17			2.085	58.0	10.15	16893	-16528[2]	16263[2]	1041		1041
	YA2	2.09	38.13			2.205	57.3	10.35	16690	-16902[2]	16073[2]	1067		1067
	YA3	2.08	38.14			2.235	57.1	10.67	17786	-	17115[1]	1098		1098
	YA4	2.10	38.26			2.117	53.0	10.24	17092	-16032	15807	1014		1014
	YA5	2.10	38.17			2.246	55.7	10.74	17492	-	16699[1]	1087		1087
	MC6[3]	2.33	38.02			2.479	50.1	8.69	-	-	-	960		960
	MC8[3]	2.34	38.03			2.600	49.2	10.15	-	-	-	1004		1004
	MC9[3]	2.34	38.03			2.495	48.6	9.73	-	-	-	958		958
3.81	XC2	2.10	38.14			1.841	53.7	8.97	14859	-14861	14152	867	1.0107	876
	XC3	2.15	38.16			1.654	52.3	7.55	12968	-12854	12019	733	1.0107	741
	XC8	2.15	38.03	25.4	76.0	1.712	51.3	8.01	13890	-14120	13022	763	1.0108	771
	XC10	2.12	38.09			1.815	54.1	8.29	14877	-16053	14562	830	1.0108	839
	XC13	2.14	38.02			1.701	53.7	7.64	13752	-14297	13138	767	1.0108	775
6.35	XB1[4]	2.12	38.12			1.587	54.8	7.13	13878	-14290	13296	721	1.0314	744
	XB2	2.12	38.26			1.603	52.8	7.64	13946	-14310	13360	731	1.0312	754
	XB3[4]	2.09	38.08			1.586	58.4	7.10	13892	-14333	13537	745	1.0315	768
	XB4	2.15	38.15			1.644	50.4	8.20	15070	-15122	14072	735	1.0314	758
	XC12	2.11	38.13			1.653	52.5	8.43	15426	-	14608[1]	765	1.0314	789
	MC10[3]	2.29	38.05			1.438	47.5	5.86	-	-	-	553	1.0316	570
	MC11[3]	2.33	38.03			1.994	45.3	8.66	-	-	-	759	1.0316	783
9.55	XA1	2.10	38.08			1.541	50.2	8.06	14832	-	14126[1]	720	1.0769	775
	XB15	2.15	38.15			1.596	47.4	8.21	15757	-16707	15128	713	1.0766	768
	XB16	2.15	38.04			1.572	46.6	8.41	16274	-	15177[1]	707	1.0771	762
	XC14	2.12	37.91			1.385	45.6	7.66	13976	-15245	13758	633	1.0777	682
	XC16	2.10	37.98			1.491	47.6	8.14	15262	-16119	14922	697	1.0774	751

…continued

Table 12: RTD OHB results and derived mechanical data

Hole ϕ (mm)	Specimen ID	Thick. (mm)	Width (mm)	Span (mm) Load	Span (mm) Supp.	P_{max} (kN)	E_1^b (GPa)	Midpt defl. (mm)	ε_1^{bu} (µε) Tens. face	ε_1^{bu} (µε) Comp. face	Strain grad. (µε mm^{-1})	F_1^{bu} (MPa)	FWCF	σ_N^∞ (MPa)
High 0° lay-up - [45 0$_2$ –45 90$_2$ 0 90$_2$]$_s$													
0.00	TC1	2.16	38.11	25.4	76.0	2.921	74.9	9.24	15773	-16813[2]	15086[2]	1305	1.0000	1305
	TB6	2.16	38.09			2.056	71.6	14.67	15867	-16325	14914	1197		1197
	TC2	2.15	38.17	31.8	95.0	2.141	72.5	16.13	16853	-	15684[1]	1279		1279
	TC3	2.17	38.02			2.101	71.1	15.81	16928	-	15624[1]	1234		1234
6.35	TC4	2.16	38.16	25.4	76.0	2.451	68.2	10.11	17235	-	15996[1]	1111	1.0314	1146
	TC5[4]	2.16	38.02	31.8	95.0	1.761	67.8	14.51	16415	-	15216[1]	1026	1.0316	1058
	TC6[4]	2.20	38.06			1.230	63.5	8.414	10674	-10542	9635	647	1.0316	667
High 45° lay-up - [45 –45 0 45 –45 90 45 –45]$_s$													
0.00	VB6	2.26	38.18	25.4	76.0	2.019	43.6	9.60	-	-16284	14410[1]	825	1.0000	825
	VC1	2.30	38.11			1.421	39.3	14.58	17005	-14258	13607	728		728
	VC2	2.29	38.10	31.8	95.0	1.441	40.7	14.71	-	-15188	13248[1]	742		742
	VC3	2.30	38.09			1.394	39.4	14.87	-	-14928	12987[1]	716		716
6.35	VC4	2.22	38.17	25.4	76.0	1.363	41.0	7.01	14814	-13353	12688	562	1.0314	580
	VC5[4]	2.25	38.10			0.895	39.7	9.31	13025	-11628	10984	456	1.0315	470
	VC6[4]	2.27	38.08	31.8	95.0	0.969	38.1	10.04	13913	-11260	11077	484	1.0315	499
	WA1	2.25	38.06			0.927	40.5	9.54	13087	-11995	11150	471	1.0316	486

[1]   Approximated by doubling the strain on the intact gauge
[2]   Strain gauge failed within 5 s of final failure. Quoted strains interpolated from valid data
[3]   Specimen photographed during loading
[4]   Specimen contained strip gauge to measure strain distribution

Table 13:   ETW OHB results and derived mechanical data (L=76.0 mm, D = 25.4 mm)

Hole φ (mm)	Specimen ID	Thick. (mm)	Width (mm)	Moist. cont. (wt%)	P_{max} (kN)	E_1^b (GPa)	Midpt defl. (mm)	ε_1^{bu} (με) Tens. face	ε_1^{bu} (με) Comp. face	Strain grad. (με mm⁻¹)	F_1^{bu} (MPa)	FWCF	σ_N^∞ (MPa)
0.00	GC6	2.40	38.07	1.32	2.401	49.6	8.11	15733	-16036	13237	857	1.0000	857
	GC7	2.36	37.95	1.31	2.213	47.3	8.18	15337	-14563	12640	820		820
1.50	GA3	2.43	38.22	1.32	1.904	45.9	6.73	13033[2]		10726[1]	652	1.0016	653
	JC7	2.34	38.06	1.28	2.235	49.8	8.47	15061	-15520	13069	843	1.0016	844
2.00	JC5	2.35	38.13	1.27	2.280	51.6	8.62	16745[2]		14251[1]	852	1.0029	854
	JC6	2.37	38.07	1.29	2.180	48.6	8.41	16345[2]		13793[1]	801	1.0029	803
2.50	FC7	2.42	37.95	1.29	1.871	45.1	6.75	13497	-12655	10807	651	1.0045	654
	GA5	2.36	38.07	1.31	1.946	49.6	7.73	-	-15203	12884[1]	742	1.0045	745
3.81	FC2	2.36	38.10	1.28	1.661	48.8	5.953	12353	-10976	9885	602	1.0107	608
	FC3	2.36	38.11	1.31	1.848	49.2	6.723	13252	-12871	11069	673	1.0107	680
	FC4	2.39	38.08	1.30	2.020	46.9	7.444	14818	-14388	12220	722	1.0108	730
6.35	FB1	2.38	38.08	1.32	2.013	45.1	8.449	17997[2]		15123[1]	733	1.0315	756
	FB4	2.34	38.15	1.32	1.940	46.8	8.328	17329	-	14811[1]	729	1.0314	752
	FB6	2.38	38.22	1.33	1.935	46.3	7.876	16175	-16526	13740	698	1.0313	720
9.55	FA4	2.36	37.99	1.29	1.551	44.5	6.353	14012	-14489	12077	565	1.0773	609
	FA5	2.38	38.20	1.29	1.417	42.8	5.758	11518	-12394	10047	503	1.0764	541
	FA6	2.40	38.14	1.30	1.508	40.5	6.260	12194	-13242	10598	529	1.0767	570

[1]   Approximated by doubling the strain on the reported strain data point

[2]   Invalid data from both strain gauges, strain approximated using mid-span displacement data
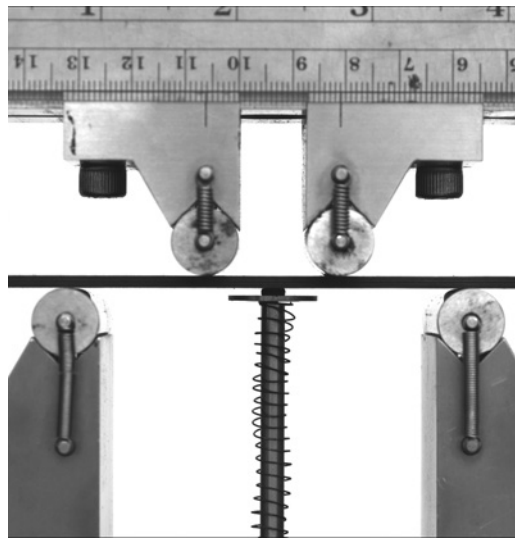
Figure 41: Photograph of specimen MC6 in the test fixture prior to the commencement of loading

Where:

$\delta_{(1)}$ = deflection of the specimen in the y direction at location l along the specimen

P = applied load/2

L = support span

a = support span – loading span

l = distance from left loading point (centre of left hand support roller)

I = second moment of inertia = $bd^3/12$ where

b = specimen width

d = specimen thickness

$$\langle l - a \rangle^3 \quad = \quad 0 \qquad \qquad \text{for } l < a$$

$$(l-a)^3 \qquad \text{for } l \geq a$$

$$\langle l - (L-a) \rangle^3 = 0 \qquad \qquad \text{for } l < (L\text{-}a)$$
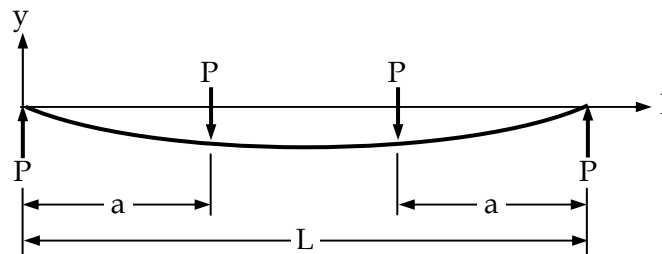
$$(l - (L-a))^3 \quad \text{for } l \geq (L\text{-}a)$$

Figure 43: Four point bend parameters as used in Equation 12

MC6 (0.00 mm hole)   MC10 (6.35 mm hole)

Photo 2: 0.0 mm displacement   Photo 2: 0.0 mm displacement

Photo 5: 3.3 mm displacement   Photo 4: 1.5 mm displacement

Photo 8: 5.8 mm displacement   Photo 7: 4.9 mm displacement

Photo 10: 7.4 mm displacement   Photo 8: 5.8 mm displacement

Photo 11: 8.2 mm displacement   Photo 16: 12.8 mm displacement

Photo 12: 10.0 mm displacement   Photo 18: 14.7 mm displacement

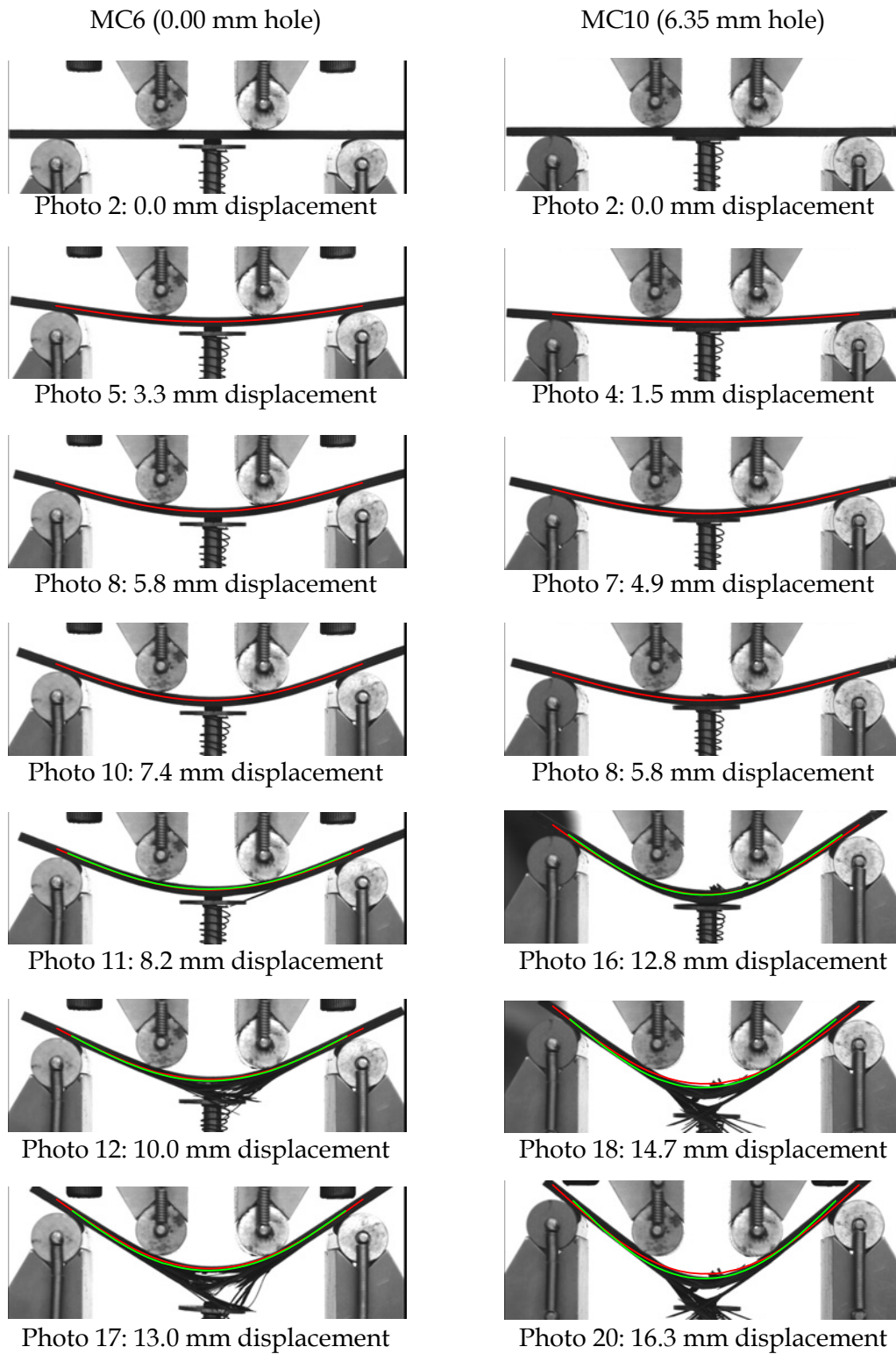Photo 17: 13.0 mm displacement   Photo 20: 16.3 mm displacement

Figure 42: Photographs of typical quasi-isotropic, RTD, OHB specimens during loading. The superimposed curves are the deformed specimen shape as predicted by Equation 12. The red curves assume constant load and support spans while the green curves correct the load and support span for specimen rotation about the finite diameter loading rollers

In Fig. 42 the red curves assumed constant load and support position while the green curves corrected for specimen rotation about the rollers. Visually the deformed specimen profiles were predicted very well by Equation 12. Only at very high deflections were there any obvious differences. These were caused by the specimens of finite thickness rotating over rolls of finite diameter changing the effective support and load spans. It is unlikely that the differences caused by this rotation would need to be corrected for because specimens were well beyond failure before significant differences occurred.

6.4 Strain distribution

A strain survey was conducted on six RTD specimens with 6.35 mm diameter holes. The specimens were:

(i)   VC 5 and VC6   with a $[\pm45/0/\pm45/90/\pm45]_s$ lay-up denoted "High 45°",
(ii) XB1 and XB3   with a $[45/0/\text{-}45/90]_{2s}$ lay-up denoted "Quasi-isotropic",
(iii) TC 5 and TC6   with a $[45/0_2/\text{-}45/90_2/0/90]_s$ lay-up denoted "High 0°".

Each specimen was instrumented with a five element strip gauge as shown in Fig. 6. The gauge was located in the ligament between the hole and the specimen edge on the opposite side of the specimen to the single back-to-back strain gauges used on all OHB specimens (denoted "opposite ligament" in Figs 44 and 45). The first element of the strip gauge was located 1.00 mm from the edge of the hole, and the remaining elements at intervals of 2.00 mm. The strip and single ("opposite ligament") gauge results for three representative specimens are shown in Fig. 44. Strains are shown at 0.8 kN to facilitate a comparison between specimens at the same load, and also at the failure load (0.97 kN for VC6, 1.59 kN for XB3 and 1.23 kN for TC6).

Also shown on Fig. 44 are the strains predicted by Equation 1. As an approximation for this comparison the far field stress (σ^{∞}) in Equation 1 was assumed to be equal to the bending stress (peak bending stress as calculated in the first term of Equation 11). This calculated stress was converted to strain by assuming linear elastic behaviour and dividing by the flexural modulus of the specimen (38.1 GPa for VC6, 58.4 GPa for XB3 and 63.5 GPa for TC6).

As shown in Fig. 44, the strains predicted by this procedure followed the same trends as the experimental data, and were quite close at large distances from the edge of the hole (5 to 12 mm). However close to the hole (1 and 3 mm) the predicted strains were 20-30% larger than that measured. It is quite surprising that the prediction was even this close, given that Equation 1 was derived for in-plane tension where through-thickness strains are uniform. In contrast the out-of-plane bending in these specimens created a strain gradient in the through-thickness direction with; peak tensile strain at the convex surface, peak compression strain at the concave surface and zero strain along the neutral axis.

It is hypothesised that the reason the surface strains close to the hole were lower than that predicted by Equation 1 was that the fibres closer to the neutral axis were less strained and therefore supported the surface fibres.
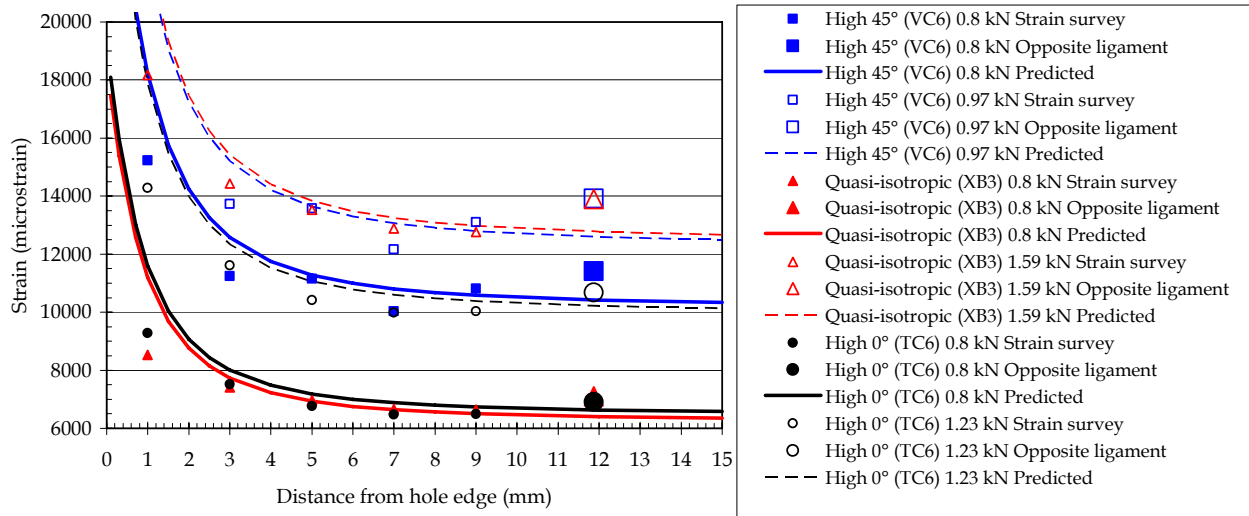
Figure 44: Measured and predicted strain distribution around the hole of three four-point bend specimens. Strains were predicted using Equation 1
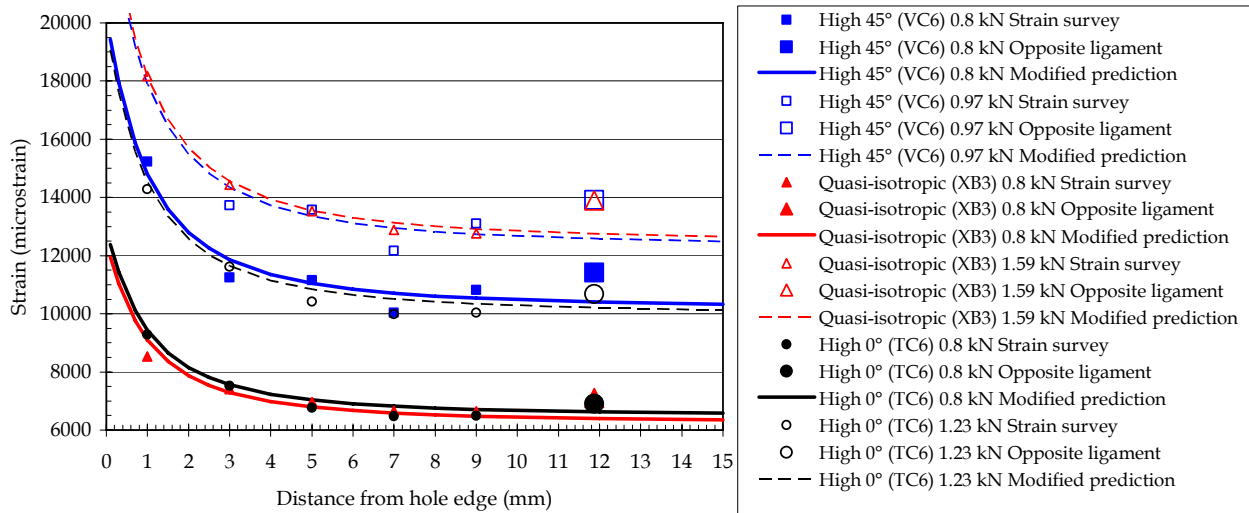

Figure 45: Measured and predicted strain distribution around the hole of three four-point bend specimens. Strains were predicted using Equation 13

In order to improve the fit with the experimental data, the factor of three for the fourth order term in Equation 1 was replaced by a factor of one. The resulting relation is shown as Equation 13 and the strain distribution arising from this equation shown in Figure 45. The predictions are an excellent match with the experimental data, with average $R^2 = 0.925$. Given the clearly superior fit of this prediction to the data, Equation 13 will be used for the ASC and PSC calculations in Section 6.9.

$$\sigma_y(x,0) = \frac{\sigma^\infty}{2}\left\{2+\left(\frac{r}{x}\right)^2+\left(\frac{r}{x}\right)^4\right\}$$ (13)

6.5 Failure locus

The failed OHB specimens were inspected visually. The compression (concave) faces contained, as shown in Fig. 46, at least one classic compression microbuckle. This was observed as a narrow raised line originating at the edge of the hole and propagating laterally to the nearest specimen edge. In most specimens this occurred on one side of the hole only, although some specimens contained microbuckles on both sides of the hole such as shown in Fig 46 (a). In contrast the tension (convex) face contained a number of longitudinal splits in the surface 45°ply. These were similar in appearance to the features on axial tension specimens shown in Fig. 14.

Long delaminations, some equal in length to the entire load-span, were observed on the long, narrow, edge of OHB specimens. These were located between the most highly compressed 0° ply and the adjacent (inboard) -45° ply. The cause of this delamination is discussed in the following paragraph.

Failure of these specimens was a two step process. The first was the initiation and propagation of a delamination between the outermost 0° ply and the adjacent -45° ply.

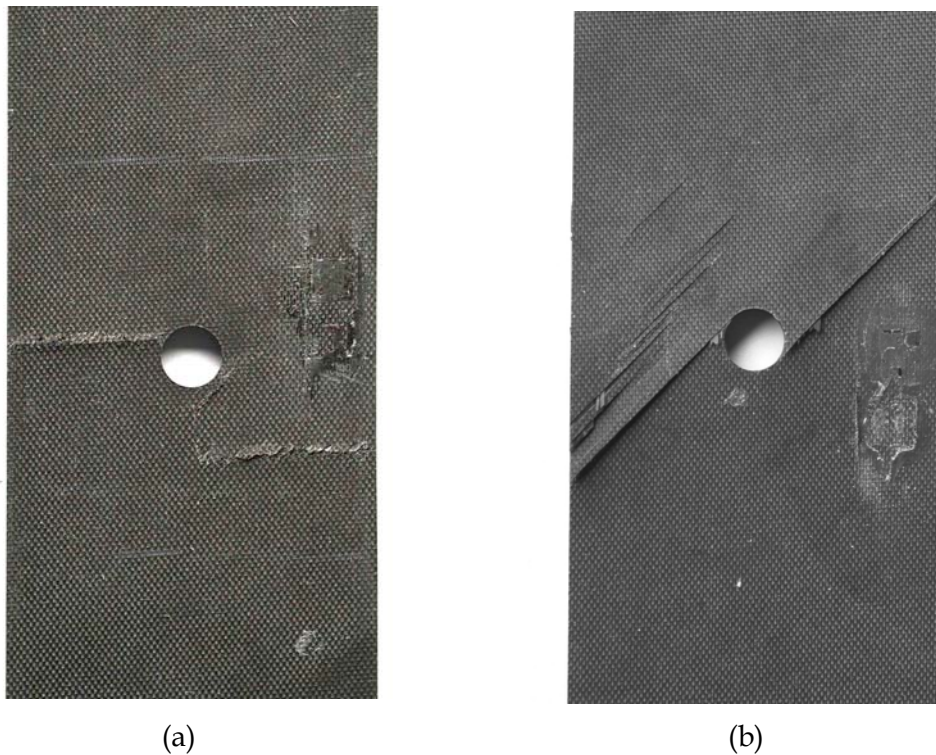(a)   (b)

Figure 46: Photographs of typical failed RTD OHB specimens showing (a) microbuckles on the compression face (specimen XB1) and, (b) split outer plies on the tension face (specimen XC12)

Presumably the driving force for this delamination was high interlaminar shear stress arising from the high strains at this location and the stiffness mismatch between the plies. It is uncertain whether the delamination propagated (i) stably, (ii) in a series of increments or (iii) unstably to its full length. Regardless of the precise length of the delamination, its presence facilitated the second and final failure process, microbuckling of the most highly compressed 0° ply at the mid-span location. The microbuckle would have initiated at the edge of the hole, where stress concentration was greatest. Initially it would have propagated stably, but once it reached a critical length it would then have propagated unstably to the edge of the specimen. This would have eliminated the load-bearing capacity of this ply and led to immediate failure of the specimen.

It is likely that specimen failure would have occurred by microbuckling of this ply even if the delamination was not present, however the delamination reduced the support given to the 0° ply and so reduced the load at which the microbuckle was able to propagate.

6.6 Modulus

The effects of hole size on E_1^b is shown in Fig. 47. The data used for this plot was obtained from Tables 12 and 13.

There was a consistent reduction in E_1^b of 0.6 to 0.9 GPa per mm of hole diameter. The consistency of the reduction over all lay-ups and environmental conditions suggest that
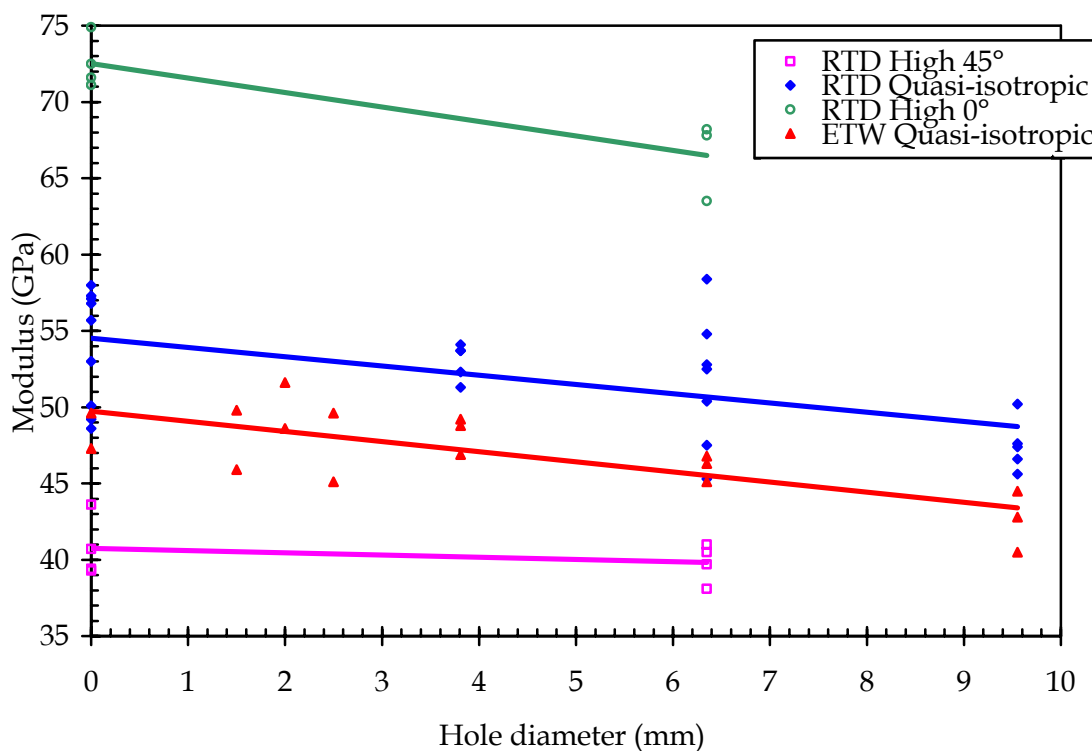

Figure 47: The effect of hole size on the modulus of OHB specimens

this effect was real. The reduction could not be attributed to the use of gross specimen width in calculating bending stress. If net-section stress were used then it was calculated that E_1^b would have risen by 0.8 to 1.1 GPa per mm of hole diameter, almost exactly the opposite effect as the reduction from using gross section stress.

In uniaxial tension and compression, E_1^t and E_1^c are considered "averaged" material properties, i.e. a measure of the bond strength between atoms throughout the entire volume of the test specimen and quite independent of specimen geometry. In contrast, E_1^b is influenced strongly by the geometry of the test. As shown in Equation 10, E_1^b is proportional to the cube of the specimen thickness and the cube of the loading span. The emphasis on specimen geometry is reinforced by the well known approach of increasing E_1^b by locating 0° plies further from the neutral axis, whereas E_1^t and E_1^c are independent of ply location.

It is hypothesised that the centrally located holes in the OHB specimens acted as elastic hinges, reducing E_1^b disproportionately more than the relatively small hole volume would suggest. This effect was subtle, certainly there was no apparent hinge in the specimens shown in Fig. 42.

6.7 Strength

The effects of hole size on the strength of OHB specimens (F_1^{bu}) is shown in Fig. 48. The data for this plot was obtained from Tables 12 and 13.

As with the equivalent OHT and OHC results the fall in OHB strength, as a function of hole size, appeared to be most rapid at the smaller hole sizes and reduced as hole size increased. However the fall in strength as a function of hole size was much more subtle than that for OHT (Fig. 16) and OHC (Fig. 31). It would not be unreasonable to model the ETW data using a straight line.

A number of the ETW observations did not follow this trend, particularly for the 2.00 and 6.35 mm diameter holes. A possible explanation was that these specimens failed to reach the full ETW condition during testing and so were actually tested closer to the RTD condition than the ETW condition. These data should therefore be treated with caution.

The high 45° and high 0° lay-ups contained only two hole sizes and so no conclusion could be made regarding the shape of the relation between strength and hole size. The average strength of these materials fell by 260 – 325 MPa from the unnotched to 6.35 mm diameter holes, a linear fall of 40-50 MPa per mm of hole diameter. This was comparable with the falls observed for the quasi-isotropic lay-up.

If all the data for the quasi-isotropic ETW and RTD was counted then $EKDF_{ETW}^{Fbu}$ = 0.86. If the data for specimens with 6.35 mm diameter holes was ignored then $EKDF_{ETW}^{Fbu}$ = 0.81,
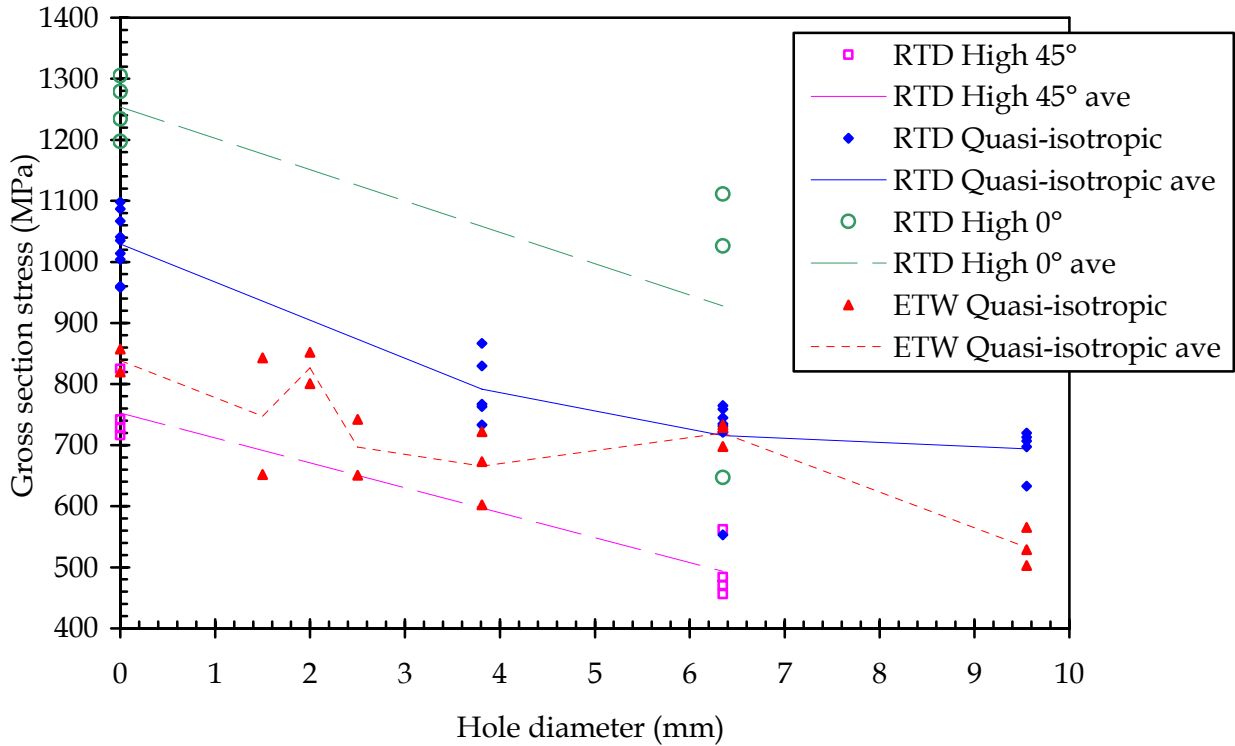
Figure 48:   The effect of hole size on OHB strength

identical to $EKDF_{ETW}^{Fcu}$. This result is reasonable given that both compression and bending are "resin-dominated" properties. Applied loads are supported by the axial fibres, but these fibres are supported by the resin. A reduction in the stiffness and strength of the resin would be expected to produce similar losses in strength for both OHC and OHB.

6.8 Strain-to-failure

The effects of hole size on the OHB strain-to-failure (ε_1^{bu}) are shown in Fig. 49. This behaviour was slightly different to that for F_1^{bu} shown in Fig. 48. Although both plots retained the broad trend of ε_1^{bu} decreasing as hole size increased, the fractional reduction in ε_1^{bu} was much less than for F_1^{bu}. For ETW specimens the loss in ε^{bu} was approximately half the loss in F_1^{bu}. ε_1^{bu} for the quasi-isotropic RTD specimens actually rose at the larger hole diameters.

The most likely cause of these reduced losses/rises was the hinge effect at the holes. The strain gauges measuring bending strain (ε_1^{b}) were located in the ligament between the edge of the hole and the side of the specimen. Although the effect was subtle and not observed visually on Fig. 42, deformation was expected to concentrate in this low stiffness region. As hole size increased the resistance to bending would have decreased, thus at least partially counteracting the expected reduction in ε^{bu} as hole size increased.
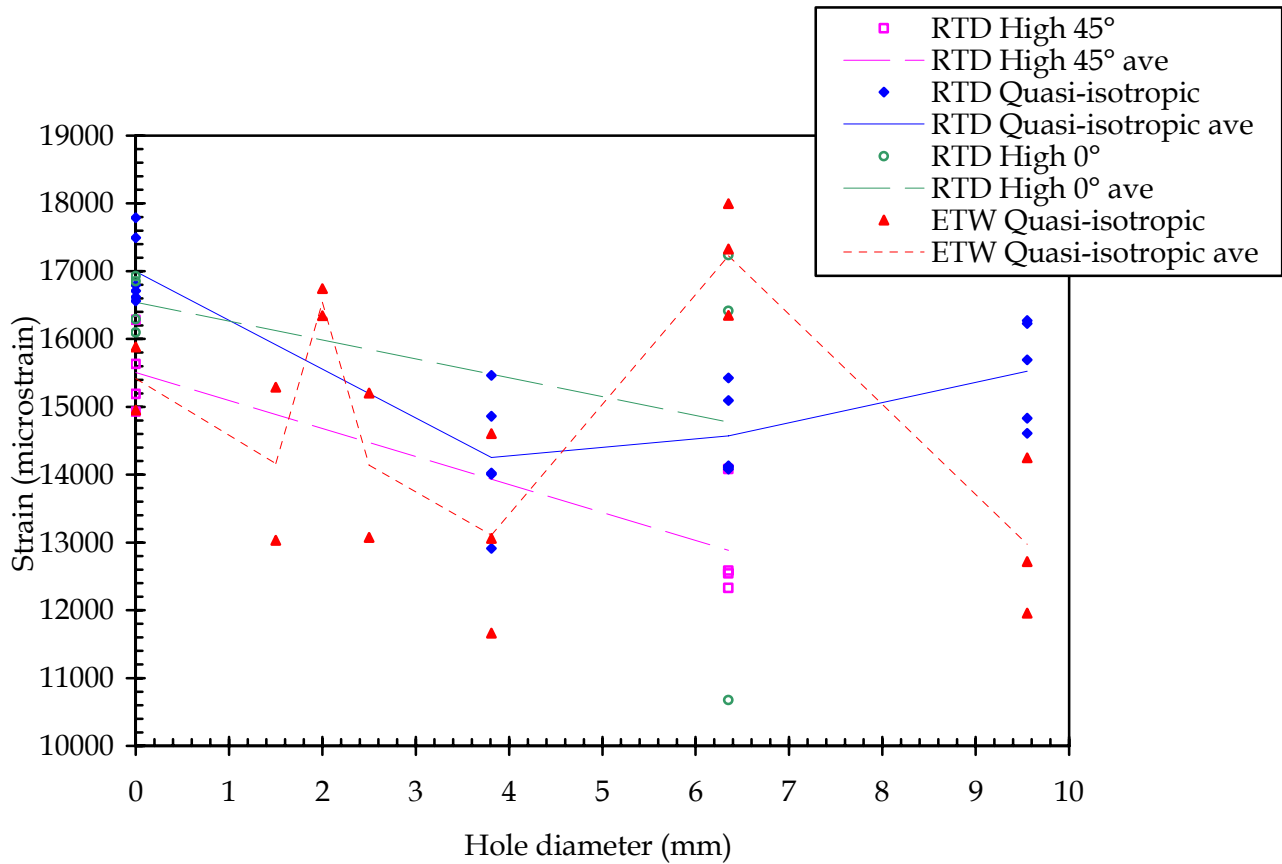
Figure 49: The effect of hole size on the average surface strain-to-failure in OHB specimens

It was found that $\text{EKDF}_{\text{ETW}}^{\varepsilon cu}$ = 0.96. This was skewed by the very high ε_1^{bu} for specimens with 2.00 and 6.35 mm diameter holes. Ignoring these produced $\text{EKDF}_{\text{ETW}}^{\varepsilon cu}$ = 0.87, a more reasonable estimation of the curves shown in Fig. 49. Upon first inspection this value appears high. Intuitively $\text{EKDF}_{\text{ETW}}^{\varepsilon cu}$ was expected to be approximately 0.8, close to that of $\text{EKDF}_{\text{ETW}}^{Fbu}$. The explanation for this discrepancy lies in the attendant fall in specimen stiffness. The load at which specimen failure occurred was approximately 20% lower in the ETW environment than the RTD environment, however bending stiffness was also approximately 10 % lower in the ETW environment. Thus, for the same load or stress, the strain measured in the ETW specimen would have been approximately 10% greater than for the equivalent RTD specimen. This should lead to an $\text{EKDF}_{\text{ETW}}^{\varepsilon cu}$ of approximately 0.9, which was close to the observed value.

6.9 Strength prediction

6.9.1 Average Stress Criterion

The average unnotched compression strength was calculated from the data in Tables 12 and 13.

Assuming that Equation 1 modelled the stress distribution around the hole then the ratio of notched to unnotched strengths for the ASC was given by Equation 5. Modifying the stress distribution to Equation 13 changed the ASC to Equation 14.

$$\frac{\sigma_N}{\sigma_0} = \frac{2(1-\xi_1)}{2 - \frac{2}{3}\xi_1 - \xi_1^2 - \frac{1}{3}\xi_1^4} \tag{14}$$

Where:

$$\xi_1 = \frac{r}{r+a_0}$$

The a_0 for both Equations 5 and 14 was calculated using least squares fits of these equations with the experimental data.

The measured strength of ETW specimens with 6.35 mm diameter holes appeared very high. Ignoring the results for these specimens and repeating the least square fit yielded moderate improvements in the determination coefficient when compared to using the full data set. It was judged that the smaller data set was a more realistic representation of the real OHB behaviour and so the parameters obtained from these regressions were used.

The resultant parameters are shown below while the experimental data and curves of best fit are shown in Fig. 50:

Equation 5

RTD	σ_0 = 1029 MPa	a_0 = 7.49 mm	R^2 = 0.777	
ETW	σ_0 = 839 MPa	a_0 = 10.33 mm	R^2 = 0.506	Full data set
	σ_0 = 839 MPa	a_0 = 7.93 mm	R^2 = 0.682	Ignoring 6.35 mm holes

Equation 14

RTD	σ_0 = 1029 MPa	a_0 = 3.63 mm	R^2 = 0.814	
ETW	σ_0 = 839 MPa	a_0 = 5.70 mm	R^2 = 0.503	Full data set
	σ_0 = 839 MPa	a_0 = 4.27 mm	R^2 = 0.670	Ignoring 6.35 mm holes

Scatter in the data made it difficult to determine whether the model derived from the more realistic model of strain distribution (Equation 14) improved the prediction of strength. R^2 increased moderately for the RTD data but decreased slightly for the ETW data. In the absence of conclusive data, it was judged to be more appropriate to use a model that reflected the experimentally measured strains and thus the parameters from Equation 14 were selected as most representing the real OHB behaviour.

6.9.2 Point Stress Criterion

Modifying the stress distribution around the hole from the uniaxial case (Equation 1) to that which matched the strain gauge data (Equation 13) changed the PSC of Equation 6 to that shown in Equation 15.

$$\frac{\sigma_N}{\sigma_0} = \frac{2}{2 + \xi_2{}^2 + \xi_2{}^4}$$ (15)

Where:

$$\xi_2 = \frac{r}{r + d_0}$$

The PSC characteristic length was calculated by using least squares fits of the experimental strength data with both Equations 6 and 15. As with the ASC, the ETW data from specimens with 6.35 mm diameter holes were both included and ignored. The calculated parameters are shown below while experimental data and curves of best fit are shown in Fig. 51:

Equation 6
RTD	σ_0 = 1029 MPa	d_0 = 2.19 mm	R^2 = 0.722	
ETW	σ_0 = 839 MPa	d_0 = 2.72 mm	R^2 = 0.401	Full data set
	σ_0 = 839 MPa	d_0 = 2.07 mm	R^2 = 0.610	Ignoring 6.35 mm holes

Equation 14
RTD	σ_0 = 1029 MPa	d_0 = 1.32 mm	R^2 = 0.812	
ETW	σ_0 = 839 MPa	d_0 = 1.81 mm	R^2 = 0.469	Full data set
	σ_0 = 839 MPa	d_0 = 1.36 mm	R^2 = 0.688	Ignoring 6.35 mm holes

The predictions for Equation 15 were selected as most representing the real OHB behaviour for the same reason as given in the previous section.

6.9.3 Comparison with tension and compression

The selected ASC and PSC parameters and coefficients of determination are summarised in Table 14. The characteristic lengths for OHB were considerably larger than the equivalent length for OHT and OHC. The physical interpretation of this result lies in the variation of longitudinal strain through-the-thickness of bend specimens. Peak tension strains occur only on the convex surface. These reduce to zero at the neutral axis and rise to a peak compression strain at the concave surface. Thus, only relatively small volumes of material near each surface of the specimen are exposed to peak bending stresses. The support offered by the less-strained inner plies reduces the strain on these surface plies and thus the stress concentration effect of the hole.

The ASC requires that a sufficient volume of material reach the unnotched strength before
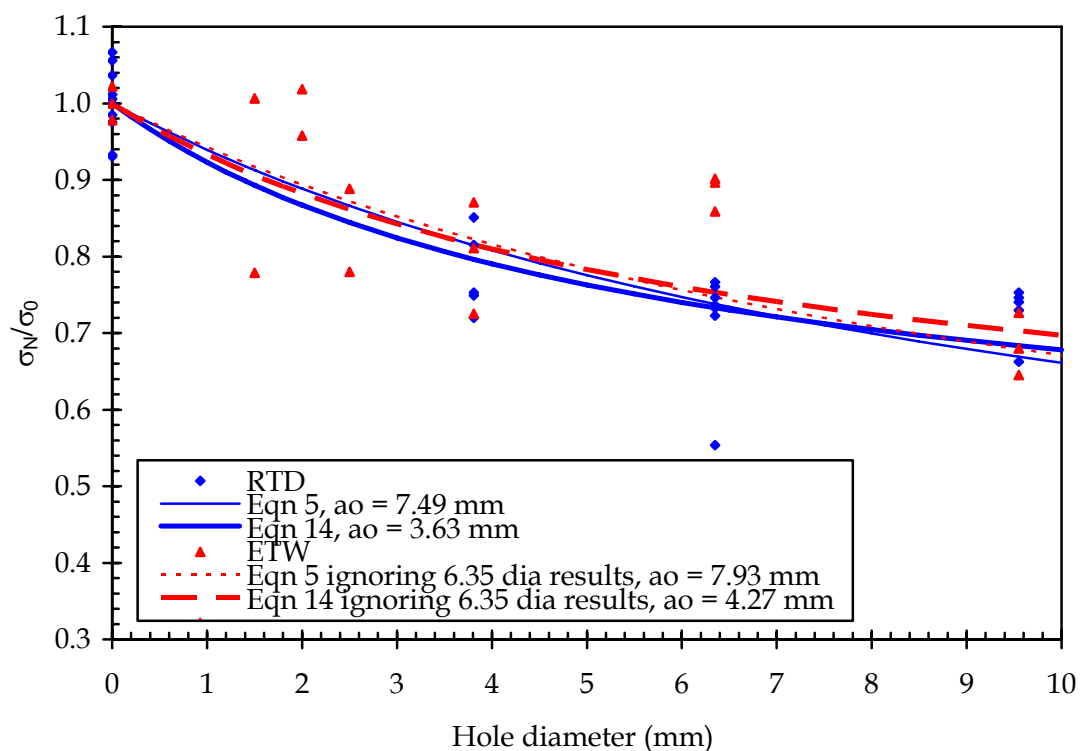
Figure 50: Notched/unnotched strength as determined experimentally and by the Equations 5 and 14 versions of the ASC for RTD and ETW OHB
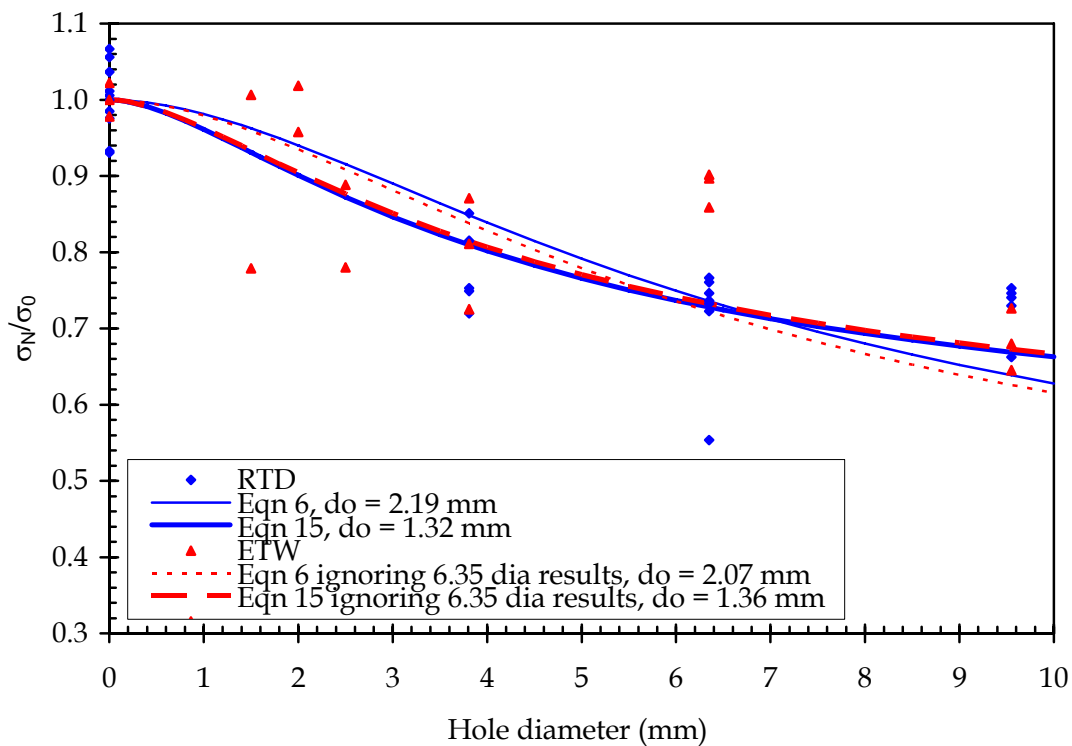

Figure 51: Notched/unnotched strength as determined experimentally and by the Equations 6 and 15 versions of the PSC for RTD and ETW OHB

Table 14: Calculated ASC and PSC parameters and coefficients of determination

Model	Parameter	OHT		OHC		OHB	
		RTD	ETW	RTD	ETW	RTD	ETW
All	σ_0 (MPa)	646	632	614	506	1029	839
Average Stress Criteria	a_o (mm)	2.61	2.26	1.71	1.49	3.63	4.27
	R^2	0.986	0.977	0.978	0.977	0.814	0.670
Point Stress Criteria	d_o (mm)	0.89	0.73	0.60	0.52	1.32	1.36
	R^2	0.957	0.943	0.954	0.965	0.812	0.688

failure. Clearly this length would be longer in the strain varying OHB specimens than in OHT/OHC specimens where strains are uniform through the entire thickness. The PSC only requires the unnotched strength to be reached at the characteristic distance (d_0) from the hole. The strain distribution from which d_0 was calculated was that on the tensile surface of the specimen, and this is strongly influenced by the strain gradient.

7 Conclusions

Open hole tension (OHT), compression (OHC) and four-point bend (OHB) tests, in the room temperature dry (RTD) and elevated temperature wet (ETW) condition, were conducted on AS4/3501-6 quasi-isotropic $[45/0/-45/90]_{2s}$ laminate coupon specimens. The following conclusions were drawn from these tests:

1. The strain distribution near the hole of an OHT specimen, in the longitudinal direction along a line through the centre of the hole and perpendicular to the loading direction, was predicted well by the model for an infinite orthotropic plate containing a circular hole subjected to a uniform, remote, in-plane, stress. A simple modification of this model predicted well the strain distribution near the hole on the tensile face of OHB specimens.

2. The elastic modulus of OHT and OHC specimens was unaffected by both hole size and test environment. The flexural modulus in OHB decreased both as hole size increased and in changing from RTD to ETW environments.

3. The OHT and OHC strength and strain-to-failure decreased rapidly as hole diameter increased from 1.50 to 3.81 mm, then much less rapidly for holes from 6.35 to 9.55 mm. This effect was much less pronounced in OHB specimens, partially due to a considerable scatter in the data.

4. ETW conditions had little effect on OHT properties but produced significant, and similar, reductions in OHC and OHB strength and strain-to-failure.

5. The deflection OHB specimens with 0.00 and 6.35 mm diameter holes was represented well by assuming no hole and using classical beam deflection theory.

6. OHT and OHC strength was predicted very well, and OHB strength moderately well, by the Whitney-Nuismer Average Stress Criterion and Point Stress Criterion when using the strain distribution for that specimen type. OHC strength was also predicted very well by the Budiansky-Soutis-Fleck Cohesive Zone Model. It is suspected that these models will not predict accurately the strength of coupons subject to combined axial and bend loading

8 Acknowledgments

The author acknowledges the contributions of Leo Mirabella (DSTO) for conducting and organising a number of the tests, Michael Bannister (CRC-ACS) for project management, Peter Haggart (Fortburn Pty Ltd) for specimen manufacture, and Mark McVilley (CRC-ACS), Neil Absolom, Rodney Gray and David Parslow are for their contribution to strain gauging and testing.

9 References

1 Whitney, J. M. and Nuismer, R. J., "Stress fracture criteria for laminated composites containing stress concentrations", Journal of Composite Materials, Vol. 8, 1974, pp. 253-265.

2 Konish, H. J. and Whitney, J. M., "Approximate stresses in an orthotropic plate containing a circular hole", Journal of Composite Materials, Vol. 9, 1975, pp. 157-166.

3 Lekhnitskii, S. G., "Anisotropic plates", Translated from the Second Russian Edition by S. W. Tsai and T. Cheron, Gordon and Breach Science Publishers Inc., New York, 1968.

4 Davis, M. J. and Jones, R., "Damage tolerance of fibre composite laminates in composites for aircraft structures", Chapter 10, Editors B.C. Hoskin and A.A. Baker, Education Series 1986.

5 Soutis, C., Fleck, N. A. and Smith, P. A., "Failure prediction technique for compression loaded carbon fibre-epoxy laminate with open holes", Journal of Composite Materials, Vol. 25, November 1991, pp. 1476-1498.

6 Tan, S., "Finite-width correction factor for anisotropic plate containing a central opening", Journal pf Composite Materials, Vol. 22, 1988, pp. 1080-1097.

7   Jones, R. M., "Mechanics of composite materials", Scripta Book Co., Washington, D. C., 1975.

8   Suppliers of Advanced Composite Materials, "SACMA recommended test method for open-hole tensile properties of oriented fiber-resin composites", SACMA SRM 5R–94 in SACMA Recommended Methods, Composites Fabricators Association, 1999, 8 pp.

9   Suppliers of Advanced Composite Materials, "SACMA recommended test method for open-hole compression properties of oriented fiber-resin composites", SACMA SRM 3R–94, in SACMA Recommended Methods, Composites Fabricators Association, 1999, 10 pp.

10 ASTM Standard D790, "Standard test method for flexure properties of unreinforced and reinforced plastics and electrical insulating materials", ASTM International, West Conshohocken, PA, www.astm.org

11 Callus, P. J., Mouritz, A. P., Bannister, M. K. and Leong, K. H., "Tensile properties and failure mechanisms of 3D woven GRP composites", Composites, 30A, June, 1999, pp. 1277-1287.

12 http://www.graphpad.com/curvefit/2_models__1_dataset.htm

13 Potti, P. K. G., Rao, B. N. and Srivastava, V. K., "Notched tensile strength of randomly oriented E-glass composite laminates", Materials Science and Engineering, A282, 2000, pp. 59-66.

14 Komadina, J., Sheppard, A., Callus, P. J. and Bannister, M., "BAE Systems/DSTO collaboration: Uniaxial coupon loading (WP2)", CRC-ACS-TM-01022, Cooperative Research Centre for Advanced Composite Structures, Melbourne, Australia, October 2001, 25 pp.

15 Sutcliffe, M. P. F., Xin, X. J., Fleck, N. A., Curtis, P. T., "Composite Compressive Strength Modeller", Version 1.4a, 1999, Engineering Department, Cambridge University, Trumpington St, Cambridge, CB2 1PZ, E-mail: mpfs@eng.cam.ac.uk

16 Adams, D. F., "Flexure test methods", High Performance Composites, November, 2005, 2 pp., http://www.compositesworld.com/hpc/issues/2005/November/1050

10 Appendix A – Correction of actuator strain

The strains determined from actuator displacement were corrected by correlating these strains with those measured from strain gauges. The correction procedure is described in this Appendix.

10.1 Calculate nominal strain

The actuator displacement was divided by a nominal specimen gauge length to produce a nominal strain. The nominal gauge lengths were 175 mm for RTD OHT and OHC, 195 mm for ETW OHT and 304.8 mm for ETW OHC.

10.2 Factor the nominal strain

The nominal strain was factored in those specimens where both actuator displacement and strain gauge (RTD OHT) or extensometer (ETW OHT) data was available. The factor was that required to match, between 1000 and 3000 με, the slope of the stress versus nominal strain plot with that of the strain gauge/extensometer plot. The factor equations for the two types of OHT and OHC test, with hole diameter in mm, are shown as Equations A1 to A4.

$$\text{RTD OHT factor} = 0.0110 \, (\text{hole diameter}) + 1.4817 \tag{A1}$$

$$\text{ETW OHT factor} = 0.0709 \, (\text{hole diameter}) + 6.2928 \tag{A2}$$

$$\text{RTD OHC factor} = 0.0173 \, (\text{hole diameter}) + 1.1592 \tag{A3}$$

$$\text{ETW OHC factor} = 0.0012 \, (\text{hole diameter}) + 1.3360 \tag{A4}$$

In specimens where strain gauge/extensometer data was available, the factor calculated from the data in that specimen was used to factor the nominal strain. In specimens where strain gauge/extensometer data was not available, the factor shown in Section 10.2 was applied to the actuator displacement based nominal strain to produce the factored nominal strain.

10.3 Offset factored strain

For all specimens the factored nominal strain was offset so that a least squares line of best fit through the stress versus strain data, from 1000-3000 με, passed through the origin.

10.4 Correct offset factored strain

The offset strain was corrected to account for non-linear displacement of the load train. The difference between the offset factored nominal strain and strain gauge/extensometer was plotted as a function of load for those specimens where data from both transducers was available. It was found that, as load increased, the difference between the strains

measured from actuator displacement and that from the strain gauge/extensometer, also increased. For the OHT and OHC specimens these differences are shown, with load in kN and strain in με, as Equations A3 and A4

RTD OHT offset strain - strain gauge strain = $0.9455(load)^2 - 20.7290(load) + 93.7115$

$$(A5)$$

ETW OHT offset strain - extensometer strain = $-0.0020(load)^5 + 0.1200(load)^4 - 3.6121(load)^3 + 58.5269(load)^2 - 450.9805(load) + 1218.7938$ $\quad$ (A6)

RTD OHC offset strain - strain gauge strain = $1.1597(load)^2 - 22.1530(load) + 93.6410$

$$(A7)$$

ETW OHC offset strain - strain gauge strain = $-0.6952(load)^2 - 10.6908(load) - 35.9244$

$$(A8)$$

10.5 Apply correction

The differences shown in Equations A5 to A8 were calculated at each actuator displacement based strain data point then subtracted from the corresponding offset factored nominal strain data point. The resultant was the corrected actuator displacement strain.

11   Appendix B

The coefficient of determination (R^2) measures the variation of sample data. It is calculated using Equation B1.

$$R^2 = 1 - SSE/SSM \tag{B1}$$

$$R^2 = 1 - \frac{\sum_{i=1}^{n}\left[\left(\frac{\sigma_n}{\sigma_0}\right)_i^{\text{Predicted}} - \left(\frac{\sigma_n}{\sigma_0}\right)_i^{\text{Experiment}}\right]^2}{\sum_{i=1}^{n}\left[\left(\frac{\sigma_n}{\sigma_0}\right)_i^{\text{Experiment}} - \left(\overline{\frac{\sigma_n}{\sigma_0}}\right)^{\text{Experiment}}\right]^2} \tag{B2}$$

Where:

SSE	=	sum of square of residuals (errors)
SSM	=	sum of squares about the mean
n	=	number of data points
$\left(\frac{\sigma_n}{\sigma_0}\right)_i^{\text{Predicted}}$	=	predicted ratio of notched/unnotched strength, for the ith data point
$\left(\frac{\sigma_n}{\sigma_0}\right)_i^{\text{Experiment}}$	=	ratio of notched/unnotched strength, for the ith data point, as obtained by experiment
$\left(\overline{\frac{\sigma_n}{\sigma_0}}\right)^{\text{Experiment}}$	=	average ratio of notched/unnotched strength for all data points as obtained by experiment

DEFENCE SCIENCE AND TECHNOLOGY ORGANISATION			
DEFENCE SCIENCE AND TECHNOLOGY ORGANISATION **DOCUMENT CONTROL DATA**			1. PRIVACY MARKING/CAVEAT (OF DOCUMENT)

| 2. TITLE

The Effects of Hole-size and Environment on the Mechanical Behaviour of a Quasi-isotropic AS4/3501-6 Laminate in Tension, Compression and Bending | 3. SECURITY CLASSIFICATION (FOR UNCLASSIFIED REPORTS THAT ARE LIMITED RELEASE USE (L) NEXT TO DOCUMENT CLASSIFICATION)

    Document   (U)
    Title   (U)
    Abstract   (U) |

| 4. AUTHOR(S)

Paul J. Callus | 5. CORPORATE AUTHOR

DSTO Defence Science and Technology Organisation
506 Lorimer St
Fishermans Bend Victoria 3207 Australia |

| 6a. DSTO NUMBER
DSTO-TR-2077 | 6b. AR NUMBER
AR-014-060 | 6c. TYPE OF REPORT
Technical Report | 7. DOCUMENT DATE
November 2007 |

| 8. FILE NUMBER
2007/1125658/1 | 9. TASK NUMBER
AIR 07/053 | 10. TASK SPONSOR
DGTA | 11. NO. OF PAGES
72 | 12. NO. OF REFERENCES
16 |

| 13. DOWNGRADING/DELIMITING INSTRUCTIONS

http://www.dsto.defence.gov.au/corporate/reports/DSTO-TR-2077.pdf | 14. RELEASE AUTHORITY

Chief, Air Vehicles Division |

15. SECONDARY RELEASE STATEMENT OF THIS DOCUMENT
Approved for public release
OVERSEAS ENQUIRIES OUTSIDE STATED LIMITATIONS SHOULD BE REFERRED THROUGH DOCUMENT EXCHANGE, PO BOX 1500, EDINBURGH, SA 5111

16. DELIBERATE ANNOUNCEMENT
No Limitations

17. CITATION IN OTHER DOCUMENTS   Yes

18. DEFTEST DESCRIPTORS
Carbon fibre reinforced composites Mechanical properties Environments Strains Failure analysis

19. ABSTRACT

This report describes the results of open-hole-tension (OHT), open-hole-compression (OHC) and open-hole-four-point-bend (OHB) tests conducted on AS4/3501-6 quasi-isotropic $[45/0/-45/90]_{2s}$ laminates in the room temperature dry (RTD) and elevated temperature wet (ETW) condition. Specimens were 38.1 mm wide with central through-holes ranging in diameter from 0.00 (unnotched) to 9.55 mm. The strain distribution near the hole in an OHT specimen was measured and found to agree well with that predicted for an infinite orthotropic plate subject to uniform remote stress. A simple modification of this model predicted well the strains near the hole on the tensile face of OHB specimens. OHT and OHC strength fell rapidly as hole size increased for small holes and less so for larger holes. This effect was much less pronounced in OHB specimens. The ETW environment had little effect on OHT properties but produced significant, and similar, reductions in OHC and OHB strength. OHT and OHC strength was predicted very well, and OHB strength moderately well, by the Whitney-Nuismer Average and Point Stress Criteria when using the strain distribution for that specimen type. OHC strength was also predicted very well by the Budiansky-Soutis-Fleck Cohesive Zone Model. However, each of these models requires experimental data in addition to the strength of the unnotched laminate and thus they are limited to applications where this data can be generated.